DISSERTATION

ANALYTICAL METHODS TO ENHANCE DETECTION OF ANTHROPOGENIC RADIONUCLIDES IN

ENVIRONMENTAL MATRICES

Submitted by

Brett L. Rosenberg

Department of Environmental and Radiological Health Sciences

In partial fulfillment of the requirements

For the Degree of Doctor of Philosophy

Colorado State University

Fort Collins, Colorado

Summer 2016

Doctoral Committee:

     Advisor: Alexander Brandl

     Thomas Borch
     Charles Henry
     John Pinder
     Georg Steinhauser

ProQuest Number: 10149820

ProQuest 10149820

ABSTRACT

ANALYTICAL METHODS TO ENHANCE DETECTION OF ANTHROPOGENIC RADIONUCLIDES IN

ENVIRONMENTAL MATRICES

The efficacy of methods that are used to detect radionuclides is dependent on the properties of

the radionuclides and the matrices being analyzed. Gamma spectroscopy is an excellent tool for detecting

very low quantities of a short-lived gamma-emitting radionuclide. However, as the probability of gamma

ray emission decreases and the half-life increases, greater quantities of a radionuclide are required for

detection by gamma spectroscopy. Since most transuranic actinides are usually not present in such

quantities or concentrations in the environment, mass spectrometry is the preferred tool. For tritium,

^{90}Sr, and other lower-Z elements that emit no easily detectable gamma rays, liquid scintillation counting is

commonly used to measure the beta particles they emit. However, this methodology requires

radiochemical extraction procedures to ensure a maximized ratio between signal and background.

Nondestructive gamma spectroscopy was used to evaluate radiocesium content in soil and vegetation

samples collected from the Fukushima prefecture exclusion zone in 2013 and 2014. Liquid scintillation

counting was used for quantifying ^{3}H in samples collected in 2013 and ^{90}Sr in samples collected in 2013

and 2014. The radiocesium and ^{90}Sr activities were found to have decreased from 2013 to 2014. Although

^{3}H activities could be quantified in most samples, a sample from Chimeiji had a specific activity that

statistically exceeded background (1.2 ± 1.6 Bq mL^{-1}); further investigation is required to ascertain if ^{3}H is

present within that sample. Reports generated by TEPCO were also evaluated; radiocesium ratios and

^{131}I/^{132}Te ratios calculated from the reports reveal the importance of considering counting statistics and

spectroscopic interference when drawing conclusions about the presence of anthropogenic radionuclides in environmental samples.

Gamma spectroscopy was then applied to explore radiochemical separation techniques that can enhance detection of anthropogenic radionuclides, especially gamma-emitting actinides like ^{239}Np shortly after a nuclear event. Ion specific extraction chromatography was found to be effective at minimizing spectroscopic interference from fission products, and addition of stable iodide carrier and a precipitating agent facilitated decreasing radioiodine activity within environmental samples. Extraction chromatography was found to reduce ^{131}I interference by at least one order of magnitude, making it preferred for reducing ^{131}I activity within an environmental sample. Extraction chromatography also avoids the potential of precipitating any analyte. The separation and measurement techniques utilized herein have effectively enhanced the ability to detect low-activity anthropogenic radionuclides; supplemental measurements gathered from the exclusion zone confirm the observed trends and prove the necessity of minimizing interference.

ACKNOWLEDGMENTS

TABLE OF CONTENTS

LIST OF TABLES

LIST OF FIGURES

1. INTRODUCTION

Environmental matrices are complex systems that require specialized methodologies to enhance the detection of trace quantities of a substance. Statistically, detection is enhanced by increasing the measurement time and the amount of a substance, the latter being more effective. However, considerations must be made regarding practicality. Is it practical to measure something by gamma spectroscopy for 200 hours? Is it practical to collect 50 kg of a sample and place it on the window of a gamma detector? Other approaches must be considered, such as changing the geometry of a sample from 2π to 4π (from *on* the detector to *in* or *around* the detector) to maximize detection efficiency. If the environmental matrix has components that interfere too much with the desired analyte, other measures must be taken to determine how much of the analyte is present – if it is present.

A nuclear event, whether it is a major incident at a nuclear power plant or the detonation of a nuclear weapon, can bring about global concern for health and safety. Most concerns revolve around the radiological effects of the radionuclides that are generated and released, although some products of a nuclear event can be chemically hazardous as well. This introduction will bring to light methods that are commonly used to detect contaminants in environmental matrices, as well as considerations for minimizing transport of contamination in the environment and radiological exposure. The projects that are presented and discussed in following chapters will highlight analytical techniques, applications, and methodological considerations for accurate detection and quantification of anthropogenic radionuclides following future nuclear events.

Common Analytical Methods

Detection of radionuclides requires an understanding of the types of emissions during their decay and the energies of these emissions. Radioactive isotopes can have half-lives ($T_{1/2}$) ranging from nanoseconds to billions of years. For example, ^{131}I has a half-life of 8 days, emits a beta particle with an

1

average energy of 192 keV during 90% of the decays, and emits a 364 keV gamma ray following 82% of the decays. Because the gamma ray has an energy in excess of 100 keV and is emitted following a high percentage of decays, detection of this radionuclide by gamma spectroscopy is preferred, as minimal sample processing may be required for detection by gamma spectroscopy.

However, there are several instances where detection of radionuclides by their radiological properties is difficult, or practically impossible. Detection of longer-lived radionuclides, such as ^{238}U ($T_{1/2}$ = 4.5×10^9 y), by their radiological properties is very difficult without large quantities present within a sample. Continuing with this example, ^{238}U emits a 113.5 keV gamma ray following 0.01% of decays; if a detector has an efficiency of 5% for detecting this gamma ray coming from a polypropylene container sitting directly on the detector, a count rate of 1 count per second would be practically impossible to obtain. The activity of the sample would have to be 200 kBq (5.4 µCi), which is more than 16 grams (0.85 mL) of pure ^{238}U. If the uranium concentration in soil is assumed to be 2.3 ppm, the amount of soil in this sample would be almost 7,000 kg [1]. For isotopes with very long half-lives, other methods like mass spectroscopy (MS) must be implemented to enhance detection of trace quantities of these radionuclides. Methods for separation can be used prior to MS to minimize interference between atoms with similar masses (isobars, such as ^{238}U and ^{238}Pu) and enhance the detection capability of the spectrometer.

Radiological interference can also make detection of radionuclides by their decay properties practically impossible. One example of this is quantifying the relative amounts of ^{239}Pu and ^{240}Pu in a sample. The half-life of ^{239}Pu is 24110 y, and it emits a 5.157 MeV alpha particle during 71% of its decays; ^{240}Pu has a half-life of 6561 y and emits a 5.168 MeV alpha particle during 73% of its decays. The resolution of a spectrum generated by alpha spectroscopy is not fine enough to distinguish between these two alpha particles. Therefore, MS is used to quantify the relative amounts of these two isotopes within a sample [2].

Similarly, detection of trace ^{239}Np ($T_{1/2}$ = 2.4 d) in a sample containing large activities of radiotellurium requires chemical separation. The most prominent gamma rays emitted from ^{239}Np have the following energies and emission probabilities: 106 keV (25%), 278 keV (15%), and 228 keV (11%). Gamma rays of similar energies are emitted from ^{129m}Te (106 keV, 0.2%), ^{129}Te (278 keV, 0.6%), and ^{132}Te (228 keV, 88%). Following a nuclear event, radiotellurium activities are orders of magnitude higher than actinide releases due to the greater volatility of tellurium and the shorter half-lives of tellurium isotopes generated following fission compared to most actinide half-lives. Unlike the previous example with plutonium isotopes, which have the same chemical behaviors, chemical separation can be conducted to sharply decrease the minimum detectable activity of ^{239}Np within a sample containing high activities of radiotellurium.

Gamma Ray Spectroscopy

Gamma ray spectroscopy is commonly performed using either a NaI(Tl) scintillation counter or a high purity Ge (HPGe) semiconductor detector. Scintillating materials can be either liquid or solid. A common scintillating crystal often used is sodium iodide doped with thallium, NaI(Tl). With a high effective atomic number and high density (3.67 g/cm^3), these scintillation counters can have rather high detection efficiencies. (However, the total detection efficiency of any system is also dependent on the geometry of the source relative to the detecting medium.) Photons that interact with the crystal induce excitations and ionizations within the crystal by the photoelectric effect, Compton scattering, or pair production. Electrons liberated by these interactions release their kinetic energy in the crystal, resulting in the excitation of electrons from the valence band to the conduction band. The return of the electrons to the valence band is accompanied by the emission of electromagnetic radiation; impurities such as Tl mediate this return to the valence band so that the energy released from this transition is in the visible spectrum. Photons produced within the crystal are funneled into a photomultiplier tube (PMT), where they interact with the photocathode and cause a cascading amplification of electrons by the dynodes. The

anode receives the final amplified signal, which is proportional to the energy of the initial gamma ray [3] [4].

Semiconductor detectors are different from NaI(Tl) scintillation counters in that they can quantify the energy of photons by the number of electron-hole pairs produced in the detecting medium. The semiconducting elements used, such as silicon or germanium, have four valence electrons; doping the silicon or germanium with elements that have three or five valence electrons creates regions with an excess of holes (p-region) or excess of electrons (n-region), respectively. The detector has both an n-region and p-region, and a depletion zone in between. Applying a reverse bias to the detector, where the n-region is connected to the positive terminal and p-region to the negative terminal, generates the depletion zone, which is the sensitive region of the detector. Ionizing radiation interacts in the depletion zone to generate electron-hole pairs that are proportional in number to the energy of the incident radiation. The holes and electrons travel through the p-region and n-region, respectively, and the electrons generate an electric pulse at the read-out [3] [4].

There are several notable differences between scintillation counters and semiconductor detectors. Scintillation counters can be used to measure low-activity samples; however, they lack the high resolution of HPGe semiconductor detectors. Because of their high resolution, HPGe detectors have a greater signal-to-noise ratio, thereby reducing measurement uncertainty. Unlike scintillation counters, HPGe semiconductor detectors require cryogenic temperatures for maintenance of structural and functional integrity. The energy required to excite electrons into the conduction band of the detecting medium is only a few electron volts, thereby requiring thermal control. Additionally, HPGe detectors utilize relatively low voltages (up to 300 V) in contrast to NaI(Tl) detectors, which can require over 1000 V [3] [4].

Mass Spectrometry

Inductively coupled mass spectrometry (ICP-MS) can detect elements at concentrations on the order of parts per trillion, which is especially useful for detecting contamination by actinides in environmental samples following a nuclear event. The sample introduction system uses a nebulizer to aerosolize the sample and mix it with argon gas. The sample is dried, atomized, and ionized by the high temperature argon laser (approximately 6000 K). The ions formed typically have a charge of +1 or +2, so elements that prefer to exist as anionic species (e.g., Cl) are selected against (unless the polarity of the electromagnets is reversed). The electromagnetic field between the sample and skimmer cones draws the sample through electrostatic lenses that separate unwanted species from the sample, reducing interference. This is accomplished by having the sample continue through an opening that is not on the axis of motion; the off-axis opening also prevents photons from interfering with the detection process. The ions then enter the quadrupole electromagnet, which filters the ions by their mass-to-charge ratios. Polyatomic ions that make it through the atomization stage are selected against using a cell gas that causes them to lose most of their kinetic energy, allowing them to be removed from the analyte. The rods of the quadrupole magnet rapidly alter their voltage, causing ions with specific mass-to-charge ratios to be systematically sampled, with resolutions between $0.7 - 1.0$ amu. A cathode is struck by the ions, liberating electrons proportional to the concentration of the ions with the specified mass-to-charge ratio and generating a signal that is amplified by dynodes (similar to the PMT of the NaI(Tl) detector) [5] [6].

Using ICP-MS for environmental samples requires destruction of the samples for analysis. Although the detection limits can be sub-ppt and range nine orders of magnitude, gamma spectroscopy can detect even smaller quantities of a substance nondestructively. Coupling gamma spectroscopy with neutron activation analysis (NAA) of a sample can help with the detection of elements that may be present in even smaller concentrations.

However, NAA does have the drawbacks of matrix effects, high activities from prominent matrix components following irradiation, and the logistics of irradiating the samples at a reactor. Furthermore, actinide analysis cannot be done with NAA because of fission probabilities, and it cannot be done by gamma spectroscopy because of the very long half-lives (low activities) of most actinides, including plutonium. Thus ICP-MS would be the preferred method of analysis for actinides.

Liquid Scintillation Counting

Some radionuclides may be present in such small quantities that MS will not be sufficient. Furthermore, these radionuclides may have very poor gamma ray emissions—if any—following decay. Therefore, a method to maximize the efficiency of detecting the emission of charged particles (especially alpha and beta) is liquid scintillation counting (LSC).

Instead of placing a sample *on* a detector (2π geometry), LSC utilizes the principle of placing a sample *in* a detecting medium (4π geometry). This method maximizes the probability of radiation interacting with the 'sensitive region' of the detector. With detection efficiencies more than ten times those of gamma spectrometry, LSC is a desirable tool to measure radiation that deposits more energy within shorter distances (higher linear energy transfer, or LET).

Liquid scintillation counting is the primary method of detecting and quantifying radionuclides that have negligible gamma ray emissions following decay (e.g., ^{90}Sr and ^{3}H). However, this method requires removal of all other potential sources of radiological interference and quench, including chemical and color quench. The higher LET radiation (beta or alpha) deposits its energy within the cocktail, exciting the organic scintillating material. The energy deposited tends to result in fluorescence in the ultraviolet energy region of the electromagnetic spectrum. The presence of specific impurities within the cocktail ensures emission of electromagnetic energy from the scintillator in the visible spectrum, thereby allowing for detection by photomultiplier tubes (PMTs); this is similar to the mechanism of NaI(Tl) inorganic scintillators. The presence of undesired chemicals or colors can decrease the signal received by the PMTs

by shifting the region of interest (ROI) towards the lower end of the spectrum. The presence of additional radionuclides, neglecting the potential chemical or color quench they may cause, can result in additional counts within the ROI and, consequently, a higher reported activity or efficiency.

The LSC detector used for low-activity beta emitters in this study is the Hidex 300 SL Liquid Scintillation Counter (see Figure 1). This detector uses three PMTs surrounding the sample vial to correct for background radiation and quench. The ideal scenario following a single decay is as follows: full deposition of the particle's energy, isotropic emission of that energy in the form of visible light, and all three PMTs detecting that light. If only two PMTs detect light, then this signal is probably attenuated due to quench. The ratio of the number of instances where all three PMTs detect a signal to two PMTs detecting a signal is referred to as the triple-to-double coincidence ratio (TDCR), which is used to correct for quench. Background interferences are accounted for through subtraction and statistical reduction algorithms [7].
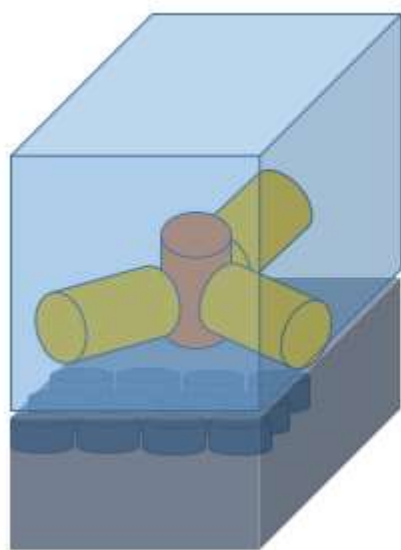
Copper-shielded measurement chamber surrounded by 3 PMTs

Sample storage tray can hold 40 20 mL vials

Figure 1: Representative diagram of the Hidex 300 SL.

Extraction Chromatography

Interference is a problem that must be minimized for detection of low-level or low-activity analytes. Interferences for gamma spectroscopy are exemplified by similar decay energies or overwhelming radioactivity from sources other than the analyte – the Compton spectrum generated by scattered photons can sufficiently drown out lower-energy signals. For mass spectroscopy, there may be spectroscopic interferences caused by matrix components with a mass-to-charge ratio similar to that of the analyte. With respect to LSC, both color and chemical quench are notorious for contributing to inaccurate results. Chromatography is an excellent tool that minimizes interference by preconcentrating and isolating the analyte based on chemical properties.

Two types of chromatography commonly used throughout the field of radiochemistry are extraction chromatography and ion exchange chromatography. Although both can use organic resins or polymers to bind the analyte, the former tends to rely on a mobile phase to alter the geometries of the central atoms of the polymers. The changes in geometry promote complexation of the polymers with tetravalent and hexavalent actinides and divalent metals, such as strontium and lead. Ion exchange chromatography, however, relies on competitive coulombic interactions between the analyte, mobile phase, and stationary phase for complete extraction. Much work has been conducted using extraction chromatography in optimizing actinide separations from various matrices [8] [9]. Ion exchange chromatography has been implemented in uranium milling and reprocessing of nuclear fuel [10] [11].

Eichrom Technologies, LLC, manufactures several types of extraction chromatography resins that are utilized in the projects that will be discussed. The stationary phase of extraction chromatography columns is made up of resins containing organic polymer extractants. The affinities of these extractants for actinides and other metals is measured by a capacity factor k'; this factor is proportional to the ratio of the volume of the stationary phase to the volume of the mobile phase that can be applied to the column (referred to as free column volumes). The equation for k' is

$$k' = D \left(\frac{v_s}{v_m} \right)$$

<div align="right">(1.1)</div>

where v_s is the volume of the stationary phase, and v_m is the volume of the mobile phase. The volume

distribution ratio D is the density of the resin multiplied by the fractional sorbed activity in a known

volume of solvent per mass of stationary phase. As the pH of the mobile phase changes, the k' of the

resin changes as well. As k' increases, the affinity of the resin to a specific ion increases. The k' value for

a specific analyte depends on the resin, acid (commonly nitric or hydrochloric), and pH.

Different extractants employ different methods of complexing ions (shown in Figure 2 below).

The use of nitric acid promotes the formation of nitrato complexes between the extractant and the

analyte for octylphenyl-N,N-di-isobutyl carbamoylphosphine oxide (CMPO) and diamyl, amylphosphonate

(DAAP). These nitrato complexes result in displacement of water molecules in the hydration spheres of

the cations. The presence of phosphonyl groups in the RE, TEVA, TRU, and UTEVA Resins from Eichrom

Technologies use this method of complexing ions. The presence of two phosphonyl groups in the Actinide

Resin makes P,P'-di(2-ethylhexyl)methanediphosphonic acid (DIPEX®) a rather potent extractant that

requires dissolution of the stationary phase for complete elution of actinides. Alternatively, crown ethers

such as 4,4'(5')-di-t-butylcyclohexano 18-crown-6 are size-specific extractants. The Sr Resin from Eichrom

Technologies uses this technology [12] [13].
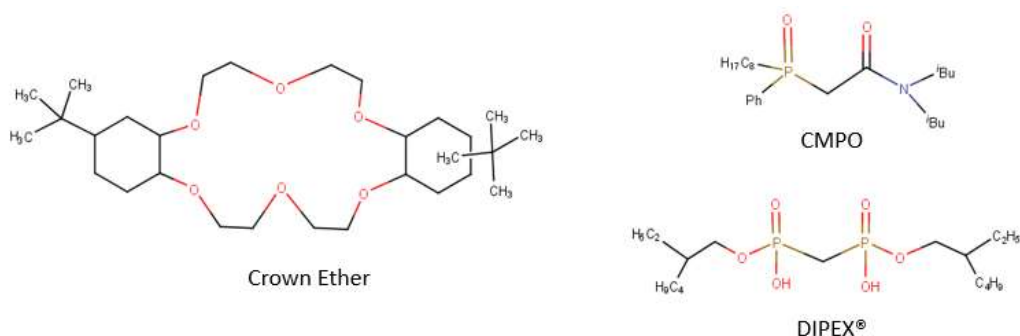
Figure 2: Extractants used in Eichrom Technologies extraction chromatography resins.

Transuranics: Production and Implications

Uranium isotopes and transuranic elements (Np, Pu, Am, Cm) are most indicative of the "state" of a reactor core in the course of a nuclear accident. As these elements exhibit the lowest volatility among those present within the fuel, these elements would be indicative of the temperatures achieved within the core [14].

The transuranic elements are produced within the core by neutron capture and consequential beta decay of uranium and the higher Z elements (see Figure 3). The probability of neutron capture depends on the nuclear properties of a given nuclide, and the successive neutron capture required for higher mass transuranics becomes increasingly less likely. Curium, americium, plutonium, and ^{237}Np all have probabilities of decaying by spontaneous fission, and undergoing fission as a result of neutron capture. When considering a sample of uranium, the probability of neutrons being captured by the same uranium atom decreases with each neutron capture as well. Therefore, the probability of detecting, for example, plutonium isotopes in the environment following a nuclear event (either reactor meltdown or nuclear weapon) is far more likely than detecting curium.
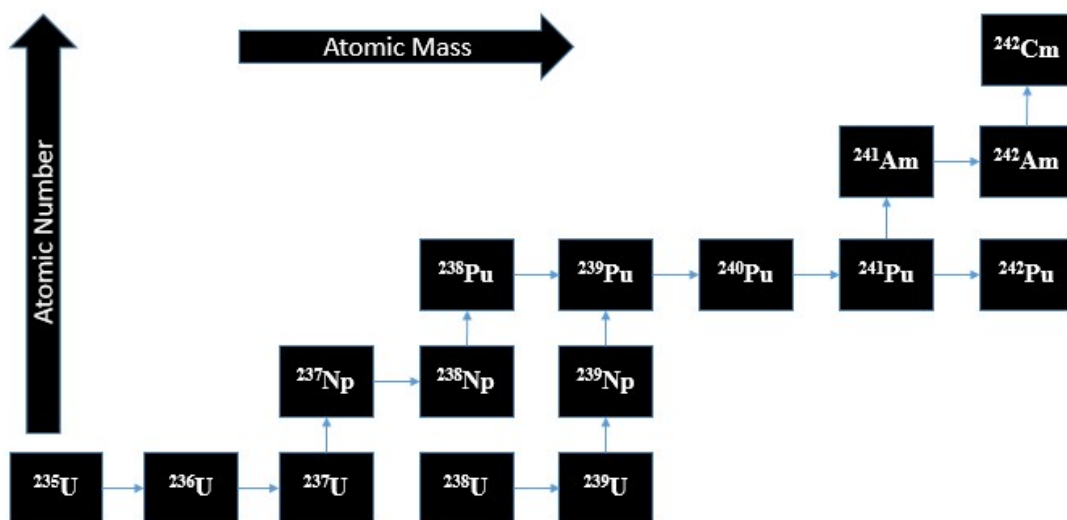
Figure 3: Generation of transuranic elements; each arrow to the right represents successful neutron capture without fission, whereas each upward arrow represents beta decay of the radionuclide.

Actinides can suggest the mechanism behind a nuclear accident as well. The nuclear power plant in Chernobyl underwent a nuclear power excursion. This is indicated by the significant quantities of actinides released [15]. The sudden heat from fission resulted in flash vaporization of the coolant and rupturing of the containment vessels. The graphite moderators were consequently exposed to air, causing their ignition under high temperatures. The resulting fire spurred the continuous release of radionuclides for 10 days [16].

Alternatively, explosions at the Fukushima Daiichi nuclear power plant were caused by the ignition of hydrogen that was vented off from the containment vessels. Upon loss of cooling capabilities, temperatures within the core were high enough (>1170 K) to oxidize the Zr cladding with the coolant present and generate H_2 gas [17]. The H_2 was vented off into the reactor buildings, mixing with the air, to prevent rupturing of the vessels from H_2 buildup. The H_2 reacted with the O_2 in the air causing explosions in Building Units 1, 3, and 4. Building Unit 2 experienced a H_2 explosion in the condensation chamber [16]. Because these explosions were chemical in nature and did not result from reactions (chemical or physical) on the level of the fuel, actinide releases were orders of magnitude less than those in Chernobyl.

Plutonium analysis following a nuclear event requires one to distinguish 'old' Pu from 'new' Pu due to the long half-lives of the most prominent isotopes generated by either nuclear explosions or reactor accidents (^{238}Pu $T_{1/2}$ = 87.74 y; ^{239}Pu $T_{1/2}$ = 2.4×10^4 y; ^{240}Pu $T_{1/2}$ = 6563 y). Distinguishing 'old' from 'new' is accomplished by evaluating the isotopic ratios ^{240}Pu/^{239}Pu and ^{238}Pu/$^{239+240}$Pu, as done by Cagno and colleagues [2]. These ratios are measured using both mass spectrometry (sector field inductively coupled plasma (SF-ICP-MS) or accelerator (AMS)) and alpha spectrometry, thus requiring two different preparatory methods. Cagno and colleagues had to dissolve and destroy alpha spectrometry samples for analysis by either SF-ICP-MS or AMS. Laser ablation quadrupole ICP-MS was also used in this study and did not require destruction of prepared samples.

Alpha spectrometry cannot be used alone to distinguish ^{239}Pu from ^{240}Pu because the monoenergetic alpha particles that are emitted during decay are very close in energy (5.157 MeV and 5.168 MeV, respectively). Because ^{238}Pu emits an alpha particle with an energy of 5.499 MeV, this energy difference provides for enough resolution in alpha spectrometry to determine the ^{238}Pu/$^{239+240}$Pu ratio.

Movement of Contaminants

Compartment Models

The release of contaminants into the environment can be modeled using compartments, such as those represented in ICRP 43, *Principles of Monitoring for the Radiation Protection of the Population*. Compartments include groundwater, plants, animals, and humans. The flow of radionuclides between compartments is represented by differential equations that assume the flow rate from a compartment is dependent only on the total activity of a radionuclide within the compartment. These differential equations are first order: The rate of change of activity is equal to a rate constant multiplied by the total activity, which is assumed to be a function of time only.

An example of a system modeled by compartments is diagrammed in Figure 4. The source can be representative of any number of scenarios, including a reactor during the course of a nuclear event or a leaking waste drum. The activities of radionuclides within a compartment change as a function of time and are assumed independent of the activities in other compartments, properties of other compartments that would affect transfer rates, etc. The first order differential equations that would represent, for example, the soil and plants compartments are, respectively:

$$\frac{dC_G}{dt} = \lambda_1 C_S + \lambda_3 C_A - \lambda_4 C_G - \lambda_5 C_G \qquad (1.2)$$

$$\frac{dC_P}{dt} = \lambda_5 C_G \qquad (1.3)$$

where C represents the activity of a contaminant within each compartment and λ represents the rate constant for transfer between compartments. The value of λ is dependent on the effective half-life (T_E) of a contaminant within the compartment and is equal to:

$$\lambda = \frac{\ln(2)}{T_E} \tag{1.4}$$

Exposure of an individual to the radiation emitted from a single radionuclide could be from standing on the soil, near the source, surrounded by plants, inhaling aerosolized particles. The different properties of these compartments would result in varying dose contributions. For example, the dose rate for an individual standing in a semi-infinite cloud of 1 Bq·m^{-3} ^{137}Cs is 1.6×10^{-1} nSv·h^{-1}, calculated using Eq. (1.5) below [18]:

$$\dot{D}_\gamma(air) = 0.25\, E_{MeV} C \tag{1.5}$$

where $\dot{D}_\gamma(air)$ is the submersion dose rate from gammas in the cloud, E_{MeV} is the photon energy (0.662 MeV), and C is the concentration in µCi mL^{-1}. If the same concentration were to be found in the soil through infinite depth (assuming uniform density, moisture content, etc.), the dose rate to an individual standing on the surface would be 6.5×10^{-5} nSv·h^{-1}.[*] This is orders of magnitude less than the submersion dose for the same volumetric concentration. Similarly, by the inverse square law, standing 1 m away from a point source that has an activity of 1 Bq would yield a dose rate of 1.1×10^{-4} nSv·h^{-1}. This is more than standing on contaminated soil, but still far less than the dose from standing in the cloud.
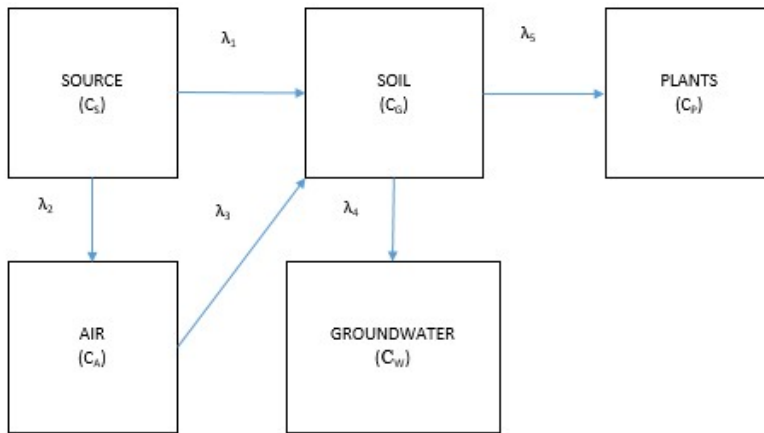
Figure 4: Example environmental transfer model, where C represents the total activity of a contaminant in each compartment and λ represents the rate constant for transfer between compartments.

---

[*] This value was obtained using effective dose coefficients for humans from [18] for ^{137m}Ba, which is the daughter of ^{137}Cs and emits the 0.662 MeV photon.

The Soil Compartment: Molecular Perspectives

Soil has many extrinsic and intrinsic variables that affect the movement of contaminants. For simplicity, only pH and soil organic matter (SOM) will be discussed in this section as they pertain to the short-lived actinide ^{239}Np and longer-lived ^{134}Cs, ^{137}Cs, and ^{90}Sr (half-lives being 2.1 y, 30.1 y, and 28.8 y, respectively). The mobility and reactivity of a radionuclide in soil depends on the soil type and the speciation of the radionuclide. Soils vary by texture (fractional composition of clay, sand, and silt) and the structural composition of the component clays. Clays can either be 1:1 in structure (e.g., kaolinites), 2:1 (e.g., micas), or combinations thereof. (The ratios refer to the organization of tetrahedral and octahedral layers, as shown in Figure 5.) The presence of SOM adds to the complexity by altering a radionuclide's mobility and its availability to both microorganisms and soil binding sites.
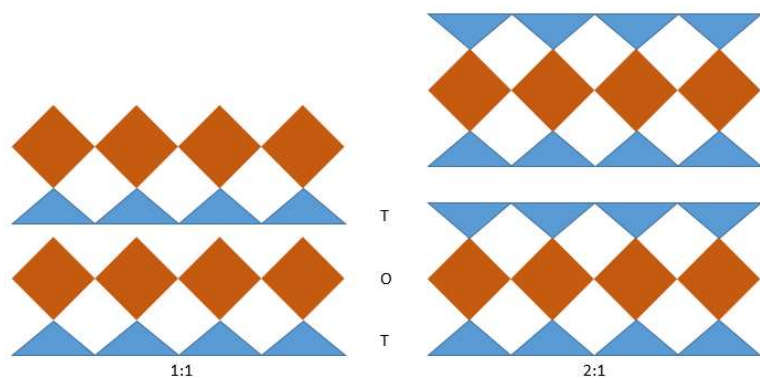
Figure 5: Diagrams of 1:1 (left) and 2:1 (right) clay structures; triangles are tetrahedral (T) layers and diamonds are octahedral (O) layers.

The speciation of a radionuclide is dependent on soil pH and the oxygen content, which is partially dependent on the hydration of the soil. For example, if soil is saturated following heavy rainfall, a reducing environment is created, resulting in changes in oxidation states and potentially solubility and reactivity. Although the causes and effects of variations in reducing potential (pe) will not be extensively discussed here, the relationship between pe and pH should be identified. As the soil pH decreases, a substance is more easily oxidized. This is especially important for actinides, which tend to exhibit multiple oxidation states, thereby impacting their speciation, solubility, and mobility.

Cesium is a relatively simple contaminant. It has been shown to behave like an alkali metal in its solubility and preferred oxidation state (+1) [19] [20]. Its ionic size and radius ratio with oxygen, however, do allow it to undergo isomorphic substitution with Rb^+, Ba^{2+}, and K^+ that are bound in minerals with coordination number 12 (cuboctahedron) geometry [21]. By extended X-ray absorption fine structure spectroscopy (EXAFS), the Cs – O bond distances have been measured between 3.2 Å and 4.3 Å. The shorter distance has been associated with outer-sphere complexes, in which the Cs ion is still hydrated. The longer distance has been associated with less mobile inner-sphere complexes with siloxane groups either at frayed edge sites or within the interlayer (see Figure 6) [19].
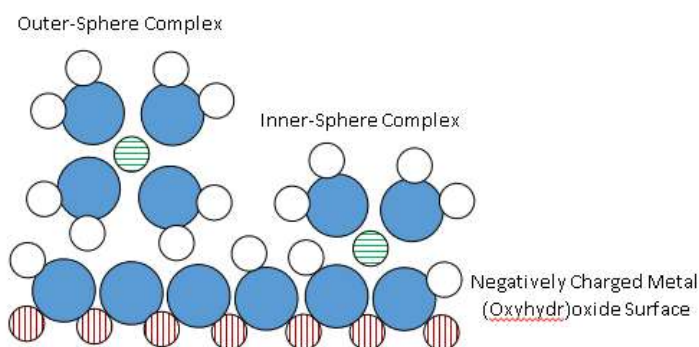
Figure 6: Complexation between metal ions (horizontal green stripes) and clay surfaces. White spheres represent hydrogen, blue spheres represent oxygen, and spheres with vertical red stripes represent metals within the clay.

The trapping of Cs in interlayer sites by heating or desiccation can result in significant retardation of the leaching of Cs [20] [21]. Rosso and colleagues discuss how opening the interlayer of muscovite promotes the diffusion of K out of the interlayer space and consequent diffusion of Cs into the interlayer and the dehydration of the Cs ion, collapsing the interlayer. The stronger the negative charge of the interlayer, the more favorable the exchange [20]. Coleman and colleagues, however, identify K^+ and NH_4^+ ions as effective Cs^+ ion exchangers for montmorillonite, illite, kaolinite, and vermiculite [22].

Strontium has an observed coordination number 8 and can therefore undergo isomorphic substitution with Rb^+, Ba^{2+}, K^+, Ca^{2+}, and Na^+ [21]. Strontium can undergo ion exchange with interlayer K^+, Ca^{2+}, and Mg^{2+} in illite and smectite clays, although its sorption is dependent on pH. Higher pH levels

result in precipitation of $SrCO_3$ [23]. Rahnemaie and colleagues evaluated the complexation of Sr on goethite, identifying Sr as having a weaker interaction than the lighter alkaline earth metals Ca and Mg. The adsorption edge of Sr on goethite suggests outer-sphere complexation, although the nature of the complex (monodentate or bidentate) is uncertain [24]. Miller and Reitemeier show that $CaCl_2$ is 10 times more effective at leaching Sr through various soils than Na, confirming the preferential binding of Ca over Sr to soil surfaces [25].

Neptunium, like other actinides, can exist in multiple oxidation states. Its most mobile form in groundwater is identified as Np(V), with its transport rate accelerated by the presence of humic acid [26]. Reduction of Np(V) to Np(IV) is possible with Fe(II) and ascorbic acid, suggesting that excessive rainfall can reduce the mobility of Np through reductive dissolution of iron and the consequential reduction of Np. Sorption of Np(V) on goethite has been characterized as mononuclear with two oxygen atoms at 1.85 Å and five oxygen atoms at 2.51 Å, similar to dissolved NpO_2^+ in water [27]. Arai and colleagues modeled Np(V) sorption as monodentate inner-sphere and bidentate outer-sphere carbonato complexes in high pH systems (pH > 8), with its adsorption on hematite, amorphous iron oxyhydroxide, manganite, and hausmanite surfaces increasing with pH [28].

A high soil pH is associated with decreased mobility of Np, Sr, and Cs within a soil column. An increase in the pH has been shown to promote sorption of Np(V) through carbonato inner- and outer-sphere complexes. Furthermore, a high pH would promote precipitation of Sr in the form of $SrCO_3$, resulting in a decrease in its ionic activity. Cesium, as observed in the laboratory setting alone, is easily removed from soil in very acidic conditions by cation exchange. Giannakopoulou and colleagues showed that the maximum sorption of Cs occurs around pH 8 for various soil textures due to the increased charge density of soil binding sites. However, above this pH, the sorption of Cs declines, possibly because of the formation of carbonate and hydroxide species in conjunction with the disruption of inner- and outer-sphere complexes [29] [30].

Organic matter tends to affect mobility of iodine more prominently than the mobility of Cs and Sr. Desorption of Cs by humic substances depends on the clay type; it was shown that the presence of humic substances does depress the sorption of Cs across clay types, but desorption was not observed for the 2:1 clay illite [31]. Sakamoto and colleagues found that humic substances greatly decrease the sorption of Np(V) in soil above pH 7. Below pH 7, there was very little effect on Np(V) sorption [32]. Similarly, it was found that actinides in the IV, V, and VI oxidation states, including U and Pu, are strongly complexed with humic acids such that carbonate complexes are prevented and humic acid mobility governs actinide mobility, especially at neutral or alkaline pH [33].

Remediation strategies revolve around maintaining pH levels around 7 or 8. Under these conditions, sorption is at a maximum for Cs [30] and Sr [34], and actinides would be complexed with the soil directly or through complexation with humic acids. Furthermore, slightly basic conditions would increase the charge density on clay particles and promote metal sorption by inner-sphere complexation such that the sorption would be less sensitive to ionic strength effects [35]. Due to the high cation exchange capacity of clays, the top layer (up to 5 cm) may be removed under these conditions with a large fraction of the contamination contained.

In the instance of radionuclide contamination following a nuclear accident, the kinetics of radiocesium, radiostrontium, and especially Np would be difficult to predict. As demonstrated in the laboratory setting, detectable activity of ^{131}I in a solution did not indicate that the iodine would behave as it would in molar concentrations (see Chapter 4). For such small quantities of radionuclides, especially actinides, we can assume that, if they are in a mobile form in soil, their ionic activities are equal to their concentrations. However, their kinetics may need to be promoted using stable carriers.

Applications to the Fukushima Daiichi Nuclear Accident

Although the March 2011 nuclear accident at the Fukushima Daiichi Nuclear Power Plant occurred five years ago, there are still detectable quantities of radiocesium (both ^{134}Cs and ^{137}Cs) in parts

of the exclusion zone contributing to the dose rates from soil and vegetation. In addition to these two compartments that have been exemplified earlier, there are several more compartments, including mushrooms that concentrate the cesium and wild boar that ingest the mushrooms. The lingering presence of radionuclides in the soil and vegetation can be explained by the half-lives of ^{134}Cs, ^{137}Cs, and ^{90}Sr; circulation and sequestration by the compartment model; and their behaviors in Japanese soils.

Soil type can influence mobility of radionuclides within a soil column. A soil map of Japan from 1971 indicates that most soils within 100 km of the NPP are cambisols or stagnosols [36] [37]. According to other studies that have been conducted on soils in the Fukushima prefecture, the predominant soil type seems to be fluvisol, although regosols, andosols, cambisols, and gleysols have been identified [38] [39] [40]. Uematsu and colleagues identified that the soils of most agricultural fields are andosols and gleysols (23 of their 51 samples were andosols, and 19 were gleysols) [41].

Radiocesium is retained more in soils with higher clay content. The percent clay content in soils studied by Lepage and colleagues ranged from 8-16%, and soil densities ranged from 0.7-1.3 g cm^{-3} [40]. Several soils from the Fukushima prefecture analyzed at Colorado State University have radiocesium in the top 5 cm only; other soils have radiocesium activities exponentially decreasing with depth. These findings suggest the presence of 2:1 clays such as vermiculite or montmorillonite, which contain Al, Mg, and Fe oxides [42]. Interstratified dioctahedral chlorite/montmorillonite has also been reported [42]. These types of clays could contribute to the trapping of radiocesium either in the top layer or in deeper layers.

Paddy cultivation of rice increases the mobility of Cs in soil and makes it more bioavailable. Paddy cultivation results in putrefaction, thus generating ammonia which, when dissolved in water, forms the ammonium ion. This ion is, as mentioned above, an efficient exchanger for Cs ions adsorbed on clay minerals [43]. The increased bioavailability of Cs results in its removal from soil by uptake in addition to leaching and decay. This could result in a larger contribution to ambient dose rate than estimated from

models that account for only leaching and radioactive decay. According to a study by Saito and colleagues, 71% of the external effective dose in 2011 was from ^{134}Cs and 28% from ^{137}Cs; based on half-lives alone, ^{137}Cs would be the main contributor to the external effective dose 3 years following the accident [44].

Project Scope

The set of radioanalytical studies that will be discussed will allow for evaluation of methods that enhance detection of anthropogenic radionuclides in the environment. These methods can be used on soil and aqueous matrices collected from an environmental site and processed within a laboratory setting. The first project is an in-depth analysis of soil and vegetation samples collected in June 2013 and July 2014 from the Fukushima prefecture. These samples were analyzed for radiocesium, ^{90}Sr, and tritium. Dose rates were mapped during the course of the collection; the maps presented herein are for demonstration purposes and provide inconclusive data regarding dose rates as they pertain to areal soil and vegetation. The second project demonstrates the capabilities of ion specific extraction chromatography. Although the methods used in this study are reflective of efforts to preconcentrate and isolate actinides from each other, this study evaluates the behaviors of volatile radionuclides through the extraction chromatography process. This project motivated an evaluation of the removal of radioiodine from soil by chemical methods, which exemplifies how radiologically detectable quantities of a substance may not behave kinetically as they would in molar concentrations.

2. FUKUSHIMA SAMPLE ANALYSIS

Introduction

Radiocesium concentrations and migration in soils around Japan following the 2011 Great Tohoku Earthquake have been analyzed extensively. Some of those analyses were summarized above (Chapter 1). However, the amount of information available on ^{90}Sr and ^{3}H in soils following the nuclear accident at Fukushima Daiichi NPP is not nearly as extensive. Potential reasons for this are the difficulties associated with detecting and quantifying these latter radionuclides.

Strontium is an alkaline earth metal that behaves like calcium chemically and, consequently, physiologically. The fission product ^{90}Sr is a pure beta-emitting radionuclide with a half-life of 28.8 y. Furthermore, its daughter ^{90}Y is also a beta-emitting radionuclide with a half-life of 64 h. Whereas the maximum energy of the ^{90}Sr beta particle is 0.55 MeV (0.20 MeV average energy), the maximum energy of its daughter is 2.28 MeV (0.93 MeV average energy). Within three weeks, these two radionuclides will reach secular equilibrium, effectively doubling the number of beta emissions interacting with the body. The danger associated with ^{90}Sr is its tendency to localize to the bone and cause leukemia or skeletal cancer. For safety, food products following the Fukushima Daiichi NPP accident were screened for the most prominent radionuclides: ^{134,137}Cs and ^{90}Sr [45]. Across the samples, ^{90}Sr tended to exhibit activities less than 10% of radiocesium activities [45].

Tritium is a naturally occurring radioisotope of hydrogen generated by cosmic rays, specifically fast neutrons, interacting with atmospheric nitrogen. Tritium has a half-life of 12.3 y and emits a 0.018 MeV (0.006 MeV average) beta particle in 100% of its decays to ^{3}He. The ^{3}H that exists in the natural background, in conjunction with its long half-life and low energy of decay, makes it difficult to quantify low levels of anthropogenic tritium. The generation of tritium as a ternary fission product and as a byproduct of reactor cooling has resulted in elevated background levels. The difference in mass between

[3]H and stable ^{1}H can result in kinetic isotopic effects in its transport through the environment [46] [47]. Although predominantly in the form of HTO (tritiated water), ^{3}H may be incorporated into organic compounds; this is referred to as organically bound tritium (OBT). Therefore, its complete isolation from soil and vegetation matrices involves heating samples to temperatures that induce combustion.

In June 2013 and July 2014, soil and vegetation samples were collected from unremediated locations within the Fukushima prefecture. The soil and vegetation samples collected in 2013 were analyzed for radiocesium by gamma spectroscopy, and then ^{90}Sr and ^{3}H by LSC. The soil samples collected in 2014 were analyzed for radiocesium and ^{90}Sr only. Specific activities are compared between sampling years and locations.

Sample Collection and Preparation

Soil and vegetation samples were collected at the locations outlined in Table 5 and represented in Figure 7. An AMS soil core sampler was used to collect the top 15 cm of soil in a plastic liner (15 cm length, 5.7 cm diameter) within 15 feet from the roadway. The samples were deep-frozen, then sliced into 2.5 cm segments. The vegetation samples were grab samples that were deep-frozen in Ziploc® bags.

Figure 7: Sample collection sites along the course of sampling in June 2013 and July 2014, which is tracked by smaller circles.

Radiocesium Analysis

Analytical Methods

Soil core sections were measured in a roll top counting shield detector for variable times to ascertain radiocesium content. Instead of placing samples on the detector window, the samples were placed within a corner of the chamber at one half of the detector height to minimize the potential for random coincidence and high dead time. Measurement times and masses are presented in Table 1.

Table 1: Measurement times and masses for gamma spectrometry of soil core segments collected in 2013.

Depth (cm):	0.0 – 2.5	2.5 – 5.0	5.0 – 7.5	7.5 – 10.0	10.0 – 12.5	12.5 – 15.0	Vegetation
F1-01	1198 s	3746 s	10989 s	14398 s	19369 s	21612 s	65817 s
	48.5 g	44.6 g	43.8 g	31.9 g	47.9 g	49.3 g	44.5 g
F1-04	8042 s	36000 s	35071 s	26657 s	36000 s	32446 s	60300 s
	83.1 g	80.3 g	70.3 g	77.8 g	64.2 g	91.9 g	55.0 g
F1-32	6593 s	20482 s	33551 s	27766 s	36000 s	36000 s	43992 s
	67.7 g	46.7 g	70.5 g	62.2 g	63.0 g	80.4 g	53.5 g
F1-09	9490 s	18691 s	19983 s	27404 s	30371 s	17819 s	59738 s
	35.4 g	76.6 g	79.8 g	78.1 g	77.4 g	79.8 g	95.6 g
F1-24	761 s	3722 s	6107 s	25392 s	35901 s	33141 s	2480 s
	75.9 g	64.0 g	76.1 g	60.5 g	74.8 g	62.3 g	50.3 g
F1-11	656 s	1471 s	1578 s	4614 s	13538 s	26055 s	28685 s
	52.9 g	59.8 g	71.1 g	54.6 g	65.1 g	62.4 g	64.4 g
F1-15	5060 s	1341 s	13057 s	3057 s	3972 s	36000 s	28800 s
	106.6 g	89.8 g	72.5 g	68.2 g	69.1 g	54.4 g	92.8 g
F1-19	542 s	3600 s	10773 s	22936 s	18033 s	17575 s	1250 s
	54.8 g	59.3 g	64.5 g	57.5 g	75.2 g	59.2 g	15.1 g

A multi-radionuclide calibration standard was created using sand and 2 M HCl. A 2.5 cm tall section of core tubing that was used for sampling was filled with sand, then water to saturation. After noting the mass of sand and volume of water added to the tubing, the tubing was emptied, cleaned, and refilled. The tubing was filled with an equivalent volume of 2 M HCl and 0.101 g Eckert & Ziegler multi-radionuclide standard (standard 1701-68, reference date December 1, 2013), followed by the same mass of sand used previously. This protocol prevented incomplete mixing of the multi-radionuclide standard with the sand. The efficiency curve is displayed in Figure 8.
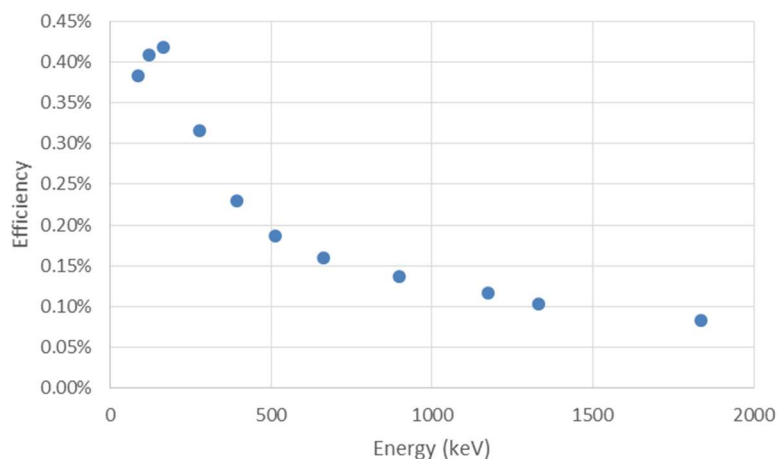
Figure 8: Efficiency curve for soil core segments situated at half detector height in the corner of a shielded detector chamber.

Vegetation samples were measured directly on the window of the detector. Aliquots of the deep-frozen samples were transferred from their respective bags and placed into separate Nalgene containers for measurement. With the exception of VegF2, which was placed in a 60 mL translucent plastic container, vegetation samples were placed in 125 mL Nalgene containers for measurement. The masses and measurement times are listed above in Table 1, and the efficiency curve for these samples is displayed in Figure 9. Since VegF2 had high levels of cesium activity, it was situated in the same geometry as the soil samples.
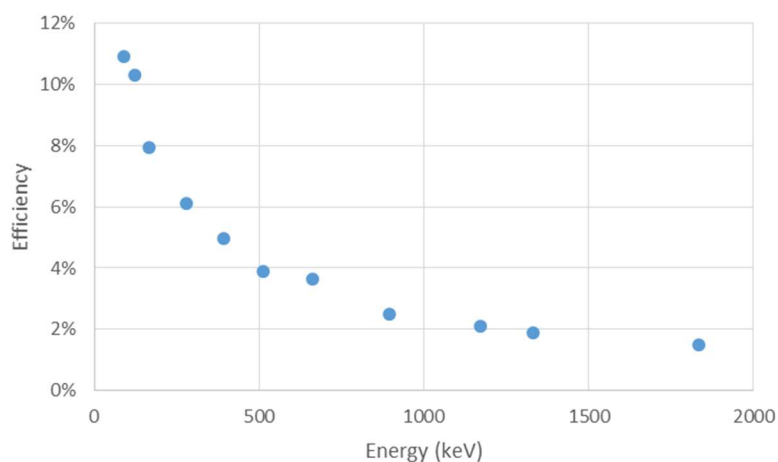
Figure 9: Efficiency curve for vegetation samples situated on the detector window inside the detector shielding.

Results and Discussion

Radiocesium tends to exhibit an exponential distribution with depth as a result of its mobility in soil [36] [38] [39] [40] [48]. The data presented in Figure 10 and Figure 11 show, respectively, ^{134}Cs and ^{137}Cs distributions at various distances from the gate of the Fukushima Daiichi Nuclear Power Plant. Activities in these figures have been time-corrected to the date of sampling (June 6, 2013). The activity of radiocesium tends to increase in lower depths for the sample collected 1 km from the gate. This trend suggests a decrease in sand content with increasing depth or a potential sink more than 5 cm below the surface. Samples collected from the gate and in Iitate Village have exponential distributions of radiocesium, although the gate sample has a surface activity in excess of a value that would be extrapolated from the other layers. The higher activity in the top layer of the soil core from the gate may be a result of loose contamination that has settled in that area.
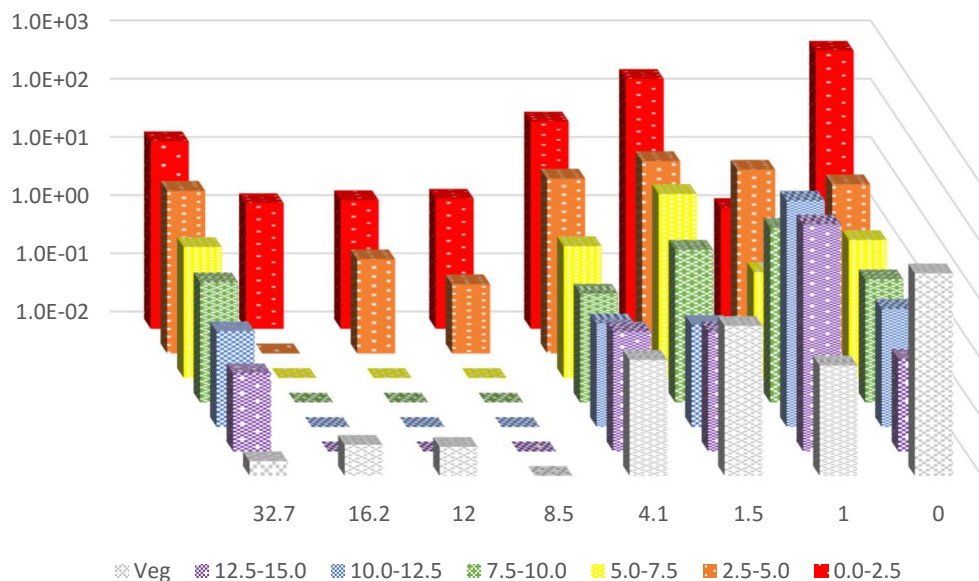
Figure 10: Specific activity of ^{134}Cs (Bq g^{-1}) in vegetation (Veg) and layers of soil (cm) at various distances from the gate of the FDNPP (0 km to 32.7 km) in 2013.
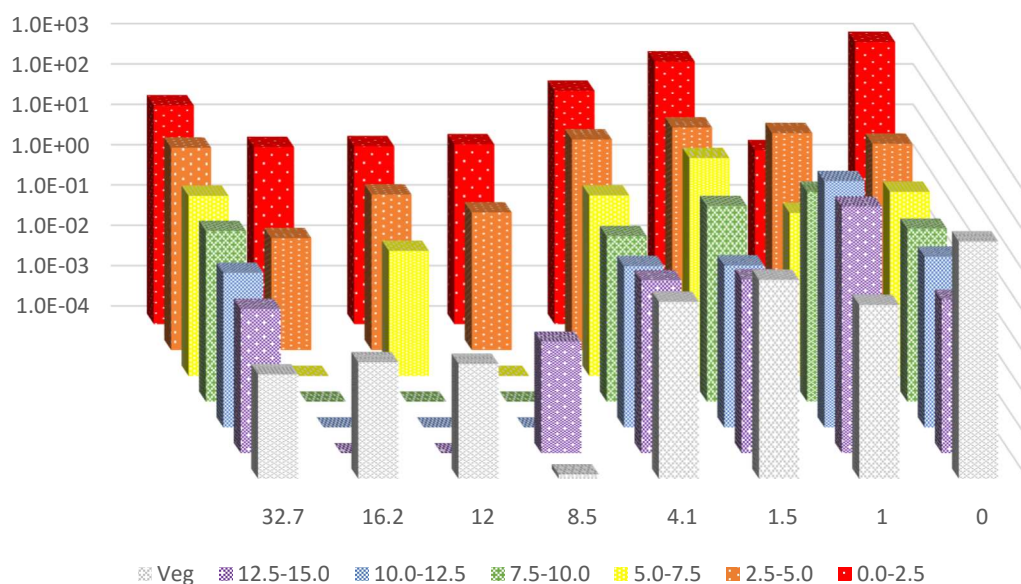
Figure 11: Specific activity of ^{137}Cs (Bq g^{-1}) in vegetation (Veg) and layers of soil (cm) at various distances from the gate of the FDNPP (0 km to 32.7 km) in 2013.

Vegetation sample activities relative to soil activities varied across the sampling sites. The specific activity of ^{134}Cs in vegetation from Iitate Village (F1-01) was well below the specific activity of ^{134}Cs in the 12.5 − 15.0 cm layer of soil. However, ^{134}Cs was not detected below the top 5 cm in Odaka Minami Soma (F1-04) and Fukushima Daini (F1-32). The presence of radiocesium in vegetation samples with specific activities similar in magnitude to some of the top layers of soil suggests the majority of the Cs detected in vegetation is from surface contamination. This could be confirmed in future samples by thoroughly cleaning the samples of any deposited radiocesium during the sample preparation phase. The specific activities of radiocesium in vegetation 4.1 km from the gate and closer are comparable to those within different layers of the soil column.

Although the vegetation activity is more than an order of magnitude lower than surface contamination levels for all sites except for F1-15, the potential for uptake should be investigated at the locations closer to the gate. The higher activities closer to the gate would propagate smaller uncertainties than those associated with activities that may approach or fall below the minimum detectable activity, as

was observed for radiocesium in several of the lower layers of soil at locations farther from the gate. The vegetation samples collected were neither characterized nor rinsed, yielding a gross count of contamination for a grab sample. Rinsing the vegetation after obtaining the gross count would yield the fraction that was incorporated into the plant tissue. This analysis could be coupled with an evaluation of the potassium content in the soil, which has been shown to affect cesium uptake in vegetation [49] [50]. Such an evaluation would provide additional information about enhancing or inhibiting radiocesium uptake by plants in that area for purposes of bioremediation or reducing the transfer of radiocesium into plant and, ultimately, animal tissues.

With few exceptions, the ^{134}Cs specific activity was consistently a factor of 2 smaller than the ^{137}Cs specific activity across the samples. If the activities are extrapolated back to the time of the accident, the $^{134/137}$Cs activity ratios were consistently under 1, with the exception of samples from Chimeiji and Odaka Minami Soma. However, all ratios were within the range of 0.907 and 1.045, as found by Komori and colleagues [51]. Based upon the ratios, and the activities of ^{134}Cs and ^{137}Cs released from each reactor, it should be possible to ascertain the extent of contamination from each reactor. To do so would require a least squares analysis based upon the assumption that the activity ratio for each reactor remained constant during the course of their releases.

Samples collected in July of 2014 were analyzed for radiocesium at The University of Tokyo.[†] The sample sites were the same as those sampled in 2013, with the exception of Iitate Village and Fukushima Daini. The results of these analyses are displayed in Figure 12 and Figure 13. Contrary to Figure 10 and Figure 11, the absence of data in these figures indicates that those layers could not be collected due to the wet terrain. Multiple samples were taken at locations, with the exception of 1 km from the gate.

[†] Samples collected in July, 2014, were analyzed for radiocesium by Katsumi Shozugawa at The University of Tokyo, Komaba. Measurements are not decay-corrected since activities calculated at the time of measurement were assumed representative of activities at the time of sampling.

These figures display the variability of the radiocesium distribution within a soil column in a single location.
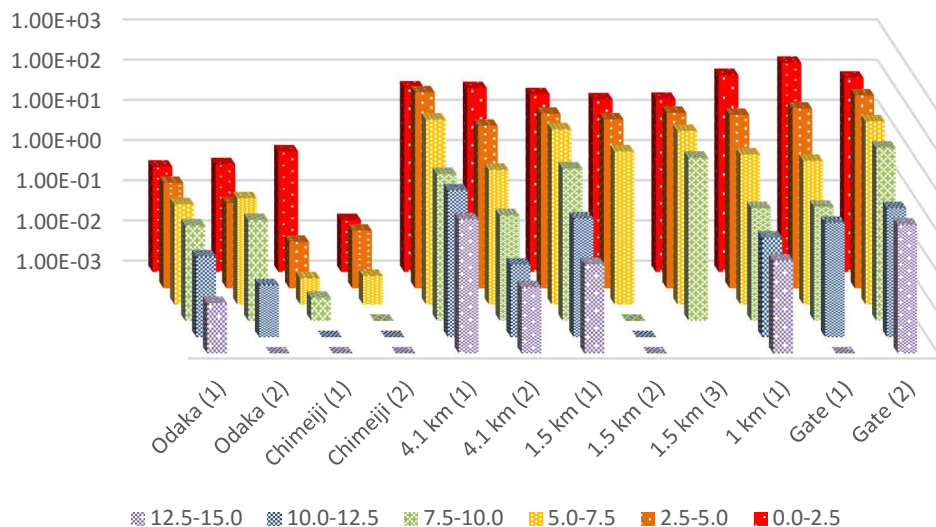
Figure 12: Specific activity (Bq g^{-1}) of ^{134}Cs in layers of soil cores (in cm) collected from Odaka Minami Soma, Chimeiji, and various distances from the gate of the NPP in 2014.
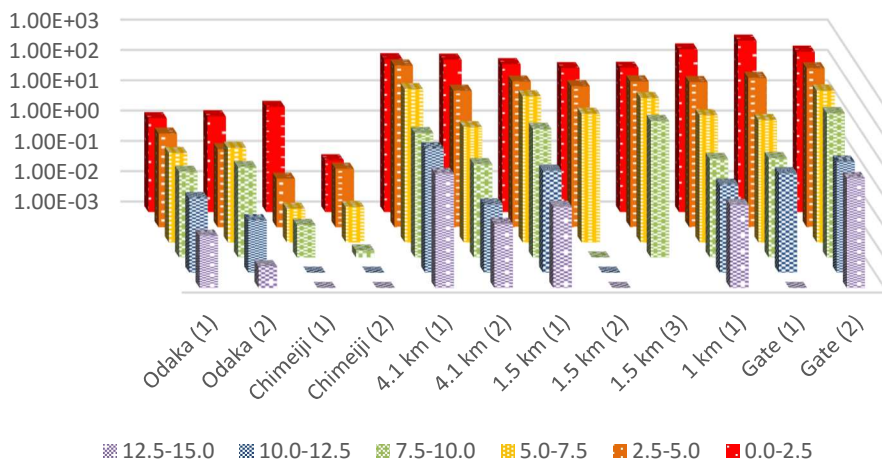
Figure 13: Specific activity (Bq g^{-1}) of ^{137}Cs in layers of soil cores (in cm) collected from Odaka Minami Soma, Chimeiji, and various distances from the gate of the NPP in 2014.

Radiocesium activities did decrease between 2013 and 2014. There are several differences, though, between samples from each year. In 2013, 6 of the 8 soil cores had more than 90% of the radiocesium activity in the top 5 cm of soil. Iitate Village and the soil 1 km from the gate had 87% and

84% of the radiocesium activity in the top 5 cm, respectively. In 2014, 5 of the 12 soil cores had more than 90% of the radiocesium activity in the top 5 cm of soil. Two of these 5 samples were a sample from the gate and a core 4.1 km from the gate. The second cores from each of these two sites had less than 70% of the activity in the top 5 cm. Since the areas sampled had not been remediated, this variation within the sites confirms the necessity of further considerations in predicting long-term behavior.

Conclusions

Although transport of radiocesium through soil is well-characterized, long-term behaviors are still difficult to predict. Micro-variations within the environment, the climate, and biota all influence the transport of ^{134,137}Cs. The samples collected from 2013 and 2014, although from the same sites, displayed different distributions. The varied distributions also held true between the samples collected in 2014.

Despite the laborious nature of collecting and slicing the soil cores, the analysis for radiocesium is rather simple and rapid. The caveat, though, is that longer analysis times are required for the minimum detectable activity to decrease.

Tritium Analysis

Analytical Methods

Aliquots of vegetation samples, the top 2.5 cm of soil samples, and the bottom 2.5 cm of soil samples were analyzed for tritium. Samples were situated in a flask inside of a Thermolyne F-A1730 benchtop muffle furnace with tubing that directed airflow through a series of traps, driven by a vacuum. The first trap, preceding the furnace, was a desiccator consisting of concentrated sulfuric acid. In line behind the furnace was a cold trap for moisture generated from drying and combustion of the samples; the cold trap was a tube submerged in a vessel of dry ice and ethanol, with dry ice added to the trap through the course of combustion to ensure temperatures within the tube were below freezing. A diagram of the setup is shown in Figure 14.

The temperature of the furnace was set to 110 °C, then increased to 440 °C. The samples were held at each temperature for 10 minutes. These temperatures were established during preliminary trials to minimize odors and coloring of the analyte in the cold trap and maintain the integrity of the setup.

After the analyte was collected, the volume was ascertained by the mass difference of the cold trap tube. The cold trap was rinsed with PerkinElmer Ultima Gold™ LLT cocktail into a plastic liquid scintillation counting vial with 18 mL cocktail. Measurements were conducted on the Hidex 300 SL Liquid Scintillation Counter (LSC) for 12 hours in triplicate with at least 8 hours of dark-adapting preceding each measurement.

Additional traps proceeded the cold trap for attempts to measure ^{14}C. An additional sulfuric acid trap was installed to minimize the flow of particulates resulting from combustion. In line behind that was a 75 mL 0.1 M NaOH trap for CO_2. This would collect any organically bound ^{14}C that was combusted. Ultima Gold (16 mL) was added to 4 mL aliquots from the NaOH trap and measured in triplicate for 12 hours. However, due to insufficient metrics to quantify the efficiency of collection and detection, preliminary results for this analyte were deemed inconclusive.
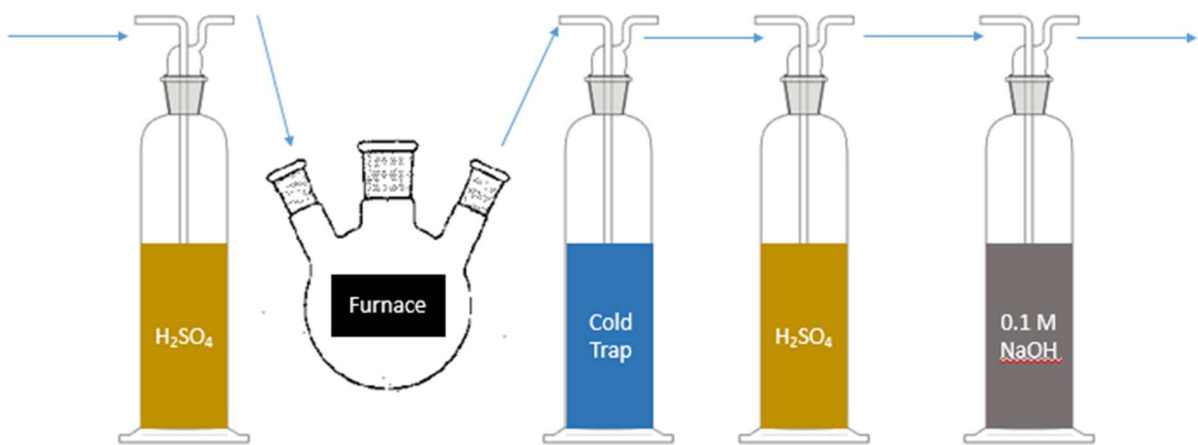
Figure 14: Schematic for sample combustion and analyte collection. Arrows indicate direction of airflow.

Calculation of tritium activity required a background tritium activity level, ambient moisture content, and extraction efficiency. A background tritium activity and moisture content was established by

executing the sample protocol in the absence of a sample. Although the purpose of the first sulfuric acid trap is to desiccate the incoming air, 0.13 mL moisture was still collected in the cold trap. A 1 mL tritium standard (Eckert & Ziegler Analytics, 86114-154; 9.308×10^3 Bq in 500 mL, reference date December 5, 2011) was then pipetted into a plastic LSC vial with 18 mL cocktail and measured for 30 minutes. The background and standard samples were used to maximize the figure of merit (FOM) and optimize the ROI using Eq. (2.1):

$$FOM = \frac{\left(\frac{CPM_s - CPM_b}{DPM_s} \times 100\right)^2}{CPM_b}$$

(2.1)

where CPM_s and CP_b refer to the counts per minute for the standard and background, respectively, and DPM_s refers to the decay-corrected activity of the standard in decays per minute. The ROI that maximized the FOM was between channels 34 and 202. The average intrinsic efficiency was calculated to be approximately 46%.

Extraction efficiency and absolute efficiency were evaluated twice using approximately 1 mL tritium standard pipetted into the flask with substrate; the flask was then subjected to the same temperatures and time durations as those of the soil and vegetation samples. The first trial was conducted using 7.94 g soil from the Colorado State University campus spiked with 0.97 g of the tritium standard. The extraction efficiency was 68%, and the absolute efficiency was 31%. The second trial was conducted using 7.12 g sand, 2.47 g dH$_2$O, and 0.99 g of the tritium standard. The extraction efficiency of this trial was 60%, and the absolute efficiency was 28%. The average extraction and absolute efficiencies were 64% and 29%, respectively.

Results and Discussion

Two noticeable trends in the tritium data are displayed in Figure 15. The top 2.5 cm of soil consistently had higher tritium activities per unit volume of water extracted than those of the bottom 2.5 cm of soil. Further investigation is required to ascertain why there is inhomogeneity in distribution within the soil column. Similarly, vegetation samples tended to have lower activity concentrations than the top

30

2.5 cm of soil. After processing vegetation samples, odors and slight yellow coloring were observed in the analytes. The presence of these odorants and colorants may have shifted the spectra for these samples to lower channels, resulting in more of the counts falling outside of the ROI. Further investigation is required to determine if quench is a contributing factor.
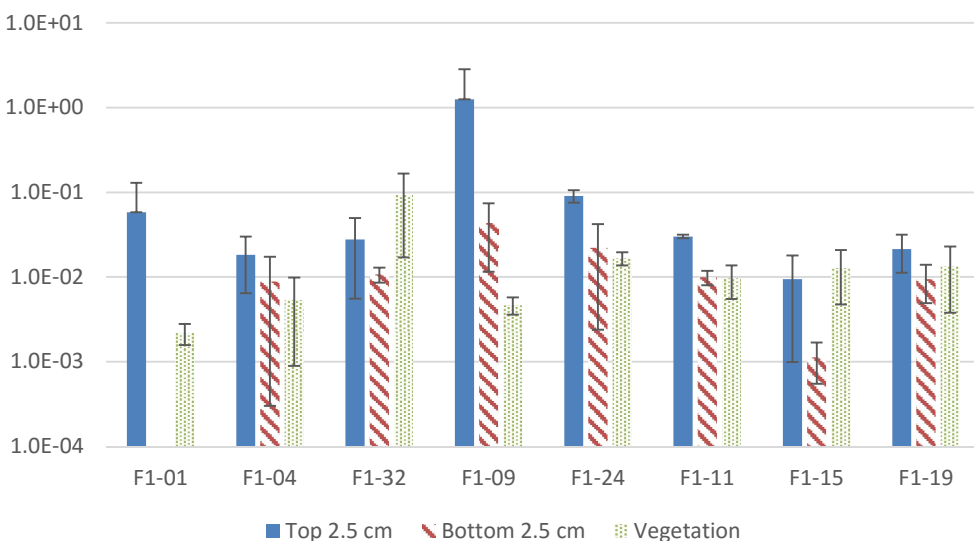
Figure 15: Specific activity (Bq mL^{-1} of collected H$_2$O) of tritium in soil and vegetation samples. Uncertainties are reported to 1 σ.

The L_C, or critical level above which there is radioactivity present with 95% certainty, was calculated to be 0.28 CPM above background (10.35 CPM) using the 0.13 mL blank sample. The top 2.5 cm of the Chimeiji soil core (1.2 ± 1.6 Bq mL^{-1}) was the only sample that had a count rate within the ROI that exceeded the L_C. However, it was one of 12 samples with count rates that declined with each successive count. It was also one of 3 samples with high count rates during the first count only; since the samples were measured for a second time within two months of the first measurement, and dark-adapted for at least 8 hours prior to measurement, the source of the high initial count rates warrants further investigation.

Although the yield was consistent for the implemented protocol, the results remain dubious. Half of the samples had decreasing consecutive counts, and three of those samples had unusually high initial

counts. Further investigation is required to determine the sources of these spikes. Potential sources are the presence of hot particles following combustion, rapid degradation of the cocktail, and rapid migration of tritium into the plastic vials. Tritium migration rates into plastic vials can be accounted for using ^{63}Ni ($T_{1/2}$ = 101.2 y); the mean energy of the beta emitted during the course of radioactive decay is 0.017 MeV. The degradation rate of cocktail, and how that degradation rate corresponds to decay energy, can be evaluated using serial dilutions of radionuclides that emit only one beta particle in each of their decay schemes. Such radionuclides may include ^{63}Ni, ^{35}S ($T_{1/2}$ = 87.4 d, 0.167 MeV mean beta energy), and ^{32}P ($T_{1/2}$ = 14.3 d, 1.711 MeV mean beta energy). These evaluations would provide a clearer picture of the source of anomalous counts and counting statistics.

Conclusions

This project has demonstrated a methodology for isolating and detecting ^{3}H in environmental matrices. Whether the environmental matrix is organic, inorganic, aqueous, or solid, tritium may be present. Since there is naturally occurring ^{3}H, detection of anthropogenic ^{3}H requires controls to be implemented to make sure luminescence reminiscent of chemical or physical interactions from the sample and system noise from the scintillation counter are minimized. The controls used in this study have failed to prove the presence of ^{3}H in the Fukushima exclusion zone in excess of background levels.

Radiostrontium Analysis

Analytical Methods

Soil and vegetation samples collected from the Fukushima exclusion zone in 2013[‡] and 2014 were analyzed for the presence of ^{90}Sr. This analysis was performed by boiling samples in reflux followed by ion specific extraction chromatography, and then counting the samples on the Hidex 300 SL Liquid Scintillation Counter. The activity distribution was assumed to be exponential through the soil column,

---

[‡] Analysis of 2013 samples was conducted and reported by Joseph E. Ball in his thesis *Deposition of Strontium-90 in Soil and Vegetation at Various Locations Surrounding the Fukushima Daiichi Nuclear Power Plant.*

similar to radiocesium; due to the expected low activities of ^{90}Sr in the soil, only the top two layers (0 cm – 2.5 cm and 2.5 cm – 5 cm) were analyzed for ^{90}Sr.

The deep-frozen samples were first dispensed into glass round-bottom flasks for massing, drying, and boiling in reflux. Samples were allowed to dry overnight at 58 °C prior to boiling. The dry masses of the aliquots are recorded in Table 2. Samples were boiled for 1 h in 8 M HNO_3 and 30% H_2O_2 using the following reagents: 4 mL 8 M HNO_3, 1 mL 1.2 mg mL^{-1} $Sr(NO_3)_2$ carrier, 1 mL 30% H_2O_2, 2 mL 16 M HNO_3. After 30 minutes of boiling, 30% H_2O_2 was added in a 1:1 ratio with 16 M HNO_3 to prevent drying of the samples and to maintain the 8 M HNO_3 concentration.

Table 2: Masses of aliquots used for ^{90}Sr analysis of soil samples collected in 2014. Information regarding samples processed in 2013 can be found in [52].

2014 Sample Masses (g)		
Depth (cm):	0.0 – 2.5	2.5 – 5.0
Odaka (1)	6.86	6.86
Odaka (2)	5.70	9.39
Chimeiji (1)	8.81	7.77
Chimeiji (2)	8.10	8.44
4.1 km (1)	1.90	5.72
4.1 km (2)	8.24	NA
1.5 km (1)	6.01	5.15
1.5 km (2)	6.25	5.29
1.5 km (3)	4.72	4.11
1 km (1)	5.11	6.49
1 km (2)	6.52	NA
Gate (1)	6.65	6.60
Gate (2)	2.59	4.09

The boiled slurry was filtered through a Büchner funnel into a vacuum flask using Carl Schleicher & Schuell Co. paper filter (no. 576). The flask was rinsed with 6 mL 8 M HNO_3 and the residue with 10 × 1 mL 8 M HNO_3 to ensure optimal yield of ^{90}Sr within the sample. The vacuum was applied to the sample for 10 minutes to maximize dryness.

The SR Resin columns were secured to the vacuum box system and primed with 10 mL H_2O followed by 7 mL 8 M HNO_3. The vacuum box system was set up in accordance with section 7.2.2 of [53]

and operated at less than 17 kPa when vacuum was applied (elution rate of approximately 1 drop per second). The filtrate was then loaded onto the resin columns and the vacuum flask rinsed with 4 × 1 mL 8 M HNO_3 to maximize yield. Complete adsorption was ensured by applying 6 × 1 mL 8 M HNO_3 to the column. An additional 10 mL 8 M HNO_3 was added to the columns without vacuum and 10 mL with vacuum for samples collected in 2014 since these samples were loaded approximately two months prior to elution.

The columns were then rinsed with 10 × 1 mL 3 M HNO_3 + 0.05 M oxalic acid solution. The k' value for actinides is high for the SR resin; oxalic acid acts as a complexing agent that prevents their retention on the column [54]. The desired eluent was 10 × 1 mL 0.01 M HNO_3 to maximize retention of Pb on the column and yield of Sr in the eluate [55].

The eluate was boiled to near dryness (less than 1 mL) 10 times, adding 1 mL autoclaved H_2O each time to prevent the flask from reaching complete dryness. The Perkin Elmer Ultima Gold™ cocktail becomes cloudy when mixed with acidic media, making its mixture with the eluate unfavorable for measurement by LSC. Driving off HNO_3 not only minimized quench, but also reduced our sample size without compromising the amount of Sr present in the sample. After boiling, the flask was rinsed with 3 × 0.5 mL autoclaved H_2O, transferring the volume to a 22 mL LSC vial by pipette each time. Approximately 18 mL of cocktail was used in each vial.

The amount of time between loading and eluting the 2014 samples was of concern and warranted investigation. Following elution of a 2014 sample column, the elution protocol was repeated on that column using 2 mL 8 M [85]Sr tracer. No detectable activity was observed in the collection tube after loading and rinsing the column. Therefore, it can be assumed that any ^{90}Sr present on the columns after the loading procedures was effectively retained until elution.

Samples were dark-adapted for more than 2 h prior to measurement to minimize residual fluorescence from mechanical or chemical stimuli. Measurements were conducted for 3 × 6000 s, with

the first measurement discarded and latter two averaged. (The first measurement allowed for adaption following mechanical disturbance.) The ROI was determined to be between channels 338 and 773 by maximizing the FOM for IAEA Standard 373 Grass (1320 mBq/g, reference date January 1, 1991) using Eq. (2.1) above. Samples were re-measured after approximately 1 year, when ^{90}Sr and its daughter ^{90}Y were in secular equilibrium.[§] A count rate that has doubled after background-subtraction would be indicative of ^{90}Sr.

The process efficiency for separation of ^{90}Sr from soil samples was established by gamma spectroscopy using a ^{85}Sr tracer. Soil samples were collected from the Colorado State University campus, spiked with 1 mL of 1 mg Sr^{2+} mL^{-1} solution (approximately 0.6 Bq µL^{-1} ^{85}Sr) and subjected to the same procedures as the Fukushima samples. The efficiency for extraction from soil matrices was determined to be 88% by gamma spectroscopy. The absolute efficiency was evaluated by spiking 1.097 g IAEA ^{90}Sr Standard 373 into soil blanks with 1.2 mg stable Sr^{2+} carrier. The sample was subjected to the separation process and allowed to reach secular equilibrium. By using this sample and a background sample generated by extracting stable Sr^{2+} carrier from a soil sample, the absolute efficiency was determined to be 66%. (The detection efficiency can be calculated by dividing the absolute efficiency by the process efficiency, yielding 75%.)

The specific activity of ^{90}Sr in a given soil sample was determined by maximizing the FOM, as performed for ^{3}H using Eq. (2.1). The optimized ROI that was associated with this FOM was found to be from channel 338 to 773. With an optimized ROI, the specific activity of the sample at the time of measurement could then be determined from the background and gross count rates (CPM_B and CPM_S, respectively) and their respective TDCR values, as shown in Eq. (2.2):

$$A = \frac{\dfrac{CPM_S}{TDCR_S} - \dfrac{CPM_B}{TDCR_B}}{2\,m\,\varepsilon} \tag{2.2}$$

[§] Secular equilibrium between ^{90}Sr and ^{90}Y can be reached after approximately 3 weeks. Data were reanalyzed after approximately 1 year for a more complete data set.

where A is the specific activity in Bq g^{-1}, m is the mass of the sample in grams, and ε is the absolute efficiency of the separation and detection process (0.66). The factor of 2 is applied in the denominator to account for the ingrowth of ^{90}Y, which would result in an effective doubling of the beta activity detected within the sample.

Results and Discussion

The specific activity of ^{90}Sr was measured in the top 5 cm of soils sampled from the Fukushima exclusion zone in 2014. The L_C for ^{90}Sr and its daughter was determined to be 1.4 CPM above background (38 CPM); all soil samples analyzed for ^{90}Sr contained radioactivity above background levels with 95% confidence. The activities were found to be no more than 93 Bq kg^{-1} in a 2.5 cm thick layer of soil, with the highest activity being in the top layer of the sample taken from the gate of the nuclear power plant. A sample collected 4.1 km from the gate had a ^{90}Sr specific activity of approximately 40 Bq kg^{-1}. However, another sample taken in the same area had approximately 16 Bq kg^{-1} ^{90}Sr. This variation in activity within a location is also observed between the two gate samples and soil samples collected 1 km from the gate (see Figure 16). Similar degrees of variation can be observed with radiocesium (Figure 12, Figure 13, and Figure 17).
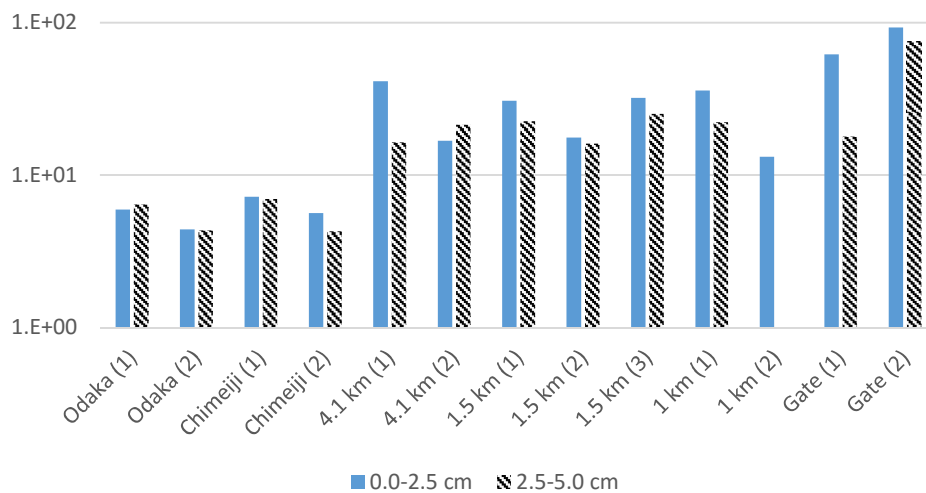
Figure 16: Specific activities (Bq kg^{-1}) of ^{90}Sr in soil cores collected from the Fukushima exclusion zone in 2014. The top 5 cm of soil were evaluated in 2.5 cm increments. Data for the 2.5-5.0 cm layer are unavailable for 1 km (2). Specific values can be found in Table 10.

The specific activity of ^{90}Sr in the top 2.5 cm of soil tended to exceed the activity in the second 2.5 cm layer of soil. This trend is observed throughout the samples with the exception of a soil sample collected in Odaka (Odaka (1)) and a soil sample collected 4.1 km from the gate (4.1 km (2)). Different specific activities within the layers are most likely due to migration within the soil column. As discussed in Chapter 1, Sr has a weaker interaction with clay surfaces than the lighter alkaline earth metals Ca and Mg. Since Sr is thought to exhibit outer-sphere complexation behavior, this type of interaction with the clay surface could justify its more rapid movement through the soil column in comparison to Cs.

Due to their half-lives, both ^{137}Cs and ^{90}Sr can be considered persistent. Their presence in the environment is attributed to fallout from nuclear weapons, releases from the meltdown of the Chernobyl nuclear power plant, and releases from other power plants. However, the difference in their specific activities in environmental matrices is a function of both physical and chemical properties. Since radiocesium is more volatile than radiostrontium, radiocesium activity releases are expected to be higher during the earlier stages of a meltdown [14]. This trend was observed in several studies, including [15], [16], [56], [57], [58], [59], [60], [61], and [62]. Furthermore, the stronger affinity for Cs on a clay matrix and its potential for being trapped within interlayers result in it being retained longer within a soil column. The presence of ^{90}Sr in the soil three years after the accident suggests that this radionuclide has become incorporated into the soil through isomorphic substitution, especially if it interacts with clay surfaces by weaker outer-sphere complexes [24].
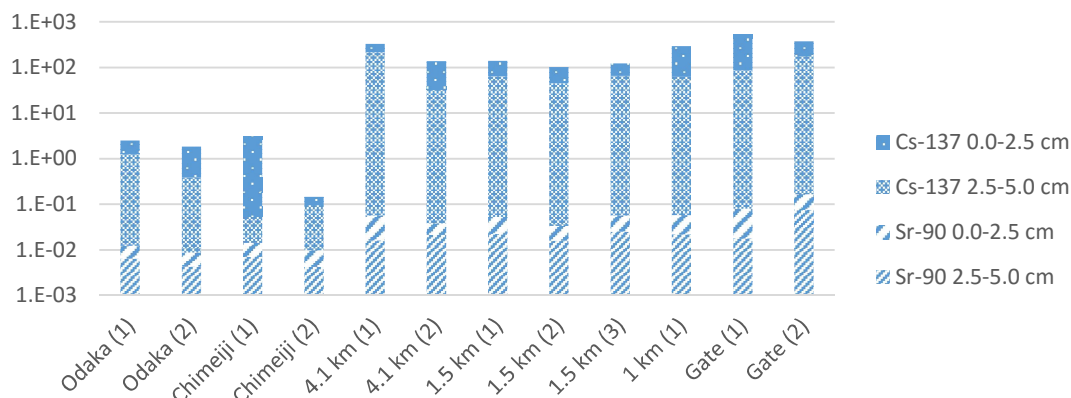
Figure 17: Specific activities (Bq g^{-1}) of ^{90}Sr and ^{137}Cs in the top 5 cm of soil samples from the Fukushima prefecture exclusion zone in 2014. Only complete data sets are shown. Specific values can be found in Table 7 and Table 10.

Conclusions

The presence of ^{90}Sr has been confirmed in soil samples from the Fukushima prefecture exclusion zone. Through acid digestion, extraction chromatography, and liquid scintillation counting, ^{90}Sr was detected and quantified.

Specific activities of ^{90}Sr reported by Ball in his analysis of soil samples collected in 2013 show a spread similar to that reported for soil samples collected in 2014. Specific activities for ^{90}Sr span one order of magnitude, with the exception of the sample from the gate, which had the highest specific activity of almost 400 Bq kg^{-1} (see Table 9). Furthermore, Ball's analysis of vegetation yielded specific activities ranging from 10 Bq kg^{-1} to 150 Bq kg^{-1}. As was addressed in the radiocesium analysis, without having washed and characterized the vegetation, the degree of surface contamination and uptake cannot be fully evaluated.

With respect to health effects, the cancer risk associated with the levels of ^{90}Sr detected in the soil samples from 2013 and 2014 can be considered negligible. The annual limit of intake for occupational exposures to ^{90}Sr is 40 µCi, which results in a committed effective dose equivalent of 5 rem. Assuming an individual ingests 100 mg soil per day (as recommended by the EPA for risk assessment), and the soil

contains 400 Bq kg^{-1} ^{90}Sr (upper limit of specific activities reported for soil samples from 2013), an individual would ingest 14.6 Bq (4×10^{-4} µCi) in one year, which would yield an annual dose of approximately 0.05 mrem. Doses from X-rays and commercial airline flights exceed this dose by orders of magnitude. Therefore, it is necessary to consider that, although anthropogenic radionuclides can be detected in trace quantities by implementing extraction techniques prior to measurement, their ubiquitous nature is not necessarily cause for alarm.

Applications to the Fukushima Exclusion Zone

The samples that have been analyzed for ^{134,137}Cs, ^{90}Sr, and ^{3}H all came from the exclusion zone in the Fukushima prefecture. Now that specific activities have been evaluated for these radionuclides, their applications to the bigger picture will be discussed. Ambient dose rates were measured during sample collection in 2013 and 2015 (2015 soil samples are not evaluated here). The dose rates were gathered from both within a vehicle and outside a vehicle, bringing to light the impact of infrastructure on dose rates.

The samples that were evaluated from 2013 and 2014 had noticeable radiocesium and radiostrontium activity. If these same locations were sampled in 2011, days and weeks following the accident, there would be much more activity in the samples, namely twice as much ^{134}Cs and substantially detectable quantities of radioiodine and radiotellurium. Fortunately, gamma analysis reports of various samples from TEPCO during this timeframe had been collected; the review of these data is enlightening, both radiologically and technologically.

Ambient Dose Rate Evaluation

The exclusion zone in the Fukushima prefecture has been undergoing constant remediation and repair. Tons of soil have been bagged and covered, and enormous amounts of debris have been consolidated. The soil and vegetation samples that have been collected and analyzed, though, are from locations that were not yet targeted by remediation efforts.

Ambient dose rates were measured in 2013 and 2015 during sampling by researchers from Colorado State University and The University of Tokyo. In 2013, two Colibri® units from Canberra Industries, Inc. attached to SVLD and STTC Canberra probes were used both within and outside of a vehicle at various heights above the ground. The dose rate from the STTC probe did not exceed 66.4 µSv (6.64 mrem) per hour in 2013 (Okuma Town, 1.5 km from the Fukushima Daiichi NPP); the highest dose rate measured by the SVLD probe did not exceed 25 µSv per hour. In 2015, a 5 cm NaI BNC SAM-940 scintillation counter coupled to a GPS unit was positioned at 1 m height above ground within a vehicle during the course of sampling. Although ambient dose rates decreased from 2013 to 2015, there are several complicating factors that prevent further conclusions from being drawn. The large degree of variation between soil types and vegetation throughout the region that was investigated only scrapes the surface. Topography and rainfall are significant contributors to the movement of radionuclides within and between compartments. Variations in data collection within and between sampling years also make these data difficult to evaluate extensively.

Figure 18: Photographs from the Fukushima exclusion zone in 2014. Top: boats and automobiles, as well as debris, were scattered across now open fields. Bottom: the top 5 cm of soil was bagged for storage.

Assuming the soil sample collected from Okuma town is representative of the soil profile of the area, the dose rate contribution from the soil 1 m above the ground can be calculated from the activities measured in the sample F1-11. The volumetric activity concentrations of ^{134}Cs and ^{137}Cs in the soil sample from Okuma Town can be calculated by dividing the total activity in each layer by the total volume of the soil column sample (5.7 cm diameter, 15 cm height). The total activity in each layer can be found by multiplying the soil activity concentrations in Table 6 by their respective soil masses in Table 1. The activity concentrations are 33.8 MBq m^{-3} ^{134}Cs and 56.2 MBq m^{-3} ^{137}Cs. These activity concentrations can be converted to dose rates using effective dose coefficients tabulated in Table 13.20 of <u>Health Physics and Radiological Health, 4th Edition</u>. The conservative assumption would be that the volumetric activity concentrations calculated above are homogeneous across the area and through the entire soil column, requiring the dose rates for infinite soil depth: 4.21×10^{-17} Sv m^3 Bq^{-1} s^{-1} for ^{134}Cs and 1.61×10^{-17} Sv m^3 Bq^{-1} s^{-1} for ^{137}Cs. [**] The dose rate for ^{134}Cs in an infinite depth of soil at the above calculated activity concentration is 5.13 µSv h^{-1}, and the dose rate for ^{137}Cs is 3.26 µSv h^{-1}. The total dose rate from radiocesium in the soil would therefore be 8.39 µSv h^{-1}. The maximum dose rate detected by one of two detectors in 2013 was 66.4 µSv h^{-1} (6.64 mrem h^{-1}) in Okuma Town, approximately 1 km from the Fukushima Daiichi NPP. This measurement was taken on the plot of a formerly residential property. The order of magnitude difference suggests that this measurement was taken closer to the ground than those measurements that were taken during transit, or there was a potential sink generated by the topography. Extensive conclusions are difficult to draw about the contribution of the soil to dose rates in the area.

Dose rates measured in 2015 along the same route of transit were within the range of those measurements taken in 2013 (Figure 19). These data are indicative of the retention of radiocesium within the environment and, as exemplified by soil data from 2014, that ^{137}Cs is still the major contributor to dose rates. Although ^{90}Sr is still present in the environment, its abundance and effective dose coefficients

---

[**] This is the value listed for ^{137m}Ba, which is the gamma-emitting daughter of ^{137}Cs.

for external exposure are both orders of magnitude lower than the abundance and effective dose

coefficients of radiocesium. The comparable dose rates on the road also reveal the shielding properties of

certain infrastructures. Because of the apparently lower retention of radionuclides on asphalt compared

to soil, roads provide a lower-dose-rate avenue of travel. Although higher dose rates were measured on

the road in 2013, it is important to note that the detectors were not secured within the vehicle and were

being moved to different elevations above the ground. Areas of data points clustered together can be

assumed to have been collected from ambulatory readings with heights above the ground less than 1 m,

resulting in dose rate readings greater than those from within the vehicle.

The results for ambient dose rates need to take into account the uncertainties associated with

the measurements. The maximum dose rate measured along the road in 2013 was 26 μSv h^{-1} (23 rem y^{-1}).

In 2015, the dose rates measured along the road did not exceed 23 μSv h^{-1} (20 rem y^{-1}). In both years, the

maximum dose rates were observed near Monitoring Post 7 of the Fukushima Daiichi Nuclear Power

Plant. The dose rate calculated from the maximum radiocesium activity observed within a collected

sample in 2013 is within 30% of these measured dose rates (see Table 3). The shielding provided by the

car also needs to be considered. If an effective half-life for the dose rate is to be established, several more

measurements that control for detector height, vehicular shielding, and measurement location should be

collected, with the upper limit of the sampling frequency being annually and the lower limit evaluated

after each measurement.

Table 3: Calculation of the total dose rate from external exposure to ^{134,137}Cs at the maximum specific activities (SA) observed within soil samples collected in 2013 (F1-19 soil core taken at the gate). The effective dose coefficient is for contamination to a depth of 15 cm for ^{134,137}Cs and 5 cm for ^{90}Sr and ^{90}Y.

June 2013	Max SA (Bq/g)	Effective Dose Coefficient (Sv m^3 Bq^{-1} s^{-1})	Dose rate from external (rem/y)
Cs-134	90	4.21E-17	11.6
Cs-137	150	1.61E-17	7.4
Sr-90+Y-90	0.4	2.72E-21/1.74E-19	1E-5
Total			19

Figure 19: Dose rates collected from the Fukushima prefecture in 2013 (top) and 2015 (bottom) along Road 252, approximately 1 km from the gate of the NPP. Dose rates are measured in µSv h⁻¹, with the scale in increments of 17.5 µSv h⁻¹.

Following the nuclear accident on March 11, 2011, Tokyo Electric Power Company (TEPCO) conducted several surveys to ascertain activities of various radionuclides across multiple matrices. Reports were obtained for surveys conducted as early as March 19, 2011, through the end of April of that year. Additional measurements were conducted from April, 2013, through October, 2013. Monitoring posts, seawater, air filters, drainage areas, trenches, subdrains, and offices were some of the surveyed areas. Sample volumes ranged from 2.5 µL of stagnant water (basement shared pool on March 27, 2011) to 6000 L of air (exhaust filter inlets and outlets on August 7, 2013).

Activity ratios, as discussed previously for Pu, can be indicative of the source, age, and behavior of the radionuclides and their progeny. For the 312 reports that were available, the ^{134}Cs/^{137}Cs and ^{131}I/^{132}Te activity ratios were evaluated using the activities that TEPCO reported by gamma spectroscopy. The activities were back-calculated to the time of the accident. The radiocesium ratio ranged in air samples from 0.09 at the west gate of Fukushima Daiichi to 1.54 at monitoring post 1 of Fukushima Daini. The radiocesium ratio is documented to have been between 0.907 and 1.045, which is characteristic of the age of the fuel within the reactors [51]. Since ^{134}Cs is produced within a reactor by neutron capture of the stable ^{133}Cs fission product, production rates of this shorter-lived cesium isotope changed during the course of releases following March 11, thereby potentially altering the ratios at surveyed loci. For calculated ratios to indicate significantly greater quantities of ^{134}Cs than ^{137}Cs given the age of the reactor fuel may be a consequence of several factors, including interference and insufficient measurement time. Several samples, though, had detectable quantities of ^{134}Cs, but not ^{137}Cs. Given the mode of production of each radionuclide, it is difficult to justify this phenomenon without addressing how the software was used for analysis.

The ^{131}I/^{132}Te ratio, on the other hand, ranged from 0.04 to 138 for activities back-calculated to the time of the accident. If a constant fission rate of reactor fuel is assumed for more than 60 days, the

ratio of the two radionuclides should be approximately 1.7 within the reactor. Within a day, ^{132}I ($T_{1/2}$ = 2.3 h) will be in transient equilibrium with its less volatile parent ^{132}Te ($T_{1/2}$ = 76.3 h). Due to their different physical and chemical properties, though, far more radioiodine will be released than radiotellurium during the initial stages of a meltdown. As temperatures within the core escalate, radiotellurium will be released in greater fractions. After the accident, Hamada and colleagues estimated a release of 1.6×10^{17} Bq of ^{131}I, and Tagami and colleagues estimated a release of 8.8×10^{16} Bq of ^{132}Te [63] [64]. The ratio calculated from these activities is 1.82. The span in the ratios calculated from TEPCO data must be discussed.

The reasoning for the large span in ratios from the reports can be justified. The most intense photopeaks from ^{131}I and ^{132}Te are 364 keV and 228 keV, respectively. These fall within the Compton spectrum for ^{137}Cs, which could interfere with their detection. The properties of the sample matrix (especially the retention and collection efficiencies for these radionuclides), intrinsic detection efficiency of the HPGe for these photons, measurement time, and sample size should all be considered. The sample with the largest ratio was 500 mL of seawater measured for 1000 s on March 26, 2011, and the sample with the smallest ratio was a 500 L air sample measured for 500 s on March 21, 2011. Different matrices, count times, and even locations are all contributing factors. Another consideration is how well the software considered interference when correcting for the contribution of these two radionuclides in the spectra; allocating too much or too little of the counts within an ROI to another radionuclide would result in over- or under-biasing the reported activity of the interfering radionuclide. This allocation depends on which radionuclides and photopeaks were included in the software library.

A curious feature of more than 10% of the reports is the absence of ^{132}I in the presence of ^{131}I and ^{132}Te. If the parent and sister isotopes of ^{132}I are detected, and ^{132}I is in equilibrium with its parent, ^{132}I should be in the sample matrix. The inability to detect ^{132}I is in the nature of the algorithms of the software. If the ^{132}I activity is less than the minimum detectable activity for the given efficiency

calibration, measurement time, and photon energies, then it should still be assumed present with an activity that approaches that of its parent ^{132}Te.

Conclusions

The radionuclides that were addressed in this section were analyzed in the order presented. Gamma spectroscopy allowed for nondestructive and rapid screening for radiocesium content in both plant and soil samples. The presence of other gamma-emitting radionuclides could be determined with minimal interference because of how monoenergetic photons interact with the HPGe. After nondestructive analyses were conducted, the samples had to be processed differently depending on the beta-emitting radionuclide of interest: ^{3}H required isolation of all water vapor arising from heating and combustion, and ^{90}Sr required isolation from all other chemicals in the matrix, including the acid used for its separation.

Radiocesium analysis brought to light numerous considerations for environmental analysis. Although radiocesium is documented to exhibit an exponential distribution through a soil column in clays, variations within a soil column can alter the flow of radiocesium within that compartment and to other compartments (e.g., vegetation) [36] [41] [48] [49] [65]. Furthermore, variations were observed between soil columns within sampling regions in 2014, sometimes by more than one order of magnitude (Figure 13).

The analysis of ^{3}H content revealed the measures that must be taken when measuring both low energy and low activity radionuclides using a low-resolution detector. As was done with both ^{3}H and ^{90}Sr, long count times and multiple counts do provide better counting statistics. Tritium measurements can be done over a long period of time without concern of the ingrowth of radioactive progeny. However, there is concern that ^{3}H can migrate into plastics, effectively decreasing the efficiency of detecting it within plastic vials like those used in this study. Further investigation is required to determine if the

consecutively decreasing count rates observed are attributed to this migration, cocktail degradation, or a combination of both.

Unlike ^{3}H, ^{90}Sr and its daughter emit high-energy beta particles and are not known to migrate into plastics. The difficulty with accurately measuring ^{90}Sr activity lies in the rapid ingrowth of its daughter ^{90}Y. Although the difference in energies between the two beta particles generate separate peaks on an LSC spectrum, the spectra for the beta particles overlap. Therefore, the simplest method for determining the activity of ^{90}Sr in a sample is to divide the net counts by two and divide by the counting efficiency for ^{90}Sr (incorporating the TDCR and separation efficiency into the calculations appropriately).

3. DETECTION OF NEPTUNIUM FOLLOWING EXTRACTION CHROMATOGRAPHY OF A HIGH ACTIVITY

MATRIX[††]

Introduction

The nuclear accidents of Chernobyl and Fukushima caused the release of large amounts of

radionuclides into the environment. Although both accidents are hardly comparable with respect to their

cause and duration as well as reactor design, safety installations, physical state of the core during and

after the accident, etc., they had in common that the main activities of their radioactive emissions were

due to radionuclides of volatile elements such as Kr, Xe, I, Cs, and Te [16]. The presence in the

environment of these radionuclides alone, therefore, does not provide much information on the nature

of a nuclear accident, including the physical state of the core, reactor vessel, containment, or release

mechanisms. Presence of nonvolatile elements such as actinides, however, provides much deeper insight

into the nature of an accident, as for example, actinide emissions (primarily plutonium) from Chernobyl

were significant, thus indicating a massive thermal destruction of the core and the release of fuel

particles [66] [67] [68] [69]. Emissions of actinides from Fukushima, in contrast, were relatively low, thus

indicating a very different type of accident [70] [71] [72] [73] [74] [75] [76] [77] [78].

After a nuclear accident, actinide analysis is therefore essential to understand the nature of the

accident and the processes inside the reactor. Actinide analysis, however, is complicated by several facts.

First, most actinides exhibit low specific activities due to their relatively long half-lives (e.g., ^{239}Pu, $T_{1/2}$ =

24,110 years; ^{240}Pu, $T_{1/2}$ = 6,563 years), thus making radiometric detection of traces more difficult.

Second, only a few relevant actinide nuclides are suitable γ-emitters. Detection by γ-spectrometry is the

fastest and most straightforward radiation detection method, especially for nondestructive assays, as it

---

[††] Results from this project have been published in [123].

requires only minimal sample preparation. For other analytical techniques such as mass spectrometry (MS) or α-spectrometry, the sample has to be treated chemically and thermally prior to separation and measurement, which sometimes introduces analytical pitfalls [79]. Third, there is a significant Pu background in the environment, caused by the releases of 8 tons of Pu (corresponding to an activity of 16 PBq) in the course of the atmospheric nuclear explosions of the 20th century [80]. Using the ^{240}Pu/^{239}Pu ratio as an isotopic signature, it is possible to distinguish between the weapons fallout (^{240}Pu/^{239}Pu ~0.18) and plutonium releases from a nuclear reactor (^{240}Pu/^{239}Pu ~0.4–0.6) [2] [81]. When α-spectrometry is applied for the determination of Pu, the discrimination of the reactor plutonium and weapons fallout plutonium via their characteristic isotopic ratio ^{240}Pu/^{239}Pu is not possible, because the α-particle energies of both nuclides cannot be resolved from each other. Plutonium analysis, therefore, usually relies on the application of MS, such as accelerator MS (AMS) or sector field inductively coupled plasma MS (SF-ICP-MS) and requires a rather laborious and time-consuming sample preparation, when compared with rapid γ-spectrometry.

To overcome this problem, ^{239}Np may be a suitable proxy for Pu in the initial assessment of the nature of a nuclear accident and may indicate fuel release into the environment. Neptunium-239 is produced by neutron capture of ^{238}U in the nuclear fuel and subsequent β$^-$-decay of the resulting ^{239}U. Neptunium-239 is a short-lived ($T_{1/2}$ = 2.356 days) γ-emitting actinide, which makes it an ideal nuclide for rapid and γ-spectrometric analysis. Because of the short half-life, there is no ^{239}Np background from global fallout in the environment, which is another important advantage. Finally, both elements Np and Pu are characterized by a similar volatility and thus^{239}Np may act as an indicator of fuel particle releases.

Analysis of ^{239}Np, however, faces one significant drawback in such a scenario: Its main γ-peak (intensity 26.3% at 106.1 keV) coincides with the γ-peak of the fission product ^{129m}Te (intensity 0.14% at 105.5 keV, $T_{1/2}$ = 33.6 days), which is usually emitted from major nuclear accident scenarios in great excess. This spectral interference has also been addressed in environmental samples after the Fukushima

accident [82]. Although not as pronounced, there is also some spectral interference of the neptunium's second-most intense γ-peak at 277.6 keV (intensity 14.4%) with a γ-photon (284.3 keV with an intensity of 6.1%) emitted by the prominent fission product ^{131}I ($T_{1/2}$ = 8.03 days).

This spectral interference calls for the separation of Np from fission products in environmental samples taken after a nuclear accident. In this study, we have screened several Np specific extraction chromatographic resins for the applicability of the attempted Np/fission product separation. Although much work has been done on the separation, isolation, and analysis of elements within the group of the actinides, separation of Np from fission products such as I, Te, and Cs by using ion specific extraction chromatography resins has not been investigated nearly as thoroughly, as they are not typically regarded as relevant interferences for actinide analysis with mass spectrometric methods and α-spectrometry [83] [84] [85] [86] [87] [88] [89] [90] [91].

The objective of this work is to establish a robust protocol for the rapid detection of ^{239}Np within aqueous and soil environmental matrices. The key of this study, however, is not only recovery of Np but also simultaneous suppression/removal of fission products, such as radioiodine, radiotellurium, and radiocesium. This scenario was accomplished through addition of commonly released volatile radionuclides to aqueous samples (simulating contaminated rainwater) and homogenized soil samples containing relatively minute, but detectable, quantities of ^{239}Np. Suppression of volatile fission products was evaluated by the yield of ^{131}I, ^{123m}Te, and ^{134}Cs through the course of the separatory procedures.

Analytical Methods

Materials and radionuclides

All chemicals used in this study were of analytical grade or higher purity. Nitric acid and hydrochloric acid were provided by Fisher Scientific, and hydrogen peroxide was purchased from Sigma-Aldrich. Radionuclides mimicking the typical mix of fission and activation products were generated by sealing into separate Suprasil quartz glass vials CsNO$_3$ (50 mg of Cs; Strem Chemicals, Newburyport, MA),

$UO_2(NO_3)_2 \cdot 6H_2O$ (20 mg of depleted U; J.T. Baker Chemical Co., Phillipsburg, NJ), and $Te(OH)_6 \cdot 2H_2O$ (30

mg of Te; Strem Chemicals, Newburyport, MA) and irradiating the vials with neutrons at the USGS TRIGA

Reactor in Denver, Colorado. Peak thermal neutron fluence rates were 4.3×10^{12} cm^{-2} s^{-1} for

$Te(OH)_6 \cdot 2H_2O$ (irradiated for 12 h and cooled for 5 days) and 1.4×10^{11} cm^{-2} s^{-1} for $CsNO_3$ and

$UO_2(NO_3)_2 \cdot 6H_2O$ (irradiated for 2 h, cooled for 48 h). Neutron activation yielded the radionuclides of

interest for this study, in particular ^{131}I, ^{123m}Te ($T_{1/2}$ = 119 days), ^{134}Cs ($T_{1/2}$ = 2.1 years), and ^{239}Np. Following

irradiation, the $CsNO_3$ sample was washed from its quartz vial using 0.5 M HNO_3 to create a 50 mL stock

solution with a concentration of 1 mg Cs mL^{-1} (7.5 mM Cs; with an initial activity concentration (A_0) of

1.32 ± 0.10 kBq mL^{-1} ^{134}Cs); the $Te(OH)_6 \cdot 2H_2O$ and $UO_2(NO_3)_2 \cdot 6H_2O$ were washed from their vials with

deionized H_2O to create 30 and 20 mL stock solutions with concentrations of 1 mg Te mL^{-1} (7.8 mM

Te; A_0 = 0.93 ± 0.12 kBq mL^{-1} ^{123m}Te) and 1 mg U mL^{-1} (4.2 mM U; A_0 = 12.44 ± 0.62 kBq mL^{-1} ^{239}Np),

respectively. The activity concentration of ^{131}I in the Te solution, after decay of the primary activation

product ^{131}Te, was 25.76 ± 0.94 kBq mL^{-1}. The radionuclides were applied in quantities that would not

only mimic the characteristic releases in the course of a nuclear accident (activities of ^{131}I > ^{129m}Te

≈ $^{134+137}$Cs > ^{239}Np) but also render the small amounts of ^{239}Np undetectable in the high background by

direct γ-spectrometric measurement of the mixture, hence requiring separation and isolation of ^{239}Np.

The chemistry of Np is highly influenced by its valence [92]; it is typically present in the

tetravalent or pentavalent form. The resin columns used in this study (Actinide-, RE-, TEVA-, TRU-, and RE-

Resins) are more selective for Np(IV) than Np(V), thereby requiring a reducing agent to reduce any Np(V)

present in the uranium solution to Np(IV) [93]. The presence of Fe(II) and ascorbic acid effectively reduces

Np(V). A 5 mg Fe(II) mL^{-1} (89.5 mM) solution was freshly prepared for every experimental series with

0.025 g of $FeSO_4 \cdot 7H_2O$ (Mallinckrodt, MO) in 10 mL of H_2O. A 1.5 M ascorbic acid (Macron Chemicals, PA)

solution was prepared by carefully heating and dissolving 13.2 g of ascorbic acid in 50 mL of H_2O.

Ion specific resins and technology

Five ion specific resins were purchased from Eichrom Technologies, LLC, and evaluated for their effectiveness in separating neptunium from volatile radionuclides released during nuclear events. The Actinide-Resin (ACT), RE-Resin, TEVA-Resin, TRU-Resin, and UTEVA-Resin have been screened for their applicability for the purpose of this study. All resins were purchased in cartridge form (2 mL) with 50–100 µm particle size. A vacuum box system was used to enhance the flow of samples through the Eichrom extraction chromatography columns. The system was set up in accordance with section 7.2.2 of [53]. Pressures within the vacuum box were maintained below 17 kPa when vacuum was applied. Prior to loading the sample solution, resins were conditioned with 5 × 1 mL (1 mL 5 times) of each respective conditioning solution to ensure homogeneity of solutions within the columns. After loading, the columns were rinsed to remove foreign substances and radionuclides. Finally, the analytes were eluted from the resin columns (see below).

Rainwater analogue preparation

Eichrom extraction chromatography columns have affinities for actinides that vary by acid type and concentration. Preconditioning, loading, rinsing, and eluting conditions for the rainwater analogues and soil are summarized in Table 4.

Table 4: Preconditioning/Loading/Rinsing and Eluting Conditions of the Ion Specific Resins Used for Recovery of ^{239}Np from Aqueous Solution (Rainwater Analogue) and Soil

Resin	Replicates	Conditioning/Loading/Rinsing	Eluting
Rainwater Analogues			
ACT	4	0.1 M HCl	10 M HCl
RE	4	8 M HNO_3	0.01 M HNO_3
RE	2	8 M HNO_3	H_2O
TRU	4	3 M HNO_3	0.1 M HNO_3
TRU	2	3 M HNO_3	H_2O
UTEVA	4	10 M HCl	0.1 M HCl
UTEVA	2	8 M HNO_3	0.1 M HNO_3
UTEVA	2	10 M HCl	H_2O
TEVA	3	2 M HNO_3	0.01 M HNO_3
TEVA	3	10 M HCl	0.1 M HCl
TEVA	3	8 M HNO_3	H_2O
Soil Matrix			
RE	2	8 M HNO_3	H_2O
UTEVA	2	8 M HNO_3	H_2O
TEVA	2	8 M HNO_3	H_2O

Natural rainwater exhibits considerable variability with respect to chemical composition and pH. It is influenced by weather phenomena [94], urbanization [95], air mass sources [96], and other factors. For the preparation of rainwater analogues, in-house deionized water (0.014 mg L^{-1} Ca^{2+}, 0.001 mg L^{-1} Cl$^-$, and each 0.0001 mg L^{-1} Mg^{2+}, Na$^+$, and K$^+$) was used, which is within 1 or 2 orders of magnitude of the composition of rainwater reported in the literature [94]. The pH of the deionized water (5.0) is within the typical range of rainwater [94]. Rainwater analogues were contaminated and made ready for loading onto the resin columns by adding, in the following order: 1.25 mL of 1.5 M ascorbic acid, 0.1 mL of 89.5 mM Fe(II) solution, 20 μL of 4.2 mM neutron-activated U, 20 mL of conditioning solution, 1 mL of 7.8 mM neutron-activated Te, and 2 mL of 7.5 mM neutron-activated Cs. Conditioning solutions were prepared from deionized water and concentrated HCl and HNO_3 stock solutions. The final concentrations of the solutes in 24.37 mL of solution were 76.9 mM ascorbic acid, 0.4 mM Fe(II), 3.4 μM U, 0.3 mM Te, and 0.6 mM Cs, the latter three being radionuclide carriers. These solutions were loaded onto their respective resin columns. The columns were then rinsed with 10 × 1 mL of conditioning solution. Additional

conditioning solution was added to bring the final volume up to 35 mL, which corresponds to the γ-spectrometry calibration geometry used. Eluents were pulled through the resin columns by vacuum into separate centrifuge tubes for collection. Eluents were applied by 10 × 1 mL. Final collected volumes were brought up to 35 mL with additional eluent (see Table 4) to ensure identical filling levels of the vial, which is important for γ-spectrometry.

Soil sample preparation

Soil from the Colorado State University campus was homogenized in a ceramic mortar to a particle size of 3 μm. The soil has a clay loam texture (28% sand, 33% silt, and 39% clay), a very high lime estimate, and a rather low organic fraction (1.5%). The 6-fold replicates of soil samples (10.0 g aliquots from the homogenized stock) were spiked with the above-mentioned stock solutions (20 μL of 4.2 mM U (^{239}Np), 2 mL of 7.5 mM Cs, 1 mL of 7.8 mM Te) and then promptly leached by boiling under reflux with a mixture of 1 mL of 30% H_2O_2, 4 mL of concentrated HNO_3(16 M), and 4 mL of 8 M $HNO_3$for 30 min. The samples were filtered through a Carl Schleicher & Schuell Co. paper filter (no. 576) using a vacuum flask and Büchner funnel. Ascorbic acid (1.25 mL, 1.5 M) and Fe(II) (0.1 mL, 89.5 mM) were added to the filtrates before loading onto the RE-, TEVA-, and UTEVA-Resin columns in duplicate (see Table 4). The columns were conditioned with 8 M HNO_3. After loading the soil extracts, the columns were rinsed with 10 × 1 mL of 8 M HNO_3. The eluent used was 10 × 1 mL of H_2O. Final eluted volumes were brought up to 35 mL for analysis by γ-spectrometry.

In preliminary trials for extraction of Np from soil, two ion specific resins (RE- and UTEVA-Resin) were used. In this case, soils were spiked with ^{239}Np (20 μL, 4.2 mM U) only and were boiled under reflux with 8 M HNO_3 in the absence of 30% H_2O_2.

Sample analysis

Final activities were determined by placing the samples on top of an ORTEC 364 cm^3 HPGe detector with a 0.76 mm Be window (2.32 keV resolution at the 1332 keV ^{60}Co peak; 87.4% relative

efficiency). Activity yields were decay-corrected to a reference time for accurate determination of the true radionuclide recovery. Samples were measured for 600 s live time in identical geometries. The Peak Locate algorithm used the Unidentified Second Differential along channels 1–4096 with a significance threshold of 3.00 and a tolerance of 1.00 keV. The Peak Area algorithm used the Sum/Nonlinear LSQ Fit with a fixed tail parameter and 4 channel continuum. For ROI (region of interest) Limits Determination, the maximum number of FWHMs (full width at half-maximum) was 5.00 between peaks, 2.00 for the left limit, and 2.00 for the right limit.

Results and Discussion

Separation from aqueous matrices

The recovery of ^{239}Np from aqueous solution and simultaneous suppression of fission products are shown in Figure 20 (uncertainties shown to 1σ). The most prominent finding that will affect the selection of conditioning/loading/rinsing and eluting solutions is not only recovery of Np but also the behavior of radiotellurium in the resin columns because ^{129m}Te will exhibit the leading spectral interference with ^{239}Np in an accident scenario. Evaluation of the ^{123m}Te (intensity of the 159 keV γ-photon is 84%) content in the eluates, resins, and loading solutions was conducted approximately 90 days following ^{239}Np isolation, after complete decay of ^{131}I and ^{239}Np.
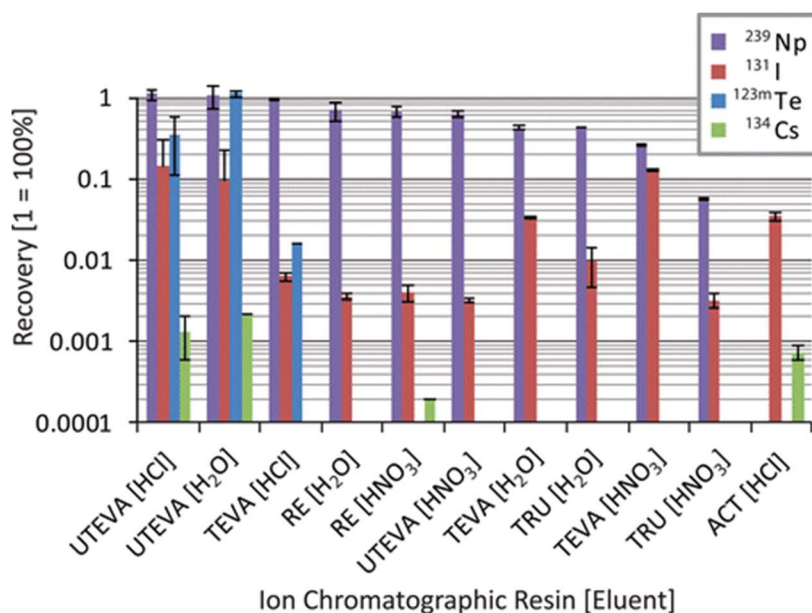
Figure 20: Recovery of ^{239}Np and associated volatile radionuclides from aqueous matrices; uncertainties are expressed to 1σ.

No detectable activity of ^{239}Np was eluted from the four replicates of the Actinide-Resin columns. According to the manufacturer, the affinity for Np on the Actinide-Resin decreases with increasing acid concentration. However, using 10 M HCl was not effective at eluting detectable quantities of ^{239}Np, resulting in effectively all of the Np being retained on the resin column (as confirmed by γ-spectrometry).

Neptunium could not be eluted in detectable amounts from two of the four replicates of the TRU-Resin columns with 0.1 M HNO$_3$. The other two replicates of the TRU-Resins using 0.1 M HNO3 as eluent yielded 5.7 ± 0.2% of the original ^{239}Np activity in the eluate (calculated using the 278 keV peak yield). Similarly, only one of the two replicates of the TRU-Resins using H$_2$O as eluent yielded detectable amounts of ^{239}Np (4.2% of the initially spiked amount). In those samples where ^{239}Np was not detected, visual analysis of the spectra suggested the presence of traces of ^{239}Np both on the column and in the eluate. However, spectral interference from prominent amounts of residual ^{131}I on the column as well as in the eluate prevented the ^{239}Np peaks from being discerned by the peak-locating algorithm used.

The RE-, TEVA-, and UTEVA-Resins exhibited the best and most consistent yield for neptunium recovery. The RE-Resins performed well in recovering ^{239}Np (yields 69.2 ± 19% for H$_2$O as eluent; 67.3 ±

11% for 0.01 M HNO$_3$ as eluent). At the same time, only 0.4 ± 0.02% ^{131}I and 0.4 ± 0.1% ^{131}I were coeluted with the ^{239}Np when H$_2$O and 0.01 M HNO$_3$ were used as eluents, respectively. Suppression of ^{123m}Te (not detectable) and ^{134}Cs worked well with RE-Resin (only minute traces of ^{134}Cs were detected in the 0.01 M HNO$_3$ eluate of one trial: 0.02%).

The TEVA-Resin is the most commonly used resin for Np separation and isolation in the literature [84] [85]. Indeed, the use of TEVA-Resin with 0.1 M HCl as eluent recovered 95.6 ± 2.7% of the initial ^{239}Np activity. However, in this experiment, the TEVA-Resin also yielded considerable amounts of ^{123m}Te (1.6 ± 0.01%) and also some ^{131}I (0.63 ± 0.07%). The use of H$_2$O or 0.01 M HNO$_3$ as eluents decreased not only the Np yield (42.1 ± 2.7% and 25.9 ± 0.001%, respectively) considerably but also diminished the separation efficiency from ^{131}I (3.3 ± 0.1% and 13.0 ± 0.4% of ^{131}I have been recovered in these trials, respectively). Both series, however, did not yield detectable ^{123m}Te in the eluate.

The manufacturer's UTEVA-Resin protocol requires elution with 0.1 M HCl. However, different eluents were also tested to seek higher yields of Np and better suppression of interfering fission products. The UTEVA-Resin seemed to have recovered all of the spiked ^{239}Np when 0.1 M HCl and H$_2$O were used for elution. Unfortunately, these trials also recovered 34 ± 24% and 100% of the ^{123m}Te, respectively, and also showed poor performance in suppressing ^{131}I (14.2 ± 15% and 9.6 ± 13%, respectively, were recovered). Also, traces of ^{134}Cs were eluted when 0.1 M HCl and H$_2$O were used as eluates. Only little ^{131}I (0.33 ± 0.02%) and no detectable ^{134}Cs and ^{123m}Te were found in the eluates when 8 M HNO$_3$ was used for conditioning/loading/rinsing and 0.1 M HNO$_3$ was used for elution. Unfortunately, however, the recovery of ^{239}Np was significantly diminished in these tests (62.8 ± 0.05%).

Separation and recovery of Np has been well investigated for these resins; however, retention of possible interfering fission products, especially radioiodine or radiotellurium, has not been studied or reported nearly as systematically. Radiocesium generally showed the lowest affinity to the resins investigated in this study. Neptunium could be separated from more than 99.9% of the radiocesium

present in the samples. In the light of the very purpose of this study, utmost exclusion of fission products (especially radiotellurium) together with a good recovery of Np, RE-Resin performed best for the rainwater analogue scenario, as it recovers a worthwhile amount of[239]Np (69%) but mostly excluded ^{131}I and [123m]Te from the eluate.

Separation from soil matrices

The RE-, TEVA-, and UTEVA-Resins were evaluated for their ability to isolate neptunium from the volatile fission products in a soil matrix. Figure 21 shows that RE- (64.8 ± 4.2%) and TEVA-Resins (53.6 ± 6.4%) had the highest yield of [239]Np, compared with the 13.9 ± 0.3% Np yield achieved by UTEVA-Resin (uncertainties shown to 1σ). The RE-Resin not only showed the highest recovery of [239]Np but also the lowest contamination with [131]I (3.9 ± 0.4%) in the eluate, compared with TEVA-Resin (4.8 ± 0.3%) and UTEVA-Resin (4.4 ± 0.3%). Again, RE-Resin outperformed the more commonly used TEVA-Resin for the very purpose of this study. No detectable [123m]Te and [134]Cs activities were observed in any of the eluates of this series (hence these were not listed in Figure 21). Furthermore, the elution of samples through TEVA-Resin columns required longer intervals of time and/or greater pressure differentials applied through the vacuum box, thereby being not as rapid as elution through the RE-Resin and potentially not as complete.
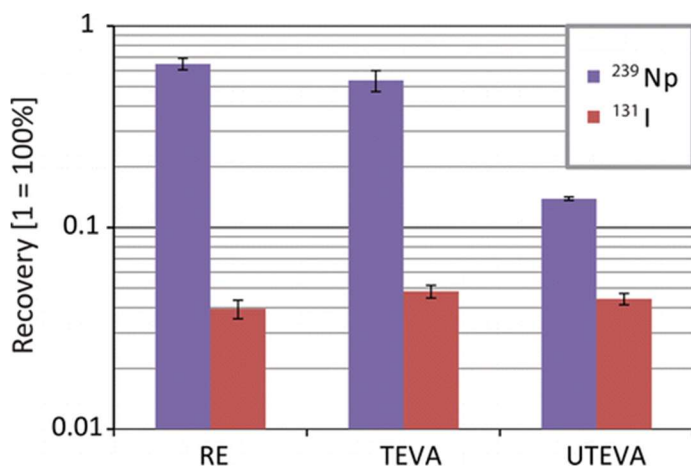
Figure 21: Recovery of [239]Np and associated volatile radionuclides from soil matrices; uncertainties are expressed to 1σ.

Separation of ^{239}Np from soil matrices was conducted by boiling samples under reflux in the presence and, in preliminary trials, absence of 30% H_2O_2. Elution of Np from the RE- and UTEVA-Resin columns with H_2O was possible only with soil samples that were refluxed with a mixture containing 30% H_2O_2. For samples refluxed in the absence of 30% H_2O_2, elution of Np from these resin columns could not be accomplished with various eluents that were supposed to either shift the pH to neutral, oxidize the Np(IV) to Np(V), or chelate the Np and thus aid its elution. The eluents used after refluxing in the absence of 30% H_2O_2 included H_2O, 0.01 M HNO_3, 30% H_2O_2, and 0.05 M oxalic acid. Removal of Np from the resin columns required dissolution of the entire stationary phase from the resin beads using acetone. However, the use of acetone cannot be recommended as a standardized protocol as it may elute any volatile radionuclides (primarily ^{131}I) remaining on the column after loading and rinsing. Apparently, the presence of H_2O_2 changes the chemistry in the soil extract during refluxing in a favorable way. We conclude that hydrogen peroxide must be used in the leaching process of soil to later effectively elute Np from the resin columns.

Conclusions

In the event of a nuclear accident, ^{239}Np detected in the environment signifies that fuel has leaked from the core elements of a reactor. Continuous monitoring of environmental samples for ^{239}Np would allow for faster and more accurate evaluations of whether or not a reactor core has emitted actinides. We present a rapid method for the isolation and detection of reactor-borne ^{239}Np using Eichrom's RE resin (Figure 22). For 25 mL of acidified rainwater, 45 min should be allotted for sample preparation, extraction chromatographic separation, and measuring each sample. Soil samples, however, would require an additional 60 min for boiling, cooling, and filtering. In our study, 600 s of γ-spectrometric measurement were sufficient to detect and quantify the radionuclides. Depending on detector efficiencies of the utilized γ-spectrometer, measurement geometry, levels of contamination, and the desired level of sensitivity, measurement time may be longer (or possibly even shorter). In addition,

chemical pretreatment for the removal of radioiodine may be required [97]. From the point of view of rapidness, the RE-Resin is also preferred as the preparation of chemicals requires the least efforts and chemical lab skills (conditioning/loading/rinsing with half-concentrated HNO_3 and elution with H_2O).

Although the TEVA- and UTEVA-Resins have also shown to be reliable in separating neptunium from volatile fission products, RE-Resin outperforms TEVA- and UTEVA-Resins when using 8 M HNO_3 as a conditioning/loading solution and H_2O as an eluent. The RE-Resin recovers a worthwhile amount of ^{239}Np in the rainwater scenario (69 ± 19%) and shows the highest yield when Np is extracted from soil (65 ± 4%). Moreover, the RE-Resin excluded ^{131}I and ^{123m}Te from the eluate to the highest degree of all resins. Therefore, the RE-Resin is favored over the TEVA-Resin (the most commonly used resin for Np separation in the literature) for the very purpose of the study, establishing a rapid method for emergency response.

Although a difference in performance is not expected, the presence of carriers (Cs, Te, and U) in this study may have a slight impact on the performance of the proposed methods when applied to real samples without any carriers. The proposed methods, of course, are only intended to act as a rapid response after a nuclear accident to answer the urgent yes-or-no question for major releases of fuel particles. Further analyses would have to be conducted in an accident scenario to establish the true quantity of actinides released.
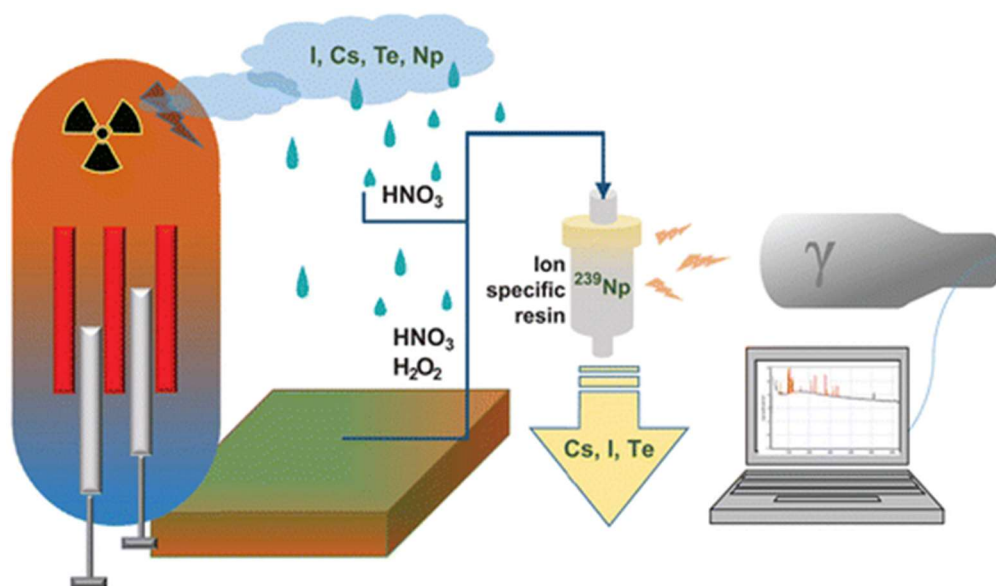
Figure 22: Graphical summary of methods.

4. REMOVAL OF RADIOIODINE FROM SOIL[‡‡]

Introduction

A great variety of radionuclides, including volatile radiocesium and radioiodine, are emitted following nuclear accidents. The Chernobyl Nuclear Power Plant (NPP) accident exhibited releases one order of magnitude greater than those of the Fukushima Daiichi NPP accident (excluding noble gases) [16]. Releases from both accidents have continued to cause global concern for health effects resulting from widespread contamination [98] [99]. Especially after the Fukushima nuclear accident, global monitoring campaigns were initiated for the tracking of radionuclides [100] [101] [102] [103] [104] [105], however, very few targeted the release of less-volatile nuclides [45] [73] [74] [76] [78] [82] [106]. Very often, the overwhelming presence of short-lived, volatile radionuclides such as ^{131}I impairs the radioanalysis of traces of bystander radionuclides [82]. In order to better analyze less volatile radionuclides in the presence of overwhelming activities of radioiodine, selective removal of ^{131}I by chemical processes may be helpful and has therefore been the objective of this study.

Radionuclide contaminations in food exhibit a severe health threat [43] [63] [107] [108] [109] [110] [111] [112] [113] [114]. There have been attempts to decrease radioiodine levels in environmental and food samples. Xu et al. have investigated a groundwater plume at the Savannah River Site contaminated with radioiodine. They found that acidic conditions result in iodination of soil organic matter (SOM), and organic-rich soils sequester a large fraction of iodine [115]. Tagami and Uchida observed negligible losses of radioiodine from tap water after boiling contaminated samples, a method recommended by the emergency-response community following the Fukushima Daiichi NPP accident [116]. Due to the decreased volume resulting from boiling, they found that the iodine was being concentrated rather than volatilized by this method. Alternatively, Mostafa et al. devised a method for

---

[‡‡] Results from this project have been published in [97].

preconcentrating, separating, and purifying radioiodine from fission products, including radiotellurium, that utilizes $AgNO_3$ as a precipitation agent for insoluble AgI [117]. Such a method yields radioiodine samples with purity sufficient for medical applications.

The goals of this study were to evaluate the potential of chemical processes for the removal of radioiodine through refluxing soil samples (thus volatilizing the ^{131}I) and the impacts of carrier, hydrogen peroxide, and silver ions (thus precipitating the ^{131}I) on the removal of radioiodine. The use of H_2O_2 was variable to identify effects of sequestration in organic soil components. The use of stable iodide carrier was also variable to evaluate if carrier behavior would promote or inhibit losses through the refluxing or precipitation processes. Radiocesium was used as a tracer for any procedural losses that may occur.

Analytical Methods

Stock Solution Preparation

The radionuclides ^{131}I and ^{134}Cs were generated by irradiation of $Te(OH)_6 \cdot 2H_2O$ (30 mg Te) and $CsNO_3$ (50 mg Cs) at the USGS TRIGA® Reactor in Denver, Colorado. Samples were brought up in 30 mL H_2O and 50 mL 0.5 M HNO_3, respectively, for the solutions to have concentrations of 1 mg cation mL^{-1}. The initial activities of the ^{131}I and ^{134}Cs stock solutions were 13.8 Bq μL^{-1} and 1.8 Bq μL^{-1}, respectively.

Stock solutions of $AgNO_3$ and NaI were produced as a precipitating agent and carrier, respectively. A stock solution with a concentration of 1 mg Ag mL^{-1} was created using 0.0787 g $AgNO_3$ in 50 mL 0.01 M HNO_3. A stock solution with a concentration of 1 mg I^- mL^{-1} was created using 0.05906 g NaI in 50 mL H_2O.

Radioiodine Removal

Several approaches for the removal of excess radioiodine from environmental soil samples were considered in this study. First, the removal of radioiodine through refluxing in 8M HNO_3 and in the presence and absence of stable iodide carrier was evaluated. Four flasks containing 5 g homogenized red soil (clay loam, 28% sand, 33% silt, 39% clay, 1.5% organic matter) from Colorado State University campus

were spiked with 1 mg Te mL^{-1} solution (200 μL). Iodide carrier solution (1 mL) was added to two of those flasks. All flasks contained ^{134}Cs (100 μL) to control for procedural losses. Water (700 μL) and concentrated HNO_3 (2 mL) were added to the flasks containing carrier to bring the HNO_3 concentration to 8 M. Water (700 μL) and concentrated HNO_3 (1 mL) were added to the flasks without carrier. Volumes were brought up to 8 mL 8 M HNO_3 with 8 M HNO_3. The flasks were refluxed for 30 minutes. The samples were filtered using a vacuum flask and Büchner funnel, with the filtrate being emptied into 50 mL polypropylene containers for measurement using γ-spectroscopy. The refluxing flask, filter, and vacuum flask were rinsed with 8 M HNO_3. The flask was rinsed with 4 × 1 mL (1 mL four times), filter with 8 × 1 mL, and vacuum flask with 3 × 1 mL. Geometry was maintained between samples by adding 8 M HNO_3 up to 35 mL total sample volume. The samples were measured for 10 minutes on the window of a Gamma Products, Inc., HPGe roll top counting shield detector.

Addition of HNO_3 to soil should be performed carefully as the carbonate fraction of soil will vigorously decompose under formation of CO_2 gas which could cause the overflow of the flask with foam. Also organic substances may react violently upon exposure to the highly oxidizing HNO_3/H_2O_2 mixture, especially when heated. The use of protective measures such as gloves and face shields is recommended [118] [119].

The next trials incorporated silver to evaluate losses by precipitation. Radioiodine from the 1 mg Te mL^{-1} stock solution (200 μL) and ^{134}Cs (100 μL) were added to six flasks containing 5 g homogenized soil. Iodide carrier (1 mL) was added to four of those flasks to evaluate the effect of carrier on precipitation. Two of the flasks containing carrier had 30% H_2O_2 (1 mL) added to assess the effects of oxidation on radioiodine losses. Concentrated HNO_3 was added to each flask to bring the concentration of HNO_3 to 8 M. Volumes of 8 M HNO_3 were added to bring solution volumes up to 7 mL. Lastly, $AgNO_3$ solution (1 mL) was added to each flask prior to refluxing for 30 minutes. After refluxing, the above

transfer and rinsing procedure was carried out. The samples were measured with identical geometry for 10 minutes.

Trials were also conducted to test the effect of hydrogen peroxide and carrier on radioiodine losses. Four flasks, each containing 5 g homogenized dirt, were spiked with radioiodine and radiocesium in quantities representative of previous trials. All four flasks were given 30% H_2O_2 (1 mL); carrier solution (1 mL) was administered to two of the flasks. The total solution volume and concentration was brought to 8 mL of 8 M HNO_3.

Two control trials were conducted with soil samples being refluxed in water. Radioiodine and radiocesium were spiked into the soils using the same volumes as before, followed by H_2O up to 8 mL total solution volume.

Results and Discussion

Effect of carrier and AgNO$_3$

According to the USGS, iodine has an average concentration of 0.75 ppm in surficial materials [1]. Therefore, the ionic activity of natural I was assumed insufficient for observing carrier effects. In order to volatilize the carrier-free ^{131}I by formation of HI Eqn. (4.1) or oxidation to I_2 Eqn. (4.2), it may be advisable to increase the amount of I present in the sample matrix by addition of an I carrier, thus promoting the kinetics of the formation of volatile species during refluxing. Figure 23 presents the results without addition of a stable I carrier; results shown in Figure 24 include the addition of a stable I carrier.

$$I^- + H^+ \rightarrow HI \uparrow \qquad\qquad (4.1)$$
$$2I^- \xrightarrow{oxidation} I_2 \uparrow + 2e^- \qquad\qquad (4.2)$$

The addition of carrier increases the removal of radioiodine during the refluxing process by 7±1%. No more than 30% of radioiodine was lost by refluxing in HNO_3 in the absence of carrier.

Similarly, silver ions did not significantly precipitate radioiodine in the absence of carrier. Silver ions in solution with carrier increased the removal of radioiodine by approximately 16±1% (Figure 24). In

samples that have very high radioiodine activities, the use of carrier and $AgNO_3$ can be used to decrease the radioiodine activity by precipitation as AgI Eq. (4.3).

$$Ag^+ + I^- \rightarrow AgI \downarrow \tag{4.3}$$

Effect of H_2O_2

Hydrogen peroxide, on the contrary, resulted in greater yield of radioiodine (less than 10% loss) in the absence of carrier. Furthermore, the presence of carrier resulted in H_2O_2 having negligible effects on ^{131}I removal when compared with refluxing in only HNO_3 in the absence of carrier. As indicated by Bray and Liebhafsky, iodide, iodine, and iodate catalytically decompose hydrogen peroxide in acidic solutions [120]. Under reflux, the fraction of hydrogen peroxide decomposed could be assumed large enough to render its oxidizing effects on organic matter negligible, thus justifying the insignificant difference in radioiodine loss between refluxing with only HNO_3 and refluxing with hydrogen peroxide and carrier (Figure 23 and Figure 24). The decomposition of hydrogen peroxide can also be observed in the insignificant radioiodine removal difference between the samples containing silver and carrier in the presence and absence of hydrogen peroxide.
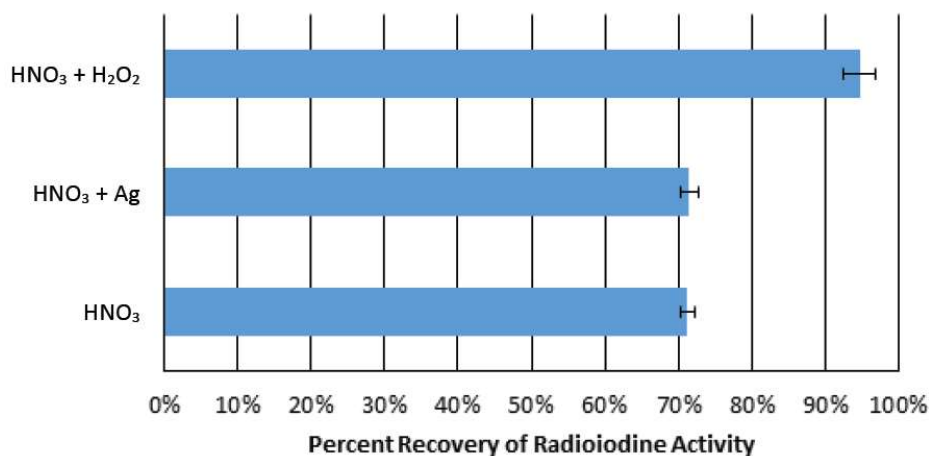
Figure 23: Radioiodine recovery in the absence of iodide carrier; refluxing was done in HNO_3 and H_2O_2; HNO_3 and $AgNO_3$; and HNO_3 only. Uncertainties are expressed to 1σ.
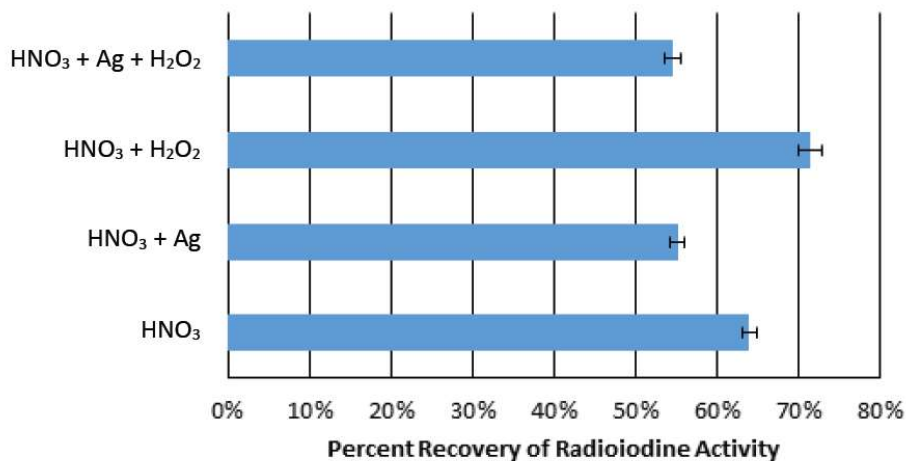
Figure 24: Radioiodine recovery in the presence of iodide carrier; refluxing was done in HNO_3, $AgNO_3$, and H_2O_2; HNO_3 and H_2O_2; HNO_3 and $AgNO_3$; and HNO_3 only. Uncertainties are expressed to 1σ.

Effect of HNO3

Refluxing radioiodine and radiocesium in water resulted in up to 80±2% recovery of radioiodine (20% removal). This finding suggests an approximate 10% removal effect through volatilization as HI Eq. (4.1) in the presence of HNO_3. However, due to the cation-exchange properties of clay within a soil sample, there was no detectable radiocesium present within the filtrate to track procedural losses; although radiocesium could not be detected in the filtrate, radioiodine could be detected in both the filter and filtrate. The presence of radioiodine in both could be attributed to retention within SOM [115]. The retention of radioiodine in SOM is supported by the increase in radioiodine yield (decrease in removal) in the presence of H_2O_2 and absence of carrier (Figure 23). The hydrogen peroxide effectively oxidized the SOM during the refluxing process, releasing any iodine retained in the organic fraction.

Conclusions

An excess of radioiodine activity in the early aftermath of a nuclear accident may thwart the analysis of bystander radionuclides that may reveal important information for accident response actions. This study shows how radioiodine can be retained in and removed from an environmental soil sample during chemical processing. The use of iodide as a carrier will facilitate loss of radioiodine from a sample.

Furthermore, the use of $AgNO_3$ as a precipitating agent is synergistic in the presence of a stable iodide carrier and appears to be less effective in the absence of carrier. However, the methods that were explored may not be sufficient for analyses that require suppression of radioiodine activity by orders of magnitude (such as the ^{239}Np isolation and detection study). Outside of extraction chromatography, radiochemical separations that remove more than 90% of radioiodine in a sample should be investigated.

Although further analysis is required, these findings also suggest the preferential degradation of hydrogen peroxide during refluxing in the presence of iodide carrier over the oxidation of SOM. Therefore, the use of carrier in processing soil samples is discouraged when evaluating organically bound radioiodine by the methods implemented in this study. Additionally, use of H_2O_2 to dissolve organic matter in a sample rich in iodine species may be less effective.

5. CONCLUSIONS

Methodologies

Detection of radionuclides in the presence of interference is important for more than health reasons. The ability to deconvolute peaks on a spectrum, for example, can reveal the radionuclides that are present and, transitively, details about their generation and transport. Fortunately, software is available to analyze spectra by subtracting out background, deconvoluting peaks, and correcting for interference. However, there may be scenarios where the algorithms behind these software programs are not as powerful as the eyes that look at the spectra. This is best demonstrated by analysis of data reported by Tokyo Electric Power Company (TEPCO) following the March, 2011, nuclear accident at Fukushima Daiichi NPP.

The projects discussed herein have demonstrated the intricacies of enhancing detection of trace quantities of radionuclides. Depending on the radiological and chemical properties of the radionuclides, some methods are more appropriate than others.

The default analytical method for any sample suspected of containing contamination from a nuclear event should be gamma spectroscopy. This nondestructive method allows for a rapid screening of radionuclides that are present and, if calibrated for a specific geometry, the activities.

Some radionuclides, such as ^{90}Sr and ^{3}H, can be present in a sample, but they are not quantifiable by gamma spectroscopy.[§§] The use of LSC is most appropriate for these radionuclides, although the time required for preparation and analysis must be considered before this method is used. Preparation is required to ensure minimal color quench and chemical quench within the cocktail. The only interference

---

[§§] In large enough quantities of beta-emitting radionuclides, bremsstrahlung may be observed on a gamma spectrum, but only photopeaks can be used to accurately assess the presence and activity of a radionuclide.

that can be corrected for systematically is background, thereby requiring potential radiochemical separations prior to analysis.

With respect to ^{90}Sr, there is one type of 'interference' that may be desirable. The ingrowth of its daughter ^{90}Y results in a doubling of beta activity within three weeks. As has been demonstrated, this doubling of activity is useful for determining the presence and activity of near-background quantities of ^{90}Sr in a sample.

Radiochemical separations may also be valuable when screening for low-activity gamma-emitting radionuclides. If a sample contains high gamma ray activity that interferes with detection, preconcentration and isolation may be more effective than larger sample sizes and longer count times. These methods may target either the desired analyte (e.g., applying ion specific extraction chromatography for ^{239}Np) or the interfering substances (e.g., boiling off ^{131}I from a sample to reduce its interference). The more effective method is strongly dependent on the physical and chemical properties of the substances in the matrix. The addition of stable carriers may be required to promote chemical kinetics.

The variations in the chemical and physical properties of environmental matrices can influence the speciation and consequential behavior of environmental contaminants and could present challenges in translating methodologies developed in a laboratory to the field. Organic matter and clay content are suspected to be the primary challenges associated with isolating radionuclides from a soil matrix. These challenges have been overcome using hydrogen peroxide and by boiling samples in 8 M HNO$_3$, respectively. Oxidation states, which are a concern for actinides, can be corrected for as well prior to the application of separation methods. Due to the relatively small ionic activities of radioactive contaminants, precipitation with agents indigenous to the environmental matrix may not present a challenge.

Characterization and migration of radionuclides through soil under controlled conditions has been conducted, for example, by Miller and Reitemeier through different well-characterized soils [25].

Such practices are essential to establishing a thorough understanding of the behavior of radionuclides in environmental matrices. Although the soils, both foreign and domestic, used in the studies herein have been uncharacterized prior to chemical processing, measures have been taken to address their variability. Well-characterized soils exposed to the same treatments as the soils from the Fukushima exclusion zone and the soils from the Colorado State University campus could be used to confirm the efficacy of the methods for these studies. Such soils can be obtained through entities like LUFA Speyer (Germany) and NIST. Upon confirmation of their efficacy, the methods that have been developed and used throughout these studies can be considered robust for isolating and detecting anthropogenic radionuclides in environmental matrices.

Lessons Learned

Environmental samples are not always representative of the system from which they were taken due to variations within a sampled region. Therefore, it is imperative to consider other factors (environmental and sampling) that can result in inconsistencies. For example, the height of the dose rate meter during the course of the measurements may not have been controlled, and topography and drainage may have induced variability in the samples within a region. Although models can be generated within a laboratory and mathematically, full characterization of a system, such as the exclusion zone in the Fukushima prefecture, requires sampling and analysis on a massive (or statistically controlled) scale. Such practices have been ongoing since the accident, and variations intrinsic and extrinsic to the sample matrices make characterization that much more difficult.

It is important for an analyst to be involved in developing the sampling plan and involved in the sample collection or production process. The collection of samples and dose rate data from the Fukushima exclusion zone, however, was conducted extemporaneously due to factors including security within the exclusion zone and analyst availability. Future sampling would require a clear scope developed by the analyst to ensure sufficient, consistent, and controlled samples and sample data are collected

across a statistically representative area. Although this can be complicated by factors outside of the analyst's control, such as access to a sampling site, the conclusions drawn from the samples would most likely be more statistically robust and provide opportunities for additional confirmatory or novel information to be shared with the scientific community. Factors for which there was no pre-determined sampling plan were sampling locations, environmental sample quality and quantity (vegetation type, soil hydration, etc.), and dose rate detector positioning within the vehicle during the course of travel. Therefore, the conclusions that have been drawn from the Fukushima exclusion zone samples should be considered confirmatory when compared to other recent studies. Unfortunately, only spurious data about the soil and vegetation are available, presenting samples and measurements of opportunity during restricted access to the site and with limited time allowed for the process.

The methods that have been developed herein can be applied following a nuclear event. Anthropogenic radionuclides released into the environment can be detected and quantified using combinations of extraction chromatography and gamma spectroscopy or liquid scintillation counting. Furthermore, these methods can reveal patterns that are characteristic of a release (e.g., relative activities of radionuclides). Since the inception of policies and remediation efforts must be expeditious, simplified and conservative assumptions can be made following radiochemical analyses by these methods in response to contamination of the environment by anthropogenic radionuclides.

6. REFERENCES

[1]   H. T. Shacklette and J. G. Boerngen, "Element Concentrations in Soils and Other Surficial Materials of the Conterminous United States," United States Government Printing Office, Washington, D.C., 1984.

[2]   S. Cagno, K. Hellemans, O. C. Lind, L. Skipperud, K. Janssens and B. Salbu, "LA-ICP-MS for Pu source identification at Mayak PA, the Urals, Russia.," *Environmental Science: Processes & Impacts,* vol. 16, no. 2, pp. 306-312, 2014.

[3]   H. Cember and T. E. Johnson, Introduction to Health Physics, Fourth Edition, New York: McGraw Hill, 2009, pp. 192-194, 639-660.

[4]   G. F. Knoll, Radiation Detection and Measurement, Fourth Edition, Hoboken: John Wiley & Sons, Inc., 2010.

[5]   "The 30-Minute Guide to ICP-MS," PerkinElmer, Inc., 2011. [Online]. Available: http://www.perkinelmer.com/PDFs/Downloads/tch_icpmsthirtyminuteguide.pdf. [Accessed 11 August 2015].

[6]   "What is ICP-MS?...and more importnatly, what can it do?," U.S. Geological Survey, 13 August 2013. [Online]. Available: http://crustal.usgs.gov/laboratories/icpms/intro.html. [Accessed 11 August 2015].

[7]   "Hidex 300 SL Liquid Scintillation Analyser," [Online]. Available: http://www.hidex.com/products.aspx. [Accessed 8 December 2015].

[8]   A. H. Thakkar, "A rapid sequential separation of actinides using Eichrom's extraction chromatographic material," *Journal of Radioanalytical and Nuclear Chemistry,* vol. 252, no. 2, p. 215, 2002.

[9]   E. P. Horwitz, "Separation and preconcentration of actinides from acidic media by extraction chromatography," *Analytica Chimica Acta ,* vol. 281, no. 2, p. 361, 1993.

[10]   C. R. Edwards and A. J. Oliver, "Uranium processing: A review of current methods and technology," *JOM,* vol. 52, no. 9, pp. 12-20, 2000.

[11]   H. Eschrich and W. Ochsenfeld, "Application of Extraction Chromatography to Nuclear Fuel Reprocessing," *Separation Science and Technology,* vol. 15, no. 4, pp. 697-732, 1980.

[12]   "Principles of extraction chromatography," Triskem, 16 10 2015. [Online]. Available: http://www.triskem-international.com/full_extraction_chromatographie.asp. [Accessed 14 12 2015].

[13] "Extraction Chromatography of actinides and Selected Fission Products: Principles and Achievement of Selectivity," Eichrom, 2015. [Online]. Available: http://www.eichrom.com/products/extraction.aspx. [Accessed 14 12 2015].

[14] T. J. McKenna and J. G. Giitter, "Source Term Estimation During Incident Response to Severe Nuclear Power Plant Accidents," U.S. Nuclear Regulatory Commission, Washington, DC, 1988.

[15] UNSCEAR, "Sources and Effects of Ionizing Radiation (annex D)," United Nations, New York, 2008.

[16] G. Steinhauser, A. Brandl and T. E. Johnson, "Comparison of the Chernobyl and Fukushima nuclear accidents: A review of the environmental impacts," *Science of The Total Environment,* Vols. 470-471, pp. 800-817, 2014.

[17] J. M. Schwantes, C. R. Orton and R. A. Clark, "Analysis of a nuclear accident: fission and activation product releases from the Fukushima Daiichi Nuclear Facility as remote indicators of source identification, extent of release, and state of damaged spent nuclear fuel," *Environmental Science & Technology,* vol. 46, pp. 8621-8627, 2012.

[18] T. E. Johnson and B. K. Birky, Health Physics and Radiological Health 4th Edition, Baltimore: Lippincott Williams & Wilkins, 2012.

[19] B. C. Bostick, M. A. Vairavamurthy, K. G. Karthikeyan and J. Chorover, "Cesium Adsorption on Clay Minerals: An EXAFS Spectroscopic Investigation," *Environmental Science & Technology,* vol. 36, no. 12, pp. 2670-2676, 2002.

[20] K. M. Rosso, J. R. Rustad and E. J. Bylaska, "The Cs/K Exchange in Muscovite Interlayers: An Ab Initio Treatment," *Clays and Clay Minerals,* vol. 49, no. 6, pp. 500-513, 2001.

[21] M. E. Essignton, Soil and Water Chemistry: An Integrative Approach, Boca Raton: CRC Press LLC, 2005.

[22] N. T. Coleman, R. J. Lewis and D. Craig, "Sorption of Cesium by Soils and Its Displacement by Salt Solutions," *Soil Science Society Proceedings,* vol. 27, pp. 287-289, 1963.

[23] C.-H. Jeong, C.-S. Kim, S.-J. Kim and S.-W. Park, "Affinity of radioactive cesium and strontium for illite and smectite clay in the presence of groundwater ions," *Journal of Environmental Science and Health Part A: Environmental Science and Engineering and Toxicology,* vol. 31, no. 9, pp. 2173-2192, 1996.

[24] R. Rahnemaie, T. Hiemstra and W. H. van Riemsdijk, "Inner- and outer-sphere complexation of ions at the goethite-solution interface," *Journal of Colloid and Interface Science,* vol. 297, no. 2, pp. 379-388, 2006.

[25] J. R. Miller and R. F. Reitemeier, "The Leaching of Radiostrontium and Radiocesium Through Soils," in *Soil Science Society Proceedings*, 1963.

[26] H. El-Naggar, M. E. El-Din and R. Sheha, "Speciation of Neptunium Migration in under Groundwater," *Journal of Radioanalytical and Nuclear Chemistry,* vol. 246, no. 3, pp. 493-504, 2000.

[27] J.-M. Combes, C. J. Chicholm-Brause, G. E. Brown, Jr., G. A. Parks, S. D. Conradson, P. G. Eller, I. R. Triay, D. E. Hobart and A. Miejer, "EXAFS Spectroscopic Study of Neptunium(V) Sorption at the a-FeOOH/Water Interface," *Environmental Science & Technology,* vol. 26, pp. 376-382, 1992.

[28] Y. Arai, P. B. Moran, B. D. Honeyman and J. A. Davis, "In Situ Spectroscopic Evidence of Neptunium(V)-Carbonate Inner-Sphere and Outer-Sphere Ternary Surface Complexes on Hematite Surfaces," *Environmental Science & Technology,* vol. 41, pp. 3940-3944, 2007.

[29] M. Gutierrez and H. R. Fuentes, "A mechanistic modeling of montmorillonite contamination by cesium sorption," *Applied Clay Science,* vol. 11, pp. 11-24, 1996.

[30] F. Giannakopoulou, C. Haidouti, A. Chronopoulou and D. Gasparatos, "Sorption behavior of cesium on various soils under different pH levels," *Journal of Hazardous Materials,* vol. 149, pp. 553-556, 2007.

[31] S. Maguire, I. D. Pulford, G. T. Cook and A. B. Mackenzie, "Cesium sorption-desorption in clay-humic acid systems," *Journal of Soil Science,* vol. 43, no. 4, pp. 689-696, 1992.

[32] Y. Sakamoto, S. Nagao, T. Ohnuki, M. Senoo, A. Ohashi, S. Sato and H. Ohashi, "Influence of Humic Acid on Sorption of Neptunium(V) onto Soil," in *MRS Proceedings*, 1994.

[33] K. Nash, S. Fried, A. M. Friedman and J. C. Sullivan, "Redox Behavior, Complexing, and Adsorption of Hexavalent Actinides by Humic Acid and Selected Clays," *Environmental Science & Technology,* vol. 15, no. 7, pp. 834-837, 1981.

[34] S. H. Wallace, S. Shaw, K. Morris, J. S. Small, A. J. Fuller and I. T. Burke, "Effect of groundwater pH and ionic strength on strontium sorption in aquifer sediments: Implicatiosn for 90Sr mobility at contaminated nuclear sites," *Applied Geochemistry,* vol. 27, no. 8, pp. 1482-1491, 2012.

[35] T. D. Small, L. A. Warren and F. G. Ferris, "Influence of ionic strenght on strontium sorption to bacteria, Fe(III) oxide, and composite bacteria-Fe(III) oxide surfaces," *Applied Geochemistry,* vol. 16, no. 7-8, pp. 939-946, 2001.

[36] N. Matsuda, S. Mikami, S. Shimoura, J. Takahashi, M. Nakano, K. Shimada, K. Uno, S. Hagiwara and K. Saito, "Depth profiles of radioactive cesium in soil using a scraper plate over a wide area surrounding the Fukushima Dai-ichi Nuclear Power Plant, Japan," *Journal of Environmental Radioactivity,* vol. 139, pp. 427-434, 2015.

[37] I. T. a. T. The Ministry of Land, "1971 MLIT 1:200,000 Land Classification Survey Soil Map," MLIT, [Online]. Available: http://nrb-www.mlit.go.jp/kokjo/tochimizu/F2/MAP/207003.jpg. [Accessed 28 December 2015].

[38] M. Honda, H. Matsuzaki, Y. Miyake, Y. Maejima, T. Yamagata and H. Nagai, "Depth profile and mobility of 129I and 137Cs in soil originating from the Fukushima Dai-ichi Nuclaer Power Plant accident," *Journal of Environmental Radioactivity,* vol. 146, pp. 35-43, 2015.

[39] A. Konoplev, V. Golosv, G. Laptev, K. Nanba, Y. Onda, T. Takase, Y. Wakiyama and K. Yoshimura, "Behavior of accidentally released radiocesium in soil-water environment: Looking at Fukushima from a Chernobyl perspective," *Journal of Environmental Radioactivity,* pp. 1-11, 2015.

[40] H. Lepage, L. Evrard, Y. Onda, I. Lefevre, P. J. Laceby and S. Ayrault, "Depth distribution of cesium-137 in paddy fields across the Fukushima pollution plume in 2013," *Journal of Environmental Radioactivity,* vol. 147, pp. 157-164, 2015.

[41] S. Uematsu, E. Smolders, L. Sweeck, J. Wannijn, M. Van Hees and H. Vandenhove, "Predicting radiocaesium sorption characteristics with soil chemical properties for Japanese soils," *Science of the Total Environment,* vol. 524, pp. 148-156, 2015.

[42] T. Sudo and S. Shimoda, Clays and Clay Minerals of Japan, 1978.

[43] S. Merz, K. Shozugawa and G. Steinhauser, "Analysis of Japanese Radionuclide Monitoring Data of Food Before and After the Fukushima Nuclear Accident," *Environmental Science & Technology,* vol. 49, pp. 2875-2885, 2015.

[44] K. Saito, I. Tanihata, M. Fujiwara, T. Saito, S. Shimoura, T. Otsuka, Y. Onda, M. Hoshi, Y. Ikeuchi, F. Takahashi, N. Kinouchi, J. Saegusa, A. Seki, H. Takemiya and T. Shibata, "Detailed deposition density maps constructed by large-scale soil sampling for gamma-ray emitting radioactive nuclides from the Fukushima Dai-ichi Nuclear Power Plant accident," *Journal of Environmental Radioactivity,* vol. 139, pp. 308-319, 2015.

[45] G. Steinhauser, V. Schauer and K. Shozugawa, "Concentration of strontium-90 at selected hot spots in Japan," *PLoS One,* vol. 8, no. 3, p. E57760, 2013.

[46] J. C. McFarlane, "Tritium fractionation in plants," *Environmental and Experimental Botany,* vol. 16, no. 1, pp. 9-14, 1976.

[47] R. Atkinson, T. Eddy, W. Kuhne, T. Jannik and A. Brandl, "Measurement of the tritium concentration in the fractionated distillate from environmental water samples," *Journal of Environmental Radioactivity,* vol. 135, pp. 113-119, 2014.

[48] D. E. Walling and Q. He, "Improved Models for Estimating Soil Erosion Rates from Cesium-137 Measurements," *Journal of Environmental Quality,* vol. 28, no. 2, pp. 611-622, 1999.

[49] E. Smolders and H. Tsukada, "The transfer of radiocesium from soil to plants: Mechanisms, data, and perspectives for potential countermeasures in Japan," *Integrated Environmental Assessment and Management,* vol. 7, no. 3, pp. 379-381, 2011.

[50] J. P. Absalom, S. D. Young, N. M. J. Crout, A. F. Nisbet, R. F. M. Woodman, E. Smolders and A. G. Gillett, "Predicting Soil to Plant Transfer of Radiocesium Using Soil Characteristics," *Environmental Sciences & Technology,* vol. 33, pp. 1218-1223, 1999.

[51] M. Komori, K. Shozugawa, M. Matsuo and N. Nogawa, "Evaluation of radioactive contamination caused by each plant of Fukushima Daiichi Nuclear Power Station using 134Cs/137Cs activity ratio as an index," *Bunseki Kagaku,* vol. 62, no. 6, pp. 475-483, 2013.

[52] J. E. Ball and G. Steinhauser, "Deposition of strontium-90 in soil and vegetation at various locations surrounding the Fukushima Daiichi nuclear power plant," DSpace, Fort Collins, 2014.

[53] Eichrom, "Americium, Neptunium, Plutonium, Throium, Curium, Uraniuum, and Strontium in Water (with Vacuum Box System)," Eichrom, 2006. [Online]. Available: http://www.eichrom.com/eichrom/radiochem/methods/eichrom/. [Accessed June 2015].

[54] Eichrom, "Sr Resin," Eichrom Technologies, LLC, [Online]. Available: http://www.eichrom.com/products/info/sr_resin.aspx. [Accessed 2015].

[55] M. Kocadag, A. Musilek and G. Steinhauser, "On the interference of 210Pb in the determination of 90Sr using a strontium specific resin," *Nuclear Technology & Radiation Protection,* vol. 28, no. 2, p. 163, 2013.

[56] V. A. Kashparov, S. M. Lundin, S. I. Zvarych, V. I. Yoschenko, S. E. Levchuk, Y. V. Khomutinin, I. M. Maloshtan and V. P. Protsak, "Territory contamination with the radionouclides representing the fuel component of Chernobyl fallout," *The Science of the Total Environment,* vol. 317, pp. 105-119, 2003.

[57] L. R. Anspaugh, R. J. Catlin and M. Goldman, "The Global Impact of the Chernobyl Reactor Accident," *Science,* vol. 242, pp. 1513-1519, 1988.

[58] M. Dreicer, A. Aarkrog, R. Alexakhin, L. Anspaugh, N. P. Arkhipov and K. J. Johansson, "Consequences of the Chernobyl accident for the natural and human environments," in *One decade after Chernobyl: summing up the consequences of the accident*, Vienna, 1996.

[59] A. Stohl, P. Seibert and G. Wotawa, "The total release of xenon-133 from the Fukushima Dai-ichi nuclear power plant accident," *Journal of Environmental Radioactivity,* vol. 112, pp. 155-159, 2012.

[60] T. Kobayashi, H. Nagai, M. Chino and H. Kawamura, "Source term estimation of atmospheric release due to the Fukushima Dai-ichi Nuclear Power Plant accident by atmospheric and oceanic dispersion simulations: Fukushima NPP Accident Related," *Journal of Nuclear Science and Technology,* vol. 50, no. 3, pp. 255-264, 2013.

[61] N. Hamada and H. Ogino, "Food safety regulations: what we learned from the Fukushima nuclear accident," *Journal of Environmental Radioactivity,* vol. 111, pp. 83-99, 2012.

[62] J. E. Ten Hoeve and M. Z. Jacobson, "Worldwide health effects of the Fukushima Daiichi nuclear accident," *Energy & Environmental Science,* vol. 5, no. 9, pp. 8743-8757, 2012.

[63] N. Hamada and H. Ogino, "Food safety regulations: what we learned from the Fukushima nuclear accident," *Journal of Environmental Radioactivity,* vol. 111, p. 83, 2012.

[64] K. Tagami, S. Uchida, N. Ishii and J. Zheng, "Estimation of Te-132 distribution in Fukushima Prefecture at the early stage of the Fukushima Daiichi nuclear power plant reactor failures," *Environmental Science & Technology,* vol. 47, no. 10, pp. 5007-5012, 2013.

[65] S. Fujimara, Y. Muramatsu, T. Ohno, M. Saitou, Y. Suzuki, T. Kobayashi, K. Yoshioka and Y. Ueda, "Accumulation of (137)Cs by rice grown in four types of soil contaminated by the Fukushima Dai-ichi Nuclear Power Plant accident in 2011 and 2012," *Journal of Environmental Radioactivity,* vol. 140, pp. 59-64, 2015.

[66] T. Bisinger, S. Hippler, R. Michel, L. Wacker and H.-A. Synal, "Determination of plutonium from different sources in environmental samples using alpha-spectormetry and AMS," *Nuclear Instruments and Methods,* vol. 268, no. 7-8, pp. 1269-1262, 2010.

[67] J. Paatero, K. Hameri, T. Jaakkola, M. Jantunen, J. Koivukoski and R. Saxen, "Airborne and deposited radioactivity from the Chernobyl accident - a review of investigations in Finland," *Boreal Environment Research,* vol. 15, pp. 19-33, 2010.

[68] K. Hirose, Y. Igarashi and M. Aoyama, "Analysis of the 50-year records of the atmospheric deposition of long-lived radionuclides in Japan," *Applied Radiation and Isotopes,* vol. 66, pp. 1675-1678, 2008.

[69] G. Shaw, "Radionuclides in forest ecosystems," *Radioactivity in the Environment,* vol. 10, pp. 127-155, 2007.

[70] W. Bu, J. Zheng, Q. Guo, T. Aono, S. Otosaka, K. Tagami and S. Uchida, "Temporal distribution of plutonium isotopes in marine sedmients off Fukushima after the Fukushima Dai-ichi Nuclear Power Plant accident," *Journal of Radioanalytical and Nuclear Chemistry,* vol. 303, no. 2, pp. 1151-1154, 2015.

[71] O. Evrard, F. Pointurier, Y. Onda, C. Chartin, A. Hubert, H. Lepage, A.-C. Pottin, I. Lefevre, P. Bonte, J. P. Laceby and S. Ayrault, "Novel Insights into Fukushima Nuclear Accident from Isotopic Evidence of Plutonium Spread along Coastal Rivers," *Environmental Science & Technology,* vol. 48, no. 16, pp. 9334-3940, 2014.

[72] W. Bu, M. Fukuda, J. Zheng, T. Aono, T. Ishimaru, J. Kanda, G. Yang, K. Tagami, S. Uchida, Q. Guo and M. Yamada, "Release of Pu Isotopes from the Fukushima Daiichi Nuclear Power Plant Accident to the Marine Environment Was Negligible," *Environmental Science & Technology,* vol. 48, no. 16, pp. 9070-9078, 2014.

[73] G. Steinhauser, "Fukushima's forgotten radionuclides: a review of the understudied radioactive emissions," *Environmental Science & Technology,* vol. 48, no. 9, pp. 4649-4663, 2014.

[74] J. Zheng, K. Tagami and S. Uchida, "Release of plutonium isotopes into the environment from the Fukushima Daiichi Nuclear Power Plant accident: what is known and what needs to be known," *Envionmental Science & Technology,* vol. 47, no. 17, pp. 9584-9595, 2013.

[75] W. T. Bu, J. Zheng, T. Aono, K. Tagami, S. Uchida, J. Zhang, M. C. Honda, Q. J. Guo and M. Yamada, "Vertical distributions of plutonium isotopes in marine sediment cores off the Fukushima coast after the Fukushima Dai-ichi Nuclear Power Plant accident," *Biogeosciences,* vol. 10, no. 4, pp. 2497-2511, 2013.

[76] S. Schneider, C. Walther, S. Bister, V. Schauer, M. Christl, H.-A. Synal, K. Shozugawa and G. Steinhauser, "Plutonium release from Fukushima Daiichi fosters the need for more detailed investigations," *Scientific Reports,* vol. 3, p. 2988, 2013.

[77] J. Zheng, K. Tagami, S. Homma-Takeda and W. Bu, "The key role of atomic spectrometry in radiation protection," *Journal of Analytical Atomic Spectrometry,* vol. 28, pp. 1676-1699, 2013.

[78] J. Zheng, K. Tagami, Y. Watanabe, S. Uchida, T. Aono, N. Ishii, S. Yoshida, Y. Kubota, S. Fuma and S. Ihara, "Isotopic evidence of plutonium release into the environment from the Fukushima DNPP accident," *Scientific Reports,* vol. 2, p. 304, 2012.

[79] Z. Wang, G. Yang, J. Zheng, L. Cao, H. Yu, Y. Zhu, K. Tagami and S. Uchida, "Effect of ashing temperature on accurate determination of plutonium in soil samples," *Analytical Chemistry,* vol. 87, no. 11, pp. 5511-5515, 2015.

[80] R. W. Perkins and C. W. Thomas, "Worldwide fallout," in *Transuranic elements in the environment*, Springfield, VA, Technical Information Center/U.S. Department of Energy, 1980, p. 53.

[81] P. W. Krey, E. P. Hardy, C. Pachucki, F. Rourke, J. Coluzza and W. K. Benson, "Mass Isotopic Composition of Global Fall-Out Plutonium in Soil," in *Transuranium Nuclides in the Environment*, San Francicso, 1975.

[82] K. Shozugawa, N. Nogawa and M. Matsuo, "Deposition of fission and activation products after the Fukushima Dai-ichi nuclear power plant accident," *Envronmental Pollution,* vol. 163, pp. 243-247, 2012.

[83] F. Quinto, R. Golser, M. Lagos, M. Plaschke, T. Schafer, P. Steier and H. Geckeis, "Accelerator Mass Spectrometry of Actinides in Ground- and Seawater: An Innovative Method Allowing for the Simultaneous Analysis of U, Np, Pu, Am, and Cm Isotopes below ppq Levels," *Analytical Chemistry,* vol. 87, no. 11, pp. 5766-5763, 2015.

[84] S. L. Maxwell, B. Culligan, J. B. Hutchison and D. R. McAlister, "Rapid fusion method for the determination of Pu, Np, and Am in large soil samples," *Journal of Radioanalytical and Nuclear Chemistry,* vol. 305, no. 2, pp. 599-608, 2015.

[85] X. Dai and S. Kramer-Tremblay, "Five-column chromatography separation for simultaneous determination of hard-to-detect radionuclides in water and swipe samples," *Analytical Chemistry,* vol. 86, no. 11, pp. 5441-5447, 2014.

[86] S. L. Maxwell, B. K. Culligan, J. B. Hutchison, R. C. Utsey and D. R. McAlister, "Rapid determination of actinides in seawater samples," *Journal of Radioanalytical and Nuclear Chemistry,* vol. 300, no. 3, pp. 1175-1189, 2014.

[87] S. L. Maxwell, B. K. Culligan and J. B. Hutchison, "Rapid determination of actinides in asphalt samples," *Jounral of Radioanalytical and Nuclear Chemistry,* vol. 299, no. 3, pp. 1891-1901, 2014.

[88] J. Qiao, X. Hou, P. Steier and R. Golser, "Sequential injection method for rapid and simultaneous determination of 236U, 237Np, and Pu isotopes in seawater," *Analytical Chemistry,* vol. 85, no. 22, pp. 11026-11033, 2013.

[89] X. Dai, M. Christl, S. Kramer-Tremblay and H. A. Synal, "Ultra-trace determination of plutonium in urine samples using a compact accelerator mass spectormetry system operating at 300kV," *Journal of Analytical Atomic Spectrometry,* vol. 27, pp. 126-130, 2012.

[90] S. H. Reboul, E. H. Borai and R. A. Fjeld, "Sequential separation of actinides by ion chromatography coupled with on-line scintillation detection," *Analytical and Bioanalytical Chemistry,* vol. 374, no. 6, pp. 1096-1100, 2002.

[91] A. Torler, F. Wegmuller, H. R. Von Gunten, K. E. Gregorich, D. Lee, D. C. Hoffman and M. M. Fowler, "Fast Radiochemical Separation of Am, Pu, Np, U, Pa, Th, Ac and Ra in Heavy Ion Reactions with Actinide Targets," *Radiochimica Acta,* vol. 43, no. 3, pp. 149-152, 1988.

[92] R. Marsac, N. Banik, J. Lutzenkirchen, C. M. Marquardt, K. Dardenne, D. Schild, J. Rothe, A. Diascorn, T. Kupcik, T. Schafer and H. Geckeis, "Neptunium redox speciation at the illite surface," *Geochimica et Cosmochimica Acta,* vol. 152, pp. 39-51, 2015.

[93] Eichrom, "Eichrom methods: Neptunium and throium in urine," 2001. [Online]. Available: http://www.eichrom.com/eichrom/radiochem/methods/eichrom/. [Accessed June 2015].

[94] K. M. Mullaugh, J. D. Willey, R. J. Kieber, R. N. Mead and G. B. Avery, "Dynamics of the chemical composition of rainwater throughout Hurricane Irene," *Atmospheric Chemistry and Physics,* vol. 13, pp. 2321-2330, 2013.

[95] Z. Xu, Y. Wu, W.-J. Liu, C.-S. Liang, J. Ji, T. Zhao and X. Zhang, "Chemical composition of rainwater and the acid neutralizing effect at Beijing and Chizhou city, China," *Atmophseric Research,* Vols. 164-165, pp. 278-285, 2015.

[96] N. Zhang, J. Cao, Y. He and S. Xiao, "Chemical composition of rainwater at Lijiang on the Southeast Tibetan Plateau: influences from various air mass sources," *Journal of Atmophseric Chemistry,* vol. 71, no. 2, pp. 157-174, 2014.

[97] B. Rosenberg and G. Steinhauser, "Preparedness for a nuclear accident: removal of radioiodine from soil by chemical processing," *Journal of Radioanalytical and Nuclear Chemistry,* pp. 1-5, 2015.

[98] P. P. Povinec, K. Hirose and M. Aoyama, Fukushima Accident: Radioactivity Impact on the Environment, Waltham, MA: Elsevier, 2013.

[99] K. H. Harada, T. Niisoe, M. Imanaka, T. Takahashi, K. Amako, Y. Fujii, M. Kanameishi, K. Ohse, Y. Nakai, T. Nishikawa, Y. Saito, H. Sakamoto, K. Ueyama, K. Hisaki, I. Ohara, T. Inoue, K. Yamamoto, Y. Matsuoka, H. Ohata, K. Toshima, A. Okada, H. Sato, T. Kuwamori, H. Tani, R. Suzuki, M. Kashikura, M. Nezu, Y. Miyachi, F. Arai, M. Kuwamori, S. Harada, A. Ohmori, H. Ishikawa and A. Koizumi, "Radiation dose rates now and in the future for residents neighboring restricted areas of the Fukushima Daiichi Nuclear Power Plant.," *Proceedings of the National Academy of Sciences of the United States of America,* vol. 111, no. 10, pp. E914-23, 2014.

[100] P. Thakur, S. Ballard and R. Nelson, "An overview of Fukushima radionuclides measured in the northern hemisphere," *Science of the Total Environment,* vol. 458, p. 577, 2013.

[101] P. Thakur, S. Ballard and R. Nelson, "Radioactive fallout in the United States due to the Fukushima nuclear plant accident," *Journal of Environmental Monitoring,* vol. 14, no. 5, p. 1317, 2012.

[102] O. Masson, A. Baeza, J. Bieringer, K. Brudecki, S. Bucci, M. Cappai, F. P. Carvalho, O. Connan, C. Cosma, A. Dalheimer, D. Didier, G. Depuydt, L. E. De Geer, A. De Vismes, L. Gini, F. Groppi, K. Gudnason, R. Gurriaran, D. Hainz, O. Halldorsson, D. Hammond, O. Hanley, K. Holey, Z. Homoki, A. Ioannidou, K. Isajenko, M. Jankovic, C. Katzlberger, M. Kettunen, R. Kierepko, R. Kontro, P. J. M. Kwakman, M. Lecomte, L. Leon Vintro, A. P. Leppanen, B. Lind, G. Lujaniene, P. McGinnity, C. McMahon, H. Mala, S. Manenti, M. Manolopoulou, A. Mattila, A. Mauring, J. W. Mietelski, B. Moller, S. P. Nielsen, J. Nikolic, R. M. W. Overwater, S. E. Palsson, C. Papastefanou, I. Penev, M. K. Pham, P. P. Povinec, H. Rameback, M. C. Reis, W. Ringer, A. Rodriguez, P. Rulik, P. R. J. Saey, V. Samsonov, C. Schlosser, G. Sgorbati, B. V. Silobritiene, C. Soderstrom, R. Sogni, L. Solier, M. Sonck, G. Steinhauser, T. Steinkopff, P. Steinmann, S. Stoulos, I. Sykora, D. Todorovic, N. Tooloutalaie, L. Tositti, J. Tschiersch, A. Ugron, E. Vagena, A. Vargas, H. Weshofen and O. Zhukova, "Tracking of Airborne Radionuclides from the Damaged Fukushima Dai-Ichi Nuclear Reactors by European Networks," *Environmental Science & Technology,* vol. 45, no. 18, p. 7670, 2011.

[103] G. Steinhauser, S. Merz, D. Hainz and J. H. Sterba, "Artificial radioactivity in environmental media (air, rainwater, soil, vegetation) in Austria after the Fukushima nuclear accident," *Environmental Science and Pollution Research,* vol. 20, no. 4, p. 2527, 2013.

[104] D. Pittauerová, B. Hettwig and H. W. Fischer, "Fukushima fallout in Northwest German environmental media," *Journal of Environmental Radioactivity,* vol. 102, no. 9, p. 877, 2011.

[105] A. Koizumi, T. Niisoe, K. H. Harada, Y. Fujii, A. Adachi, T. Hitomi and H. Ishikawa, "137Cs trapped by biomass within 20 km of the Fukushima Daiichi nuclear power plant," *Environmental Science & Technology,* vol. 47, no. 17, p. 9612, 2013.

[106] G. Lujaniene, D. Valiulis, S. Bycenkiene, J. Sakalys and P. P. Povinec, "Plutonium isotopes and 241Am in the atmosphere of Lithuania: A comparison of different source terms," *Atmospheric Environment,* vol. 61, p. 419, 2012.

[107] N. Nihei, K. Tanoi and T. M. Nakanishi, "Inspections of radiocesium concentration levels in rice from Fukushima Prefecture after the Fukushima Dai-ichi Nuclear Power Plant accident," *Scientific Reports,* vol. 5, 2015.

[108] A. Koizumi, K. H. Harada, T. Niisoe, A. Adachi, Y. Fujii, T. Hitomi, H. Kobayashi, Y. Wada, T. Watanabe and H. Ishikawa, "Preliminary assessment of ecological exposure of adult residents in Fukushima Prefecture to radioactive cesium through ingestion and inhalation," *Environmental Health,* vol. 17, no. 4, p. 292, 2012.

[109] K. H. Harada, Y. Fujii, A. Adachi, A. Tsukidate, F. Asai and A. Koizumi, "Dietary intake of radiocesium in adult residents in Fukushima prefecture and neighboring regions after the Fukushima nuclear power plant accident: 24-h food-duplicate survey in December 2011," *Environmental Science & Technology,* vol. 47, no. 6, pp. 2520-2526, 2012.

[110] S. Tagami, S. Uchida and N. Ishii, "Extractability of radiocesium from processed green tea leaves with hot water: the first emergent tea leaves harvested after TEPCO's Fukushima Daiichi Nuclear Power Plant accident," *Journal of Radioanalytical and Nuclear Chemistry,* vol. 292, no. 1, p. 243, 2012.

[111] S. Merz, G. Steinhauser and N. Hamada, "Anthropogenic radionuclides in Japanese food: environmental and legal implications," *Environmental Science & Technology,* vol. 47, no. 3, pp. 1248-1256, 2013.

[112] N. Hamada, H. Ogino and Y. Fujimichi, "Safety regulations of food and water implemented in the first year following the Fukushima nuclear accident," *Journal of Radiation Research,* vol. 53, no. 5, pp. 641-671, 2012.

[113] K. Nishizawa, K. Takata, N. Hamada, Y. Ogata, S. Kojima, O. Yamashita, M. Ohshima and Y. Kayama, "Iodine-131 in milk and rain after Chernobyl," *Nature,* vol. 324, p. 308, 1986.

[114] I. G. Travnikova, G. J. Bruk, V. N. Shutov, A. B. Bazjukin, M. I. Balonov, T. Rahola and M. Tillander, "Contribution of different foodstuffs to the internal exposure of rural inhabitants in Russia after the Chernobyl accident," *Radiation Protection Dosimetry,* vol. 93, no. 4, pp. 331-339, 2001.

[115] C. Xu, E. J. Miller, S. Zhang, H. P. Li, Y. F. Ho, K. A. Schwehr, D. I. Kaplan, S. Otosaka, K. A. Roberts, R. Brinkmeyer, C. M. Yeager and P. H. Santschi, "Sequestration and remobilization of radioiodine (129I) by soil organic matter and possible consequences of the remedial action at Savannah River Site," *Environmental Science & Technology,* vol. 45, no. 23, p. 9975, 2011.

[116] K. Tagami and S. Uchida, "Can we remove iodine-131 from tap water in Japan by boiling?-Experimental testing in response to the Fukushima Daiichi Nuclear Power Plant accident," *Chemosphere,* vol. 84, no. 9, p. 1282, 2011.

[117] M. Mostafa, A. F. El-Gharbawy, M. A. El-Absy, S. E. Soliman and F. A. Aly, "Preconcentration of radioiodine as AgI and purification from radiotellurium waste," *Journal of Radioanalytical and Nuclear Chemistry,* vol. 300, no. 3, p. 1089, 2014.

[118] T. M. Klapötke, B. Krumm, F. X. Steemann and G. Steinhauser, "Hands on explosives: safety testing of protective measures," *Safety Science,* vol. 48, no. 1, p. 28, 2010.

[119] G. Steinhauser and T. M. Klapötke, "Using the chemistry of fireworks to engage students in learning basic chemical principles: a lesson in eco-friendly pyrotechnics," *Journal of Chemical Education,* vol. 87, no. 2, p. 150, 2010.

[120] W. C. Bray and H. A. Liebhafsky, "Reactions involving hydrogen peroxide, iodine and iodate ion. I. Introduction," *Journal of the American Chemical Society,* vol. 53, no. 1, p. 38, 1931.

[121] J. Pudykiewicz, "Numerical simulation of the transport of radioactive cloud from the Chernobyl nuclear accident," *Tellus B,* vol. 40, no. 4, pp. 241-259, 1988.

[122] A. S. Rogowski and T. Tamura, "Environmental mobility of cesium-137," *Radiation Botany,* vol. 10, pp. 33-45, 1970.

[123] B. L. Rosenberg, K. Shozugawa and G. Steinhauser, "Detection of Fuel Release in a Nuclear Accident: A method for preconcentration and isolation of reactor-borne 239Np using ion-specific extraction chromatography," *Analytical Chemistry,* vol. 87, no. 17, pp. 8651-8656, 2015.

Table 5: Fukushima sample descriptions and labels from June, 2013, and July, 2014..

Distance to NPP (km)	Site Description	Sample Code	Sample Type	GPS Coordinates 2013	GPS Coordinates 2014
32.7	Iitate Village	Veg A1	Vegetation	37.61270 N 140.74905 E	N/A
		F1-01	Soil		
16.2	Odaka Minami Soma	Veg B1	Vegetation	37.56556 N 140.99194 E	37.565961 N 140.992462 E
		F1-04	Soil		
12	Fukushima Daini	Veg H1	Vegetation	37.3147 N 141.01325 E	N/A
		F1-32	Soil		
8.5	Chimeiji	Veg C1	Vegetation	37.49556 N 141.00139 E	37.495397 N 141.001808 E
		F1-09	Soil		
4.1	4.1 km from NPP	Veg G1	Vegetation	37.38854 N 141.00825 E	37.388553 N 141.008240 E
		F1-24	Soil		
1.5	Okuma Town	Veg D1	Vegetation	37.41742 N 141.01012 E	37.417534 N 141.010255 E
		F1-11	Soil		
1	Okuma Town	Veg E1	Vegetation	37.41770 N 141.01510 E	37.417783 N 141.014911 E
		F1-15	Soil		
0	NPP Entrance Gate, MP7	Veg F2	Vegetation	37.41736 N 141.02329 E	37.415693 N 141.026747 E
		F1-19	Soil		

Table 6: Specific activities of ^{134}Cs (top) and ^{137}Cs (bottom) in vegetation and varying depths of soil collected from the Fukushima prefecture in June, 2013. Activities are reported in Bq kg^{-1}.

Depth (cm):	0.0-2.5	2.5-5.0	5.0-7.5	7.5-10.0	10.0-12.5	12.5-15.0	Veg
F1-01	1.7E+04	6.2E+03	1.8E+03	1.2E+03	4.5E+02	2.2E+02	1.8E+01
	2.7E+04	1.0E+04	2.9E+03	1.7E+03	7.0E+02	3.9E+02	4.1E+01
F1-04	1.4E+03	ND	ND	ND	ND	ND	3.5E+01
	2.5E+03	5.9E+01	ND	ND	ND	ND	8.2E+01
F1-32	1.6E+03	4.2E+02	ND	ND	ND	ND	3.2E+01
	2.6E+03	7.2E+02	1.3E+02	ND	ND	ND	7.5E+01
F1-09	1.7E+03	1.5E+02	ND	ND	ND	ND	ND
	2.9E+03	2.6E+02	ND	ND	ND	6.0E+01	1.3E-01
F1-24	3.6E+04	1.0E+04	1.8E+03	7.5E+02	6.1E+02	1.2E+03	1.0E+03
	6.1E+04	1.7E+04	3.0E+03	1.3E+03	1.0E+03	2.0E+03	2.6E+03
F1-11	2.0E+05	2.0E+04	1.5E+04	4.2E+03	5.8E+02	1.2E+03	3.9E+03
	3.2E+05	3.3E+04	2.5E+04	7.2E+03	1.1E+03	2.1E+03	9.0E+03
F1-15	1.2E+03	1.4E+04	6.6E+02	1.0E+04	7.9E+04	8.1E+04	8.1E+02
	2.0E+03	2.4E+04	1.1E+03	1.6E+04	1.3E+05	1.3E+05	2.2E+03
F1-19	5.9E+05	8.1E+03	2.4E+03	1.3E+03	1.1E+03	4.0E+02	3.1E+04
	9.9E+05	1.3E+04	3.7E+03	2.0E+03	1.8E+03	6.6E+02	8.1E+04

Table 7: Specific activities (Bq kg^{-1}) of ^{134}Cs (top) and ^{137}Cs (bottom) in soil samples collected from the Fukushima prefecture exclusion zone in July, 2014.

Depth (cm):	0.0-2.5	2.5-5.0	5.0-7.5	7.5-10.0	10.0-12.5	12.5-15.0
Odaka (1)	4.2E+02	4.2E+02	3.1E+02	2.3E+02	1.0E+02	1.8E+01
	1.3E+03	1.2E+03	9.1E+02	6.9E+02	3.0E+02	5.4E+01
Odaka (2)	4.8E+02	1.3E+02	4.4E+02	3.2E+02	1.9E+01	ND
	1.5E+03	3.8E+02	1.3E+03	1.0E+03	5.5E+01	5.2E+00
Chimeiji (1)	1.0E+03	1.4E+01	4.5E+00	3.8E+00	ND	ND
	3.0E+03	4.1E+01	1.3E+01	1.2E+01	ND	ND
Chimeiji (2)	2.0E+01	2.7E+01	5.2E+00	ND	ND	ND
	5.1E+01	8.6E+01	1.5E+01	1.7E+00	ND	ND
4.1 km (1)*	3.9E+04	7.5E+04	4.0E+04	4.5E+03	4.5E+03	2.1E+03
	1.1E+05	2.2E+05	1.2E+05	1.3E+04	1.3E+04	6.0E+03
4.1 km (2)	3.8E+04	1.1E+04	2.2E+03	4.2E+02	6.3E+01	4.4E+01
	1.1E+05	3.2E+04	6.5E+03	1.2E+03	1.9E+02	1.3E+02
1.5 km (1)	2.7E+04	2.2E+04	2.3E+04	6.2E+03	8.9E+02	1.7E+02
	7.6E+04	6.5E+04	6.7E+04	1.8E+04	2.4E+03	5.0E+02
1.5 km (2)	2.0E+04	1.6E+04	6.4E+03	ND	ND	ND
	5.6E+04	4.5E+04	1.8E+04	ND	ND	ND
1.5 km (3)	2.0E+04	2.3E+04	2.1E+04	1.1E+04	7.9E+04	2.1E+04
	5.8E+04	6.6E+04	5.9E+04	3.3E+04	2.3E+05	6.2E+04
1 km (1)	7.9E+04	2.1E+04	5.4E+03	6.3E+02	3.0E+02	2.0E+02
	2.3E+05	6.2E+04	1.6E+04	1.9E+03	8.3E+02	5.8E+02
Gate (1)	1.6E+05	2.9E+04	3.8E+03	6.8E+02	6.9E+02	ND
	4.5E+05	8.6E+04	1.1E+04	2.0E+03	2.0E+03	ND
Gate (2)	6.8E+04	6.2E+04	3.6E+04	2.0E+04	1.6E+03	1.6E+03
	2.0E+05	1.8E+05	1.0E+05	6.0E+04	4.7E+03	4.4E+03

The soil content between 7.5 cm and 12.5 cm was consolidated into a single sample. The reported specific activities for the 7.5-10.0 cm depth and for the 10.0-12.5 cm depth are the total activity halved.

Table 8: Tritium activity in 15 cm soil cores and vegetation samples collected in 2013. Activities are reported in Bq L^{-1} H$_2$O collected. Uncertainties are expressed to 1σ.

Distance to NPP (km)	Sample	Top 2.5 cm	Bottom 2.5 cm	Vegetation
0	F1-19	21.5±10.2	9.5±4.6	13.4±9.6
1	F1-15	9.5±8.5	1.1±0.6	12.8±8.1
1.5	F1-11	30.1±1.4	9.9±1.9	9.6±4.1
4.1	F1-24	90.9±15.2	22.2±19.8	16.6±2.9
8.5	F1-09	1249.3±1573.8	42.7±31.2	4.7±1.1
12	F1-32	27.7±22.2	535.2±2.1	91.8±74.7
16.2	F1-04	18.3±11.8	8.8±8.5	5.4±4.5
32.7	F1-01	58.2±71.2	ND	2.2±0.6
Blank		10.35 CPM		

Table 9: Specific activities of ^{90}Sr in the top 5 cm of soil cores and vegetation samples collected in 2013. Activities are reported in Bq kg^{-1} dry mass. Data originally reported by Ball, J.: Deposition of strontium-90 in soil and vegetation at various locations surrounding the Fukushima Daiichi nuclear power plant, 2015 [52].

Distance to NPP (km)	Sample	0.0-2.5 cm	2.5-5.0 cm	Veg
0	F1-19	385.3±2.2	28.7±1.2	59.8±4.2
1	F1-15	9.1±0.6	11.4±0.7	147.8±2.8
1.5	F1-11	86.5±2.7	16.7±1.5	56.1±0.2
4.1	F1-24	12.9±0.2	14.2±0.8	16.4±0.3
8.5	F1-09	8.9±0.5	7.7±1.6	49.1±0.8
12	F1-32	12.6±2.0	9.1±1.5	10.3±3.5
16.2	F1-04	5.6±0.9	10.8±0.6	21.1±5.0
32.7	F1-01	17.1±1.4	11.0±0.4	30.3±1.2

Table 10: Specific activities of ^{90}Sr in the top 5cm of soil cores collected from the Fukushima exclusion zone in July, 2014. Activities are reported in Bq kg^{-1} dry mass and are corrected to the date of sampling.

	2.5 cm	5.0 cm
Odaka (1)	7.0	6.3
	4.9	6.5
Odaka (2)	6.1	4.7
	2.7	4.0
Chimeiji (1)	7.4	7.5
	7.0	6.4
Chimeiji (2)	7.0	3.7
	4.3	4.9
4.1 km (1)	39.1	16.0
	43.5	16.7
4.1 km (2)	16.9	20.9
	16.7	21.8
1.5 km (1)	31.3	22.4
	30.0	22.6
1.5 km (2)	17.1	16.0
	18.1	16.1
1.5 km (3)	32.1	22.6
	32.1	27.9
1 km (1)	36.2	20.3
	35.6	24.0
1 km (2)	14.5	N/A
	11.8	N/A
Gate (1)	60.2	18.3
	63.5	17.5
Gate (2)	89.1	76.0
	96.4	73.7

Table 11: Percent recovery of radionuclides from rainwater analogues using combinations of ion specific extraction chromatography resins and eluents. Uncertainties are expressed to 1σ.

Resin [Eluent]	^{123m}Te	^{131}I	^{134}Cs	^{239}Np
UTEVA [HCl]	34.7±23.6%	14.2±15.4%	0.1±0.1%	115.0±8.6%
UTEVA [H$_2$O]	111.7%	9.6±13.0%	0.2%	103.4±31.6%
TEVA [HCl]	1.6±0.01%	0.6±0.1%	ND	95.9±2.7%
RE [H$_2$O]	ND	0.4±0.02%	ND	69.2±19.2%
RE [HNO3]	ND	0.4±0.1±	0.02%	67.3±10.6%
UTEVA [HNO3]	ND	0.3±0.02%	ND	62.7±5.4%
TEVA [H2O]	ND	3.3±0.1%	ND	42.5±2.9%
TRU [H2O]	ND	0.9±0.5%	ND	42.1%
TEVA [HNO3]	ND	13.0±0.4%	ND	25.9±0.1%
TRU [HNO3]	ND	0.3±0.1%	ND	5.7±0.2%
ACT [HCl]	ND	3.4±0.4%	0.1±0.01%	ND

Table 12: Percent recovery of radionuclides from soil matrices using ion specific extraction chromatography resins. Uncertainties are expressed to 1σ.

Resin	^{123m}Te	^{131}I	^{134}Cs	^{239}Np
RE	ND	3.9±0.4%	ND	64.8±4.2%
TEVA	ND	4.8±0.3%	ND	53.6±6.4%
UTEVA	ND	4.4±0.3%	ND	13.9±0.3%

Table 13: Percent recovery of ^{131}I from soil using combinations of reagents in the presence and absence of stable iodide carrier. Reagents included HNO_3, $AgNO_3$ (Ag), and 30% H_2O_2.

Reagents	W/Carrier	W/O Carrier
HNO_3	61%	73%
	67%	70%
HNO_3 + Ag	59%	70%
	52%	73%
HNO_3 + H_2O_2	76%	93%
	67%	96%
HNO_3 + Ag + H_2O_2	60%	N/A
	55%	

Table 14: Compilation of ^{131}I, ^{132}I, ^{132}Te, ^{134}Cs, and ^{137}Cs activities (Bq mL^{-1}) reported by TEPCO. Ratios were calculated based on activities back-calculated to March 11, 2011. Sample descriptions were translated from the reports. Samples were collected from monitoring posts (MP) at Fukushima Daiichi (1F) and Fukushima Daini (2F). Some information was not provided in the reports (U).

Measurement Day/Time	Sample Description	Volume (mL)	Live Time (s)	I-131 A	I-132 A	Te-132 A	^{131}I/^{132}Te Ratio	Cs-134 A	Cs-137 A	^{134}Cs/^{137}Cs ratio
3/19/2011 10:39	MP-1 charcoal measurement	3.00E+05	1000	2.70E-04	ND	7.05E-05	1.26E+00	6.32E-05	ND	
3/19/2011 10:58	MP-1 dust	3.00E+05	1000	1.38E-04	1.24E-04	ND		ND	ND	
3/19/2011 14:12	1F main bldg office (before drainage)	8.38E+05	500	5.94E-03	2.20E-03	3.72E-05	5.15E+01	ND	ND	
3/19/2011 14:22	1F main bldg office N (before drainage)	8.38E+05	500	1.07E-03	3.82E-04	3.02E-05	1.15E+01	2.17E-05	2.44E-05	8.95E-01
3/19/2011 19:08	charcoal	3.00E+05	1000	2.51E-04	1.23E-04	ND		ND	ND	
3/19/2011 19:26	DST filter paper	3.00E+05	1000	1.26E-04	ND	ND		ND	ND	
3/20/2011 16:17	MP-1	5.00E+05	500	5.25E-05	ND	8.70E-06	1.69E+00	ND	7.89E-06	
3/20/2011 16:29	MP-1	5.00E+05	500	2.59E-05	ND	4.16E-06	1.74E+00	ND	ND	
3/20/2011 21:11	MP-1	5.00E+05	500	2.23E-04	ND	ND		ND	ND	

Measurement Day/Time	Sample Description	Volume (mL)	Live Time (s)	I-131 A	I-132 A	Te-132 A	^{131}I/^{132}Te Ratio	Cs-134 A	Cs-137 A	^{134}Cs/^{137}Cs ratio
3/20/2011 21:20	MP-1	5.00E+05	500	8.20E-05	ND	ND		ND	ND	
3/21/2011 12:15	MP-1 dust	5.00E+05	500	2.25E-04	2.42E-04	3.16E-04	1.78E-01	1.23E-05	1.84E-05	6.75E-01
3/21/2011 12:28	MP-1	5.00E+05	500	1.51E-04	2.50E-04	4.48E-04	8.44E-02	4.41E-05	4.71E-05	9.45E-01
3/21/2011 13:12	1F main bldg office N of unit 1	8.41E+05	500	1.27E-03	ND	2.18E-04	1.45E+00	2.84E-05	2.89E-05	9.91E-01
3/21/2011 13:28	1F main bldg office N of unit 1	8.41E+05	500	2.30E-03	ND	2.89E-04	1.98E+00	4.05E-05	3.93E-05	1.04E+00
3/21/2011 13:38	1F main bldg office N of unit 1	8.40E+05	500	9.16E-04	1.14E-04	1.62E-04	1.41E+00	3.38E-05	3.80E-05	8.98E-01
3/21/2011 13:48	1F main bldg office N of unit 1	8.40E+05	500	1.52E-03	2.54E-04	2.30E-04	1.64E+00	3.14E-05	3.59E-05	8.83E-01
3/21/2011 19:00	MP-1 area	5.00E+05	500	1.58E-04	8.10E-04	9.15E-04	4.17E-02	1.73E-05	1.80E-05	9.69E-01
3/21/2011 19:11	1F units 1-4 drainage seawater S side	5.00E+02	1000	5.07E+00	2.14E+00	2.37E+00	5.16E-01	1.49E+00	1.48E+00	1.01E+00
3/21/2011 19:14	MP-1 area	5.00E+05	500	1.25E-04	3.94E-04	5.22E-04	5.76E-02	3.02E-05	3.31E-05	9.21E-01
3/22/2011 2:31	3 4 drainage opening side seawater	5.00E+02	1000	1.09E+00	1.60E-01	1.77E-02	1.42E+01	4.82E-02	5.28E-02	9.20E-01
3/22/2011 2:53	Iwasawa coast seawater	5.00E+02	1000	6.56E-01	1.21E-01	3.18E-02	4.77E+00	3.11E-02	3.29E-02	9.54E-01
3/22/2011 3:18	Tomioka River estuary seawater	5.00E+02	1000	3.211	8.76E-01	1.59E-01	4.66E+00	7.54E-02	7.76E-02	9.80E-01

Measurement Day/Time	Sample Description	Volume (mL)	Live Time (s)	I-131 A	I-132 A	Te-132 A	^{131}I/^{132}Te Ratio	Cs-134 A	Cs-137 A	^{134}Cs/^{137}Cs ratio
3/22/2011 8:27	1F units 1-4 drainage seawater 100m from coast	5.00E+02	1000	1.19E+00	1.36E+00	ND		1.50E-01	1.54E-01	9.89E-01
3/22/2011 11:53	2F MP-1	5.00E+05	500	1.42E-04	ND	3.19E-05	9.79E-01	2.65E-05	2.32E-05	1.15E+00
3/22/2011 12:05	2F MP-1	5.00E+05	500	6.94E-05	ND	2.19E-05	6.97E-01	1.29E-05	1.02E-05	1.28E+00
3/22/2011 14:50	1F main gate	8.31E+05	500	2.24E-03	ND	ND		1.13E-05	1.35E-05	8.47E-01
3/22/2011 15:01	1F main gate monitoring post dust	8.31E+05	500	4.69E-04	ND	1.59E-05	6.38E+00	1.59E-05	1.89E-05	8.51E-01
3/22/2011 16:53	2F 3 4 drainage opening area	5.00E+02	1000	1.14E+00	ND	ND		4.63E-02	3.93E-02	1.19E+00
3/22/2011 17:14	2F Iwasawa coast area	5.00E+02	1000	6.66E-01	ND	ND		3.93E-02	4.36E-02	9.09E-01
3/22/2011 17:32	2F MP-1	5.00E+05	500	1.35E-04	ND	ND		1.87E-05	2.15E-05	8.78E-01
3/22/2011 17:42	2F MP-1	5.00E+05	500	7.92E-05	4.15E-05	ND		1.35E-05	1.37E-05	9.98E-01
3/23/2011 12:50	1F S side drainage opening area 1 (S spillway)	5.00E+02	1000	5.87E+00	6.39E+00	4.10E-01	2.75E+00	2.50E-01	2.53E-01	9.97E-01
3/23/2011 13:06	1F N side drainage opening area	5.00E+02	1000	2.66E+00	2.94E+00	1.56E+00	3.28E-01	1.79E+00	1.93E+00	9.40E-01
3/23/2011 14:17	2F MP-1	5.00E+05	500	2.66E-04	2.76E-04	9.30E-05	5.45E-01	4.33E-05	ND	

Measurement Day/Time	Sample Description	Volume (mL)	Live Time (s)	I-131 A	I-132 A	Te-132 A	^{131}I/^{132}Te Ratio	Cs-134 A	Cs-137 A	^{134}Cs/^{137}Cs ratio
3/23/2011 14:54	1F main gate	8.41E+05	500	6.68E-04	ND	2.95E-04	4.30E-01	2.18E-05	2.29E-05	9.63E-01
3/23/2011 15:00	2F MP-1	5.00E+05	500	1.46E-04	ND	7.14E-05	3.89E-01	ND	1.74E-05	
3/23/2011 15:06	1F main gate	8.41E+05	500	4.32E-04	ND	1.39E-04	5.90E-01	1.71E-05	1.34E-05	1.29E+00
3/23/2011 15:19	3 4 drainage opening	5.00E+02	1000	7.44E-01	1.96E-01	ND		5.08E-02	5.46E-02	9.40E-01
3/23/2011 15:37	Iwasawa beach	5.00E+02	1000	7.64E-01	3.32E-01	ND		3.27E-02	4.26E-02	7.77E-01
3/23/2011 17:38	2F MP-1	6.00E+02	500	2.13E-04	2.77E-04	4.03E-04	9.90E-02	2.34E-05	2.01E-05	1.17E+00
3/23/2011 17:47	2F MP-1	5.00E+05	500	8.19E-05	2.59E-04	3.03E-04	5.05E-02	1.69E-05	1.72E-05	9.94E-01
3/24/2011 10:18	Iwasawa beach seawater	5.00E+02	1000	5.03E-01	ND	ND		3.47E-02	3.80E-02	9.22E-01
3/24/2011 10:23	3 4 seawater drainage opening	2.50E+02	1000	1.14E+00	1.23E-01	4.95E-02	3.92E+00	9.88E-02	9.43E-02	1.06E+00
3/24/2011 10:39	MP-1	5.00E+05	500	1.15E-04	1.73E-04	2.01E-04	9.70E-02	2.08E-05	2.03E-05	1.04E+00
3/24/2011 10:49	MP-1	5.00E+05	500	1.91E-04	3.02E-04	3.59E-04	9.07E-02	2.83E-05	2.98E-05	9.59E-01
3/24/2011 17:42	Turbine basement water	5.00E-01	500	2.10E+05	ND	ND		1.59E+05	1.82E+05	8.86E-01
3/24/2011 19:43	1F anti-N water discharge	5.00E+02	1000	9.47E-01	4.50E-01	1.35E-01	1.14E+00	1.11E-01	1.10E-01	1.02E+00

Measurement Day/Time	Sample Description	Volume (mL)	Live Time (s)	I-131 A	I-132 A	Te-132 A	^{131}I/^{132}Te Ratio	Cs-134 A	Cs-137 A	^{134}Cs/^{137}Cs ratio
3/24/2011 20:32	1F seawater south drainage opening area	5.00E+02	500	4.15E+00	1.662	7.99E-02	8.39E+00	4.46E-01	4.45E-01	1.01E+00
3/24/2011 22:03	1F main gate	8.38E+05	500	1.49E-03	ND	2.28E-04	1.05E+00	3.20E-05	3.10E-05	1.04E+00
3/24/2011 22:13	1F main gate	8.38E+05	500	4.99E-04	ND	1.30E-04	6.13E-01	1.08E-05	1.19E-05	9.14E-01
3/24/2011 22:56	Subdrain water	2.50E+02	500	3.65E+02	1.28E+01	1.40E+01	4.15E+00	3.09E+01	3.17E+01	9.86E-01
3/24/2011 23:03	1F turbine bldg basement water intrusion	1.00E-01	500	1.22E+06	ND	ND		1.79E+05	1.80E+05	1.01E+00
3/25/2011 0:40	MP-1	5.00E+05	500	6.37E-05	ND	2.50E-05	4.03E-01	ND	2.13E-05	
3/25/2011 0:45	2F MP-1	5.00E+05	500	1.66E-04	ND	3.25E-04	8.05E-02	1.6E-05	2.94E-05	5.49E-01
3/25/2011 11:35	1F seawater N side	5.00E+02	1000	1.14E+01	1.90E-01	1.25E-01	1.35E+01	1.68E+00	1.67E+00	1.02E+00
3/25/2011 11:54	1F seawater S side	5.00E+02	1000	5.00E+01	3.31E+00	2.25E-01	3.30E+01	7.04E+00	7.16E+00	9.95E-01
3/25/2011 12:16	Iwasawa beach	5.00E+02	1000	3.66E-01	1.16E-01	ND		2.01E-02	2.15E-02	9.45E-01
3/25/2011 12:20	MP-1 area	5.00E+05	500	1.01E-04	5.96E-05	3.72E-05	4.01E-01	ND	ND	
3/25/2011 12:29	MP-1 area	5.00E+05	500	2.08E-04	1.60E-04	6.89E-05	4.46E-01	3.13E-05	ND	
3/25/2011 12:34	3 4 drainage opening	5.00E+02	1000	4.27E-01	5.80E-02	1.27E-02	4.98E+00	2.63E-02	3.41E-02	7.81E-01

Measurement Day/Time	Sample Description	Volume (mL)	Live Time (s)	I-131 A	I-132 A	Te-132 A	^{131}I/^{132}Te Ratio	Cs-134 A	Cs-137 A	^{134}Cs/^{137}Cs ratio
3/25/2011 13:38	1F main gate	8.47E+05	500	3.17E-04	ND	2.98E-05	1.57E+00	1.60E-05	1.61E-05	1.01E+00
3/25/2011 13:51	1F main gate	8.47E+05	500	8.75E-04	ND	5.23E-05	2.46E+00	3.17E-05	2.40E-05	1.33E+00
3/25/2011 18:33	2F MP-1 area	5.00E+05	500	1.74E-04	2.21E-04	2.56E-04	9.73E-02	2.65E-05	3.51E-05	7.64E-01
3/25/2011 18:43	2F MP-1 area	5.00E+05	500	6.79E-05	1.13E-04	1.30E-04	7.48E-02	1.04E-05	1.08E-05	9.68E-01
3/26/2011 11:40	1F seawater S side	5.00E+02	1000	3.00E+01	2.047	2.84E-02	1.38E+02	4.73E+00	4.81E+00	9.97E-01
3/26/2011 12:03	1F seawater N side	5.00E+02	1000	2.88E+01	1.15E-01	ND		5.02E+00	5.08E+00	1.00E+00
3/26/2011 12:24	1F main gate	8.44E+05	500	3.02E-04	ND	1.36E-04	2.88E-01	1.24E-05	8.83E-06	1.43E+00
3/26/2011 12:26	1F main gate	8.44E+05	500	2.62E-04	ND	2.34E-05	1.45E+00	1.85E-05	1.55E-05	1.21E+00
3/26/2011 12:35	2F MP-1	5.00E+05	500	1.03E-04	1.56E-04	2.05E-04	6.51E-02	1.28E-05	1.57E-05	8.29E-01
3/26/2011 12:37	2F MP-1	5.00E+05	500	8.37E-05	ND	3.24E-05	3.35E-01	1.85E-05	1.65E-05	1.14E+00
3/26/2011 16:38	1F seawater S side	5.00E+02	1000	7.40E+01	3.777	1.03E+00	9.08E+00	1.18E+01	1.20E+01	9.96E-01
3/26/2011 16:43	1F seawater N side	5.00E+02	1000	1.27E+01	3.22E-01	6.70E-02	2.40E+01	2.18E+00	2.18E+00	1.01E+00
3/26/2011 17:17	2F Iwasawa seawater	5.00E+02	1000	3.03E-01	ND	ND		1.32E-02	1.42E-02	9.42E-01
3/26/2011 17:18	2F seawater (3 4 drainage opening)	5.00E+02	1000	4.11E-01	ND	ND		2.62E-02	2.65E-02	1.00E+00

Measurement Day/Time	Sample Description	Volume (mL)	Live Time (s)	I-131 A	I-132 A	Te-132 A	^{131}I/^{132}Te Ratio	Cs-134 A	Cs-137 A	^{134}Cs/^{137}Cs ratio
3/26/2011 18:46	Turbine bldg basement water intrusion	1.00E-02	500	1.34E+07	ND	ND		2.27E+06	2.27E+06	1.01E+00
3/26/2011 19:19	2F MP-1 particulate	5.00E+05	500	8.84E-04	ND	3.17E-04	3.49E-01	1.77E-04	2.11E-04	8.54E-01
3/26/2011 19:41	2F MP-1 volatile	5.00E+05	500	1.58E-04	ND	3.44E-05	5.72E-01	ND	ND	
3/26/2011 19:44	1F turbine bldg basement water intrusion	5.00E-01	500	3.24E+05	ND	ND		55000	5.58E+04	9.99E-01
3/26/2011 22:12	1F turbine basement moveable elements	1.00E-01	500	1.53E+05	ND	ND		1.19E+05	1.33E+05	9.07E-01
3/27/2011 10:19	2F Iwasawa Beach Seawater	5.00E+02	1000	2.94E-01	ND	ND		2.03E-02	2.36E-02	8.74E-01
3/27/2011 11:09	1F seawater S side	5.00E+02	1000	1.09E+01	3.43E-01	1.52E-02	8.26E+01	1.90E+00	1.93E+00	9.99E-01
3/27/2011 11:10	1F seawater N side	5.00E+02	1000	8.11E+00	ND	ND		1.63E+00	1.68E+00	9.86E-01
3/27/2011 11:38	1F W gate	8.45E+05	500	4.45E-04	ND	9.94E-05	5.12E-01	1.20E-05	1.41E-05	8.62E-01
3/27/2011 11:41	1F W gate	8.45E+05	500	2.10E-04	ND	1.72E-05	1.39E+00	1.56E-05	1.36E-05	1.17E+00
3/27/2011 11:56	2F MP-1 area	5.00E+05	1500	1.29E-04	1.38E-04	1.66E-04	8.86E-02	1.89E-05	1.93E-05	9.97E-01
3/27/2011 11:56	2F MP-1 area	5.00E+05	500	7.33E-05	3.25E-05	2.45E-05	3.41E-01	2.29E-05	1.60E-05	1.45E+00

Measurement Day/Time	Sample Description	Volume (mL)	Live Time (s)	I-131 A	I-132 A	Te-132 A	^{131}I/^{132}Te Ratio	Cs-134 A	Cs-137 A	^{134}Cs/^{137}Cs ratio
3/27/2011 12:46	Turbine bldg underground water intrusion	1.00E-02	500	1.33E+07	ND	ND		2.24E+06	2.24E+06	1.01E+00
3/27/2011 15:16	2F seawater (3 4 drainage opening)	5.00E+02	1000	3.77E+00	1.49E-02	ND		5.40E-01	5.65E-01	9.70E-01
3/27/2011 16:22	1F seawater N side	5.00E+02	1000	4.58E+01	ND	ND		9.76E+00	9.78E+00	1.01E+00
3/27/2011 16:22	1F seawater S side	5.00E+02	1000	1.04E+01	3.50E-01	ND		1.85E+00	1.82E+00	1.03E+00
3/27/2011 18:03	2F MP-1	5.00E+05	500	7.60E-05	6.30E-05	7.51E-05	1.12E-01	5.31E-06	4.68E-06	1.15E+00
3/27/2011 20:42	2F MP-1	5.00E+05	500	4.26E-05	ND	ND		ND	ND	
3/27/2011 22:32	Shared pool BFL building stagnant water	2.50E-03	500	1.33E+07	ND	ND		3075000	3.03E+06	1.03E+00
3/28/2011 11:05	1F seawater S side	5.00E+02	1000	1.36E+00	ND	ND		2.77E-01	2.93E-01	9.58E-01
3/28/2011 11:06	1F seawater N side	5.00E+02	1000	3.26E+01	ND	ND		6.62E+00	6.65E+00	1.01E+00
3/28/2011 11:41	1F W gate dust routine	8.42E+05	1000	3.59E-04	2.46E-04	2.69E-04	1.34E-01	8.88E-06	8.08E-06	1.12E+00
3/28/2011 11:42	1F W gate dust routine	8.42E+05	1000	2.10E-04	ND	ND		ND	7.48E-06	
3/28/2011 13:10	2F MP-1	5.00E+05	1000	3.06E-05	ND	ND		ND	ND	
3/28/2011 13:10	2F MP-1	5.00E+05	1000	ND	ND	ND		ND	ND	

Measurement Day/Time	Sample Description	Volume (mL)	Live Time (s)	I-131 A	I-132 A	Te-132 A	^{131}I/^{132}Te Ratio	Cs-134 A	Cs-137 A	^{134}Cs/^{137}Cs ratio
3/28/2011 13:50	2F Iwasawa Beach Seawater	5.00E+02	1000	2.35E+00	ND	ND		0.3301	3.77E-01	8.89E-01
3/28/2011 14:07	2F 3 4 drainage opening	5.00E+02	1000	3.82E+00	ND	ND		6.06E-01	6.19E-01	9.93E-01
3/28/2011 16:37	1F seawater N side	5.00E+02	1000	2.66E+01	ND	ND		5.63E+00	5.71E+00	1.00E+00
3/28/2011 16:58	1F seawater S side	5.00E+02	1000	1.11E+00	ND	ND		2.44E-01	2.41E-01	1.02E+00
3/28/2011 17:49	2F MP-1	5.00E+05	1000	ND	ND	ND		ND	ND	
3/28/2011 18:02	2F MP-1	5.00E+05	1000	4.64E-05	2.80E-05	1.43E-05	3.14E-01	7.79E-06	ND	
3/28/2011 21:56	1F central process bldg controlled area	2.50E+02	500	8.67E-01	ND	ND		4.37E+00	4.416	1.00E+00
3/28/2011 22:05	1F central process bldg non-tube area	2.30E+02	500	6.25	ND	ND		2.657	2.80E+00	9.62E-01
3/29/2011 10:57	1F seawater S side	5.00E+02	1000	1.03E+02	ND	ND		2.37E+01	2.41E+01	9.99E-01
3/29/2011 11:18	1F seawater N side	5.00E+02	1000	4.94E+01	ND	ND		1.15E+01	1.17E+01	1.00E+00
3/29/2011 11:46	Vertical shaft furnace B	5.00E+02	500	5.38E+00	1.761	1.77E+00	2.67E-01	6.95E-01	7.85E-01	8.99E-01
3/29/2011 12:17	1F W gate routine segment	8.42E+05	1000	1.20E-04	ND	ND		1.13E-05	1.39E-05	8.23E-01
3/29/2011 12:35	1F W gate routine segment	8.42E+05	1000	2.37E-04	ND	ND		2.34E-05	2.31E-05	1.03E+00

Measurement Day/Time	Sample Description	Volume (mL)	Live Time (s)	I-131 A	I-132 A	Te-132 A	^{131}I/^{132}Te Ratio	Cs-134 A	Cs-137 A	^{134}Cs/^{137}Cs ratio
3/29/2011 12:38	2F 3 4 drainage opening	5.00E+02	1000	1.64E+00	ND	ND		3.22E-01	3.25E-01	1.01E+00
3/29/2011 13:06	2F Iwasawa coast	5.00E+02	1000	1.28E+00	ND	ND		2.35E-01	0.2303	1.03E+00
3/29/2011 13:24	2F MP-1	5.00E+05	500	1.29E-04	ND	ND		1.55E-04	1.80E-04	8.79E-01
3/29/2011 13:32	2F MP-1	5.00E+05	500	2.01E-04	ND	ND		3.26E-05	4.29E-05	7.73E-01
3/29/2011 15:49	1F N side seawater	5.00E+02	1000	5.05E+01	1.25E-01	ND		1.21E+01	1.23E+01	1.00E+00
3/29/2011 16:09	1F seawater S side	5.00E+02	1000	1.34E+02	2.22E-01	ND		3.12E+01	3.17E+01	1.00E+00
3/29/2011 18:18	2F MP-1 routine dust	5.00E+05	500	7.92E-05	3.89E-05	4.91E-05	1.36E-01	4.26E-05	3.91E-05	1.11E+00
3/29/2011 18:28	2F MP-1 routine dust	5.00E+05	500	1.44E-04	8.31E-05	9.62E-05	1.27E-01	6.02E-05	6.28E-05	9.74E-01
3/30/2011 10:42	2F MP-1 routine dust	5.00E+05	1000	8.14E-04	3.28E-04	8.44E-05	7.47E-01	8.18E-05	7.43E-05	1.12E+00
3/30/2011 10:56	2F seawater (3 4 drainage opening)	5.00E+02	1000	1.58E+00	ND	ND		3.60E-01	3.41E-01	1.07E+00
3/30/2011 11:04	2F MP-1 routine dust	5.00E+05	1000	6.79E-04	2.27E-04	1.18E-04	4.46E-01	8.69E-04	8.25E-04	1.07E+00
3/30/2011 11:14	2F Iwasawa seawater	5.00E+02	1000	8.82E-01	ND	ND		1.79E-01	1.95E-01	9.37E-01
3/30/2011 11:32	1F seawater S side	5.00E+02	1000	3.18E+01	ND	ND		8.29E+00	8.32E+00	1.01E+00
3/30/2011 11:51	1F seawater N side	5.00E+02	1000	5.72E+01	ND	ND		1.46E+01	1.47E+01	1.01E+00

Measurement Day/Time	Sample Description	Volume (mL)	Live Time (s)	I-131 A	I-132 A	Te-132 A	^{131}I/^{132}Te Ratio	Cs-134 A	Cs-137 A	^{134}Cs/^{137}Cs ratio
3/30/2011 12:05	1F W gate	8.40E+05	1000	4.14E-04	ND	5.52E-05	5.76E-01	4.30E-05	3.99E-05	1.10E+00
3/30/2011 12:24	1F W gate	8.40E+05	1000	1.87E-04	ND	2.83E-05	5.06E-01	2.95E-05	3.00E-05	9.99E-01
3/30/2011 12:29	1F seawater pit water	1.00E+02	1000	2.03E+02	1.6	1.06E+01	1.47E+00	2.05E+01	2.12E+01	9.85E-01
3/30/2011 12:52	Pit water	1.00E-02	1000	6.85E+06	ND	ND		1.99E+06	2.01E+06	1.01E+00
3/30/2011 16:26	1F seawater S side	5.00E+02	1000	1.75E+02	ND	ND		4.70E+01	4.75E+01	1.01E+00
3/30/2011 17:09	1F seawater N side	5.00E+02	1000	4.71E+01	ND	ND		1.24E+01	1.24E+01	1.02E+00
3/30/2011 17:52	Subdrain water	5.00E+02	500	1.56E+00	ND	1.03E-01	1.13E+00	2.49E-01	2.72E-01	9.33E-01
3/30/2011 18:08	Subdrain water	5.00E+02	500	2.02E+01	5.81E-01	5.98E-01	2.50E+00	4.71E+00	4.90E+00	9.76E-01
3/30/2011 20:05	2F MP-1 charcoal	5.00E+05	1000	2.43E-04	7.48E-05	6.57E-05	2.72E-01	7.11E-05	7.50E-05	9.64E-01
3/30/2011 20:08	Subdrain water	2.00E+02	500	4.29E+02	8.296	3.00E+00	1.05E+01	5.17E+00	5.897	8.91E-01
3/30/2011 20:19	Subdrain water	2.00E+02	500	7.96E+01	ND	3.86E-01	1.51E+01	0.7003	6.31E-01	1.13E+00
3/30/2011 20:22	2F MP-1 particulate	5.00E+05	1000	1.51E-04	3.66E-05	3.90E-05	2.85E-01	5.22E-05	4.88E-05	1.09E+00
3/30/2011 20:30	Subdrain water	2.00E+02	500	2.23E+01	1.26E+01	5.36E-01	3.05E+00	1.02E+01	1.04E+01	9.97E-01
3/30/2011 23:32	Trench water	5.00E+02	500	5.52E+00	ND	2.46E-01	1.62E+00	1.05E+00	1.14E+00	9.32E-01

Measurement Day/Time	Sample Description	Volume (mL)	Live Time (s)	I-131 A	I-132 A	Te-132 A	^{131}I/^{132}Te Ratio	Cs-134 A	Cs-137 A	^{134}Cs/^{137}Cs ratio
3/30/2011 23:36	1F-6 N side trench water	5.00E+02	500	1.59E+00	ND	5.60E-02	2.05E+00	5.68E-01	5.78E-01	9.99E-01
3/31/2011 11:12	2F Iwasawa seawater	5.00E+02	1000	7.96E-01	ND	ND		1.55E-01	1.77E-01	8.92E-01
3/31/2011 11:33	2F 3 4 drainage opening	5.00E+02	1000	1.48E+00	ND	ND		3.57E-01	3.55E-01	1.02E+00
3/31/2011 11:58	1F seawater S side	5.00E+02	1000	7.44E+01	ND	ND		2.12E+01	2.13E+01	1.01E+00
3/31/2011 12:18	1F seawater N side	5.00E+02	1000	4.48E+01	ND	ND		1.18E+01	1.19E+01	1.01E+00
3/31/2011 12:26	1F W gate	8.35E+05	1000	6.42E-04	ND	4.20E-05	1.03E+00	4.20E-05	4.53E-05	9.43E-01
3/31/2011 12:44	1F W gate	8.35E+05	1000	1.89E-04	ND	2.25E-05	5.63E-01	3.28E-05	3.58E-05	9.32E-01
3/31/2011 13:02	2F MP-1	5.00E+05	1000	1.65E-04	4.14E-05	6.67E-05	1.65E-01	6.93E-05	7.28E-05	9.70E-01
3/31/2011 13:19	2F MP-1	5.00E+05	1000	1.30E-04	4.02E-05	5.60E-05	1.55E-01	7.28E-05	7.14E-05	1.04E+00
3/31/2011 16:16	1F seawater N side	5.00E+02	1000	8.25E+01	ND	ND		2.57E+01	2.58E+01	1.01E+00
3/31/2011 16:18	1F seawater S side	5.00E+02	1000	8.74E+01	1.22E-01	ND		2.54E+01	2.53E+01	1.02E+00
3/31/2011 18:21	2F MP-1	5.00E+05	1000	1.46E-04	3.24E-05	5.45E-05	1.74E-01	6.81E-05	6.85E-05	1.01E+00
3/31/2011 18:39	2F MP-1	5.00E+05	1000	7.84E-05	1.56E-05	3.14E-05	1.62E-01	4.22E-05	4.34E-05	9.91E-01
4/10/2011 9:54	2F MP-1	5.00E+05	1000	1.43E-05	ND	ND		ND	ND	

Measurement Day/Time	Sample Description	Volume (mL)	Live Time (s)	I-131 A	I-132 A	Te-132 A	^{131}I/^{132}Te Ratio	Cs-134 A	Cs-137 A	^{134}Cs/^{137}Cs ratio
4/10/2011 10:40	2F MP-1 volatile	5.00E+05	1000	1.94E-05	ND	ND		ND	ND	
4/10/2011 19:13	2F MP-1 afternoon dust	5.00E+05	1000	2.63E-05	ND	1.31E-06	3.50E-01	1.17E-05	1.16E-05	1.03E+00
4/10/2011 19:16	2F MP-1 afternoon charcoal	5.00E+05	1000	2.11E-05	ND	ND		ND	ND	
4/11/2011 10:16	2F MP-1 dust	5.00E+05	1000	1.67E-05	ND	ND		ND	ND	
4/11/2011 10:36	2F MP-1 particulate	5.00E+05	1000	1.18E-05	ND	ND		ND	ND	
4/11/2011 11:59	1F W gate volatile	8.22E+05	1000	1.13E-04	ND	1.06E-06	1.68E+00	1.14E-05	1.36E-05	8.61E-01
4/11/2011 12:09	1F W gate particulate	8.22E+05	1000	4.00E-05	ND	ND		ND	5.79E-06	
4/11/2011 17:11	2F MP-1 afternoon volatile	5.00E+05	1000	1.64E-05	ND	1.21E-06	2.09E-01	8.92E-06	8.47E-06	1.08E+00
4/11/2011 17:13	2F MP-1 afternoon particulate	5.00E+05	1000	8.39E-06	ND	ND		ND	ND	
4/12/2011 11:00	1F W gate particulate	8.38E+05	1000	1.13E-04	ND	1.95E-06	8.12E-01	3.28E-05	3.85E-05	8.77E-01
4/12/2011 11:30	1F W gate volatile	8.38E+05	1000	1.31E-04	ND	1.95E-06	9.37E-01	2.25E-05	2.89E-05	7.99E-01
4/12/2011 12:44	2F MP-1 volatile	5.00E+05	1000	2.10E-05	ND	1.93E-06	1.50E-01	1.19E-05	7.92E-06	1.54E+00
4/12/2011 13:03	2F MP-1 particulate	5.00E+05	1000	2.27E-05	ND	ND		1.13E-05	9.36E-06	1.24E+00

Measurement Day/Time	Sample Description	Volume (mL)	Live Time (s)	I-131 A	I-132 A	Te-132 A	^{131}I/^{132}Te Ratio	Cs-134 A	Cs-137 A	^{134}Cs/^{137}Cs ratio
4/12/2011 16:26	2F MP-1 particulate	5.00E+05	1000	7.29E-06	ND	ND		ND	ND	
4/12/2011 16:54	2F MP-1 volatile	5.00E+05	1000	1.91E-05	ND	ND		0.000124	ND	
4/13/2011 10:28	1F W gate particulate	8.27E+05	1000	1.10E-04	ND	1.58E-06	8.52E-01	2.30E-05	2.64E-05	8.97E-01
4/13/2011 10:30	1F W gate charcoal	8.27E+05	1000	9.75E-05	ND	ND		ND	1.12E-05	
4/13/2011 10:47	2F MP-1 particulate	5.00E+05	1000	2.12E-05	2.11E-06	ND		9.11E-06	9.53E-06	9.84E-01
4/13/2011 10:49	2F MP-1 charcoal	5.00E+05	1000	1.81E-05	ND	ND		ND	ND	
4/13/2011 18:44	2F MP-1 charcoal	5.00E+05	1000	1.99E-05	ND	1.16E-06	2.02E-01	8.95E-06	7.70E-06	1.20E+00
4/13/2011 18:46	2F MP-1 afternoon particulate	5.00E+05	1000	8.90E-06	ND	ND		ND	ND	
4/14/2011 11:26	2F MP-1 dust	5.00E+05	1000	1.02E-05	ND	ND		6.1E-06	6.64E-06	9.46E-01
4/14/2011 11:44	2F MP-1 charcoal	5.00E+05	1000	1.68E-05	ND	1.37E-06	1.31E-01	9.66E-06	8.57E-06	1.16E+00
4/14/2011 17:27	1F W gate monitoring post dust	8.12E+05	1000	4.16E-04	5.51E-05	3.60E-06	1.20E+00	1.92E-04	1.90E-04	1.04E+00
4/14/2011 17:27	1F W gate	8.12E+05	1000	7.65E-04	1.31E-05	ND		7.49E-05	8.13E-05	9.49E-01
4/14/2011 18:58	2F MP-1 charcoal	5.00E+05	1000	1.88E-05	ND	ND		1.02E-05	1.10E-05	9.59E-01

Measurement Day/Time	Sample Description	Volume (mL)	Live Time (s)	I-131 A	I-132 A	Te-132 A	^{131}I/^{132}Te Ratio	Cs-134 A	Cs-137 A	^{134}Cs/^{137}Cs ratio
4/14/2011 19:21	2F MP-1 dust	5.00E+05	1000	1.27E-05	ND	ND		7.92E-06	6.26E-06	1.30E+00
4/15/2011 11:12	2F MP-1 morning	5.00E+05	1000	4.65E-05	ND	ND		ND	ND	
4/15/2011 11:31	2F MP-1 morning	5.00E+05	1000	1.87E-05	ND	ND		1.02E-05	1.05E-05	9.98E-01
4/15/2011 17:00	1F W gate	8.26E+05	1000	2.16E-04	ND	ND		7.59E-05	8.09E-05	9.67E-01
4/15/2011 17:19	1F W gate	8.26E+05	1000	1.27E-04	ND	ND		4.24E-05	4.17E-05	1.05E+00
4/15/2011 20:41	2F MP-1 afternoon dust	5.00E+05	1000	1.16E-05	ND	ND		6.53E-06	7.70E-06	8.74E-01
4/15/2011 20:59	2F MP-1 afternoon charcoal	5.00E+05	1000	1.63E-05	ND	ND		8.21E-06	8.90E-06	9.50E-01
4/16/2011 10:41	2F MP-1	5.00E+05	1000	1.24E-05	ND	ND		ND	1.8E-05	
4/16/2011 11:03	2F MP-1	5.00E+05	1000	1.14E-05	ND	ND		ND	ND	
4/16/2011 17:07	2F MP-1	5.00E+05	1000	1.38E-05	ND	ND		8.76E-06	9.93E-06	9.10E-01
4/16/2011 17:12	2F MP-1 particulate	5.00E+05	1000	1.28E-05	ND	ND		ND	ND	
4/16/2011 18:25	1F W gate charcoal routine	8.14E+05	1000	1.07E-04	ND	ND		1.45E-06	1.64E-05	9.17E-02
4/16/2011 18:27	1F W gate particulate routine	8.14E+05	1000	5.78E-05	ND	ND		ND	ND	

Measurement Day/Time	Sample Description	Volume (mL)	Live Time (s)	I-131 A	I-132 A	Te-132 A	^{131}I/^{132}Te Ratio	Cs-134 A	Cs-137 A	^{134}Cs/^{137}Cs ratio
4/17/2011 10:27	2F MP-1 charcoal	5.00E+05	1000	1.90E-05	ND	ND		1.18E-05	1.43E-05	8.52E-01
4/17/2011 10:27	2F MP-1 particulate	5.00E+05	1000	1.50E-05	ND	ND		ND	9.64E-06	
4/17/2011 16:45	2F MP-1 charcoal	5.00E+05	1000	2.10E-05	ND	ND		ND	ND	
4/17/2011 17:40	2F MP-1 particulate	5.00E+05	1000	1.39E-05	ND	ND		ND	ND	
4/17/2011 18:01	1F W gate charcoal	8.22E+05	1000	5.68E-04	7.79E-05	ND		1.14E-05	ND	
4/17/2011 18:22	1F W gate particulate	8.22E+05	1000	3.46E-04	8.66E-05	ND		1.15E-04	1.07E-04	1.11E+00
4/18/2011 11:07	2F MP-1 morning	5.00E+05	1000	1.18E-05	ND	ND		ND	ND	
4/18/2011 11:11	2F MP-1 morning	5.00E+05	1000	2.07E-05	ND	ND		1.04E-05	1.27E-05	8.46E-01
4/18/2011 16:12	1F W gate	8.15E+05	1000	7.06E-05	ND	2.38E-06	1.83E-01	1.58E-05	1.43E-05	1.14E+00
4/18/2011 16:32	1F W gate	8.15E+05	1000	3.19E-05	ND	ND		ND	6.05E-06	
4/18/2011 21:00	1F MP-1 dust particulate	5.00E+05	1000	9.52E-06	ND	ND		7.12E-06	6.59E-06	1.12E+00
4/18/2011 21:19	2F MP-1 charcoal	5.00E+05	1000	2.25E-05	ND	ND		1.03E-05	7.79E-06	1.36E+00
4/19/2011 12:15	2F MP-1	5.00E+05	1000	1.51E-05	ND	ND		7.99E-06	1.21E-05	6.84E-01
4/19/2011 16:36	1F W gate particulate	8.32E+05	1000	7.50E-05	ND	ND		7.34E-06	6.96E-06	1.09E+00

Measurement Day/Time	Sample Description	Volume (mL)	Live Time (s)	I-131 A	I-132 A	Te-132 A	^{131}I/^{132}Te Ratio	Cs-134 A	Cs-137 A	^{134}Cs/^{137}Cs ratio
4/19/2011 16:44	1F W gate charcoal	8.32E+05	1000	5.01E-05	ND	ND		1.22E-05	1.36E-05	9.33E-01
4/19/2011 17:37	2F MP-1	5.00E+05	1000	6.99E-05	ND	ND		ND	ND	
4/19/2011 18:01	2F MP-1	5.00E+05	1000	1.58E-05	ND	ND		9.62E-06	1.09E-05	9.10E-01
4/19/2011 19:18	2F MP-1 particulate	5.00E+05	1000	6.38E-05	ND	ND		ND	ND	
4/20/2011 11:15	2F MP-1	5.00E+05	1000	1.45E-05	ND	ND		8.49E-06	1.01E-05	8.74E-01
4/20/2011 11:53	2F MP-1	5.00E+05	1000	8.67E-06	ND	ND		8.64E-06	6.63E-06	1.35E+00
4/20/2011 16:02	1F W gate	8.25E+05	1000	3.34E-05	ND	ND		7.98E-06	9.13E-06	9.04E-01
4/20/2011 16:20	1F W gate	8.25E+05	1000	7.01E-05	ND	ND		1.55E-05	1.68E-05	9.53E-01
4/20/2011 16:49	2F MP-1 afternoon	5.00E+05	1000	3.28E-05	ND	ND		ND	ND	
4/20/2011 19:01	2F MP-1	5.00E+05	1000	1.91E-05	ND	ND		7.29E-06	9.90E-06	7.62E-01
4/21/2011 10:57	2F MP-1 morning	5.00E+05	1000	1.38E-05	ND	ND		8.51E-06	1.25E-05	7.08E-01
4/21/2011 11:16	2F MP-1 morning	5.00E+05	1000	7.78E-06	ND	ND		5.38E-06	7.32E-06	7.61E-01
4/21/2011 18:44	1F W gate particulate	8.25E+05	1000	5.16E-05	ND	ND		ND	7.61E-06	
4/21/2011 18:45	1F W gate charcoal	8.25E+05	1000	7.57E-05	ND	ND		1.79E-05	1.35E-05	1.38E+00

Measurement Day/Time	Sample Description	Volume (mL)	Live Time (s)	I-131 A	I-132 A	Te-132 A	^{131}I/^{132}Te Ratio	Cs-134 A	Cs-137 A	^{134}Cs/^{137}Cs ratio
4/21/2011 19:11	2F MP-1 dust	5.00E+05	1000	2.52E-05	ND	1.33E-06	7.72E-02	ND	ND	
4/21/2011 19:12	2F MP-1 afternoon iodine	5.00E+05	1000	1.43E-05	ND	ND		1.2E-05	1.27E-05	9.81E-01
4/22/2011 11:58	2F MP-1 morning	5.00E+05	1000	1.83E-05	ND	ND		1.26E-05	1.39E-05	9.41E-01
4/22/2011 12:20	2F MP-1 morning	5.00E+05	1000	1.83E-05	ND	ND		ND	ND	
4/22/2011 17:09	1F W gate charcoal	8.31E+05	1000	3.72E-05	ND	ND		8.35E-06	9.04E-06	9.58E-01
4/22/2011 17:13	1F W gate	8.31E+05	1000	3.83E-05	ND	ND		ND	6.30E-06	
4/22/2011 20:49	2F MP-1 charcoal	5.00E+05	1000	1.26E-05	ND	ND		9.69E-06	7.09E-06	1.42E+00
4/22/2011 21:08	2F MP-1 particulate	5.00E+05	1000	9.04E-06	ND	ND		5.79E-06	6.12E-06	9.81E-01
4/23/2011 11:49	2F MP-1 morning charcoal	5.00E+05	1000	1.46E-05	ND	ND		9.76E-06	1.06E-05	9.60E-01
4/23/2011 12:07	2F MP-1 morning particle	5.00E+05	1000	8.28E-06	ND	ND		9.37E-06	7.71E-06	1.26E+00
4/23/2011 16:25	1F W gate monitoring car	8.31E+05	1000	4.03E-05	ND	ND		1.07E-05	1.52E-05	7.30E-01
4/23/2011 16:44	1F W gate monitoring car	8.31E+05	1000	2.71E-05	ND	ND		1.28E-05	1.45E-05	9.18E-01
4/23/2011 17:37	2F MP-1 afternoon charcoal	5.00E+05	1000	1.41E-05	ND	ND		1.10E-05	1.10E-05	1.04E+00

Measurement Day/Time	Sample Description	Volume (mL)	Live Time (s)	I-131 A	I-132 A	Te-132 A	^{131}I/^{132}Te Ratio	Cs-134 A	Cs-137 A	^{134}Cs/^{137}Cs ratio
4/23/2011 17:55	2F MP-1 afternoon dust	5.00E+05	1000	7.51E-06	ND	ND		1.02E-05	8.56E-06	1.23E+00
4/24/2011 11:08	2F MP-1 morning charcoal	5.00E+05	1000	9.85E-06	ND	ND		1.08E-05	1.50E-05	7.46E-01
4/24/2011 11:25	2F MP-1 morning dust	5.00E+05	1000	7.91E-06	ND	ND		7.81E-06	7.30E-06	1.11E+00
4/24/2011 16:18	1F W gate charcoal	8.28E+05	1000	4.84E-05	ND	ND		1.33E-05	1.73E-05	7.98E-01
4/24/2011 16:20	1F W gate particulate	8.28E+05	1000	4.21E-05	ND	ND		1.84E-05	1.59E-05	1.20E+00
4/24/2011 16:39	2F MP-1 afternoon particulate	5.00E+05	1000	1.12E-05	ND	ND		ND	ND	
4/24/2011 16:44	2F MP-1 afternoon charcoal	5.00E+05	1000	1.29E-05	ND	ND		1.26E-05	1.34E-05	9.79E-01
4/25/2011 11:22	2F MP-1 morning particle	5.00E+05	1000	6.18E-06	ND	ND		5.42E-06	5.81E-06	9.69E-01
4/25/2011 11:40	2F MP-1 morning charcoal	5.00E+05	1000	7.77E-06	ND	ND		9.73E-06	8.29E-06	1.22E+00
4/25/2011 15:56	2F MP-1 afternoon charcoal	5.00E+05	1000	9.48E-06	ND	ND		5.96E-06	1.04E-05	5.96E-01
4/25/2011 16:14	2F MP-1 afternoon particulate	5.00E+05	1000	6.72E-06	ND	ND		9.55E-06	1.01E-05	9.79E-01
4/25/2011 18:29	1F W gate charcoal	8.09E+05	1000	3.06E-05	ND	ND		9.53E-06	1.04E-05	9.54E-01

Measurement Day/Time	Sample Description	Volume (mL)	Live Time (s)	I-131 A	I-132 A	Te-132 A	^{131}I/^{132}Te Ratio	Cs-134 A	Cs-137 A	^{134}Cs/^{137}Cs ratio
4/25/2011 18:47	1F W gate particulate	8.09E+05	1000	1.41E-05	ND	ND		7.20E-06	8.60E-06	8.70E-01
4/26/2011 9:57	2F MP-1 morning charcoal	5.00E+05	1000	1.08E-05	ND	ND		9.75E-06	1.13E-05	8.98E-01
4/26/2011 13:49	2F MP-1 morning particle	5.00E+05	1000	5.63E-06	ND	ND		3.62E-06	6.09E-06	6.18E-01
4/26/2011 16:02	2F MP-1 afternoon charcoal	5.00E+05	1000	1.08E-05	ND	ND		9.52E-06	1.46E-05	6.78E-01
4/26/2011 16:04	2F MP-1 afternoon	5.00E+05	1000	9.53E-06	ND	ND		ND	ND	
4/26/2011 16:49	1F W gate monitoring car	8.25E+05	1000	4.95E-05	ND	ND		1.22E-05	1.40E-05	9.08E-01
4/26/2011 17:11	1F W gate monitoring car	8.25E+05	1000	ND	ND	ND		9.69E-06	1.00E-05	1.01E+00
4/27/2011 10:17	2F MP-1 charcoal	5.00E+05	1000	8.92E-06	ND	ND		8.97E-06	1.00E-05	9.32E-01
4/27/2011 10:39	2F MP-1 dust	5.00E+05	1000	4.01E-06	ND	ND		6.97E-06	6.37E-06	1.14E+00
4/27/2011 16:16	1F W gate charcoal	8.16E+05	1000	5.11E-05	ND	ND		ND	1.18E-05	
4/27/2011 16:34	1F W gate particulate	8.16E+05	1000	4.72E-05	ND	ND		1.27E-05	1.27E-05	1.05E+00
4/27/2011 18:56	2F MP-1 afternoon dust	5.00E+05	1000	4.81E-06	ND	ND		6.59E-06	8.27E-06	8.30E-01
4/27/2011 19:13	2F MP-1 charcoal dust afternoon	5.00E+05	1000	5.19E-06	ND	ND		1.26E-05	1.48E-05	8.88E-01

Measurement Day/Time	Sample Description	Volume (mL)	Live Time (s)	I-131 A	I-132 A	Te-132 A	^{131}I/^{132}Te Ratio	Cs-134 A	Cs-137 A	^{134}Cs/^{137}Cs ratio
4/28/2011 9:49	2F MP-1 morning charcoal	5.00E+05	1000	7.65E-06	ND	ND		1.06E-05	1.22E-05	9.03E-01
4/28/2011 10:26	2F MP-1 morning dust	5.00E+05	1000	7.26E-06	ND	ND		ND	ND	
4/28/2011 15:44	2F MP-1 afternoon charcoal	5.00E+05	1000	7.03E-06	ND	ND		8.73E-06	7.37E-06	1.23E+00
4/28/2011 16:01	2F MP-1 afternoon dust	5.00E+05	1000	4.68E-06	ND	ND		7.38E-06	6.75E-06	1.14E+00
4/28/2011 19:39	1F W gate	8.15E+05	1000	1.63E-04	ND	ND		1.55E-05	ND	
4/28/2011 19:56	1F W gate	8.15E+05	1000	6.60E-05	ND	ND		3.27E-05	3.01E-05	1.13E+00
4/29/2011 11:16	2F MP-1 morning charcoal	5.00E+05	1000	5.77E-06	ND	ND		9.10E-06	1.22E-05	7.77E-01
4/29/2011 13:02	2F MP-1 morning dust	5.00E+05	1000	2.72E-06	ND	ND		5.14E-06	4.87E-06	1.10E+00
4/29/2011 21:39	1F W gate monitoring car	8.34E+05	1000	4.38E-05	ND	ND		1.83E-05	2.04E-05	9.36E-01
4/29/2011 22:22	2F MP-1 afternoon	5.00E+05	1000	5.81E-06	ND	ND		8.03E-06	7.65E-06	1.10E+00
4/29/2011 22:43	1F W gate monitoring car	8.34E+05	1000	6.30E-05	ND	ND		3.93E-05	4.52E-05	9.06E-01
4/29/2011 23:12	2F MP-1	5.00E+05	1000	5.27E-06	ND	ND		ND	ND	
4/30/2011 12:09	2F MP-1 morning charcoal	5.00E+05	1000	6.41E-06	ND	ND		7.75E-06	1.02E-05	7.92E-01

Measurement Day/Time	Sample Description	Volume (mL)	Live Time (s)	I-131 A	I-132 A	Te-132 A	^{131}I/^{132}Te Ratio	Cs-134 A	Cs-137 A	^{134}Cs/^{137}Cs ratio
4/30/2011 12:27	2F MP-1 morning dust	5.00E+05	1000	3.16E-06	ND	ND		6.50E-06	7.8E-06	8.70E-01
4/30/2011 16:43	1F W gate charcoal	8.31E+05	1000	3.33E-05	ND	ND		1.79E-05	2.51E-05	7.47E-01
4/30/2011 17:00	1F W gate particulate	8.31E+05	1000	1.33E-05	ND	ND		1.20E-05	1.21E-05	1.04E+00
4/30/2011 17:45	2F MP-1 charcoal	5.00E+05	1000	5.73E-06	ND	ND		9.14E-06	1.27E-05	7.49E-01
4/30/2011 18:03	2F MP-1 dust	5.00E+05	1000	3.79E-06	ND	ND		5.79E-06	6.60E-06	9.16E-01
4/1/2013 10:05	Shallow draft quay seawater morning	2.00E+03	2000	ND	ND	ND		3.03E+00	4.88E+00	1.18E+00
4/2/2013 11:54	Shallow draft quay seawater morning	2.00E+03	2000	ND	ND	ND		U	U	
4/3/2013 10:17	Shallow draft quay seawater morning	2.00E+03	2000	ND	ND	ND		2.654	4.89E+00	1.03E+00
4/4/2013 10:35	Shallow draft quay seawater morning	2.00E+03	2000	ND	ND	ND		3.24E+00	4.864	1.27E+00
5/27/2013 19:07	N drainage marine soil	5.00E+02	1000	ND	ND	ND		2.08E-01	4.18E-01	9.94E-01
7/1/2013 9:37	1F seawater N side	2.00E+03	1000	ND	ND	ND		ND	U	
7/1/2013 9:39	Shallow draft quay seawater morning	2.00E+03	500	ND	ND	ND		2.502	6.53E+00	7.87E-01
7/18/2013 9:05	Turbine bldg SE	5.00E+02	500	ND	ND	ND		ND	ND	

Measurement Day/Time	Sample Description	Volume (mL)	Live Time (s)	I-131 A	I-132 A	Te-132 A	$^{131}I/^{132}Te$ Ratio	Cs-134 A	Cs-137 A	$^{134}Cs/^{137}Cs$ ratio
8/1/2013 9:15	Incineration workshop bldg 6 W	5.00E+02	500	ND	ND	ND		0.0233	8.02E-02	6.13E-01
8/3/2013 13:03	PCV gas piping outlet charcoal	1.98E+06	2000	ND	ND	ND		ND	ND	
8/3/2013 13:10	PCV gas piping outlet	6.70E+05	2000	ND	ND	ND		U	U	
8/7/2013 16:26	Exhaust filter inlet particulate	6.00E+06	2000	ND	ND	ND		3.92E-06	7.61E-06	1.09E+00
8/7/2013 16:57	RB exhaust filter outlet particulate	6.00E+06	2000	ND	ND	ND		ND	ND	
8/7/2013 17:32	Exhaust filter inlet charcoal	6.00E+06	2000	ND	ND	ND		ND	ND	
8/7/2013 17:38	Exhaust filter outlet charcoal	6.00E+06	2000	ND	ND	ND		ND	ND	
8/15/2013 9:01	Incineration workshop bldg 6 W	5.00E+02	500	ND	ND	ND		0.04415	0.09419	1.00E+00
8/22/2013 17:49	Reactor well top A below particulate	1.50E+05	3000	ND	ND	ND		U	U	
8/22/2013 18:41	Reactor well top A below charcoal	1.50E+05	3000	ND	ND	ND		ND	2.12E-05	
8/22/2013 19:33	Reactor well top A side charcoal	1.50E+05	3000	ND	ND	ND		U	ND	
8/22/2013 20:24	Reactor well top A below charcoal	1.50E+05	3000	ND	ND	ND		U	2.59E-05	
8/22/2013 20:26	Reactor well top A side particulate	1.50E+05	3000	ND	ND	ND		U	ND	

Measurement Day/Time	Sample Description	Volume (mL)	Live Time (s)	I-131 A	I-132 A	Te-132 A	^{131}I/^{132}Te Ratio	Cs-134 A	Cs-137 A	^{134}Cs/^{137}Cs ratio
8/22/2013 21:19	Reactor well top A side charcoal	1.50E+05	3000	ND	ND	ND		ND	ND	
8/22/2013 21:24	Reactor well top A below particulate	1.50E+05	3000	ND	ND	ND		ND	1.22E-05	
8/22/2013 22:17	Reactor well top B below charcoal	1.50E+05	3000	ND	ND	ND		U	ND	
8/22/2013 22:19	Reactor well top A side particulate	1.50E+05	3000	ND	ND	ND		U	ND	
8/22/2013 23:14	Reactor well top B below particulate	1.50E+05	3000	ND	ND	ND		0.001247	0.002625	1.02E+00
8/22/2013 23:17	Reactor well top B side charcoal	1.50E+05	3000	ND	ND	ND		U	2.75E-05	
8/23/2013 0:06	Reactor well top B side particulate	1.50E+05	3000	ND	ND	ND		3.15E-05	7.58E-05	8.94E-01
8/23/2013 0:56	Reactor well top B below particulate	1.50E+05	3000	ND	ND	ND		1.73E-04	0.000364	1.02E+00
8/23/2013 1:03	Reactor well top B below charcoal	1.50E+05	3000	ND	ND	ND		ND	U	
8/23/2013 1:52	Reactor well top B side particulate	1.50E+05	3000	ND	ND	ND		8.72E-06	1.84E-05	1.02E+00
8/23/2013 1:56	Reactor well top B side charcoal	1.50E+05	3000	ND	ND	ND		ND	ND	
9/1/2013 9:06	Incineration workshop bldg 6 W	5.00E+02	500	ND	ND	ND		0.0621	0.1436	9.37E-01
9/1/2013 11:02	Bar screen front seawater	2.00E+03	500	ND	ND	ND		1.46E+01	33.69	9.36E-01

Measurement Day/Time	Sample Description	Volume (mL)	Live Time (s)	I-131 A	I-132 A	Te-132 A	$^{131}I/^{132}Te$ Ratio	Cs-134 A	Cs-137 A	$^{134}Cs/^{137}Cs$ ratio
10/1/2013 8:47	Incineration workshop bldg 6 W	5.00E+02	500	ND	ND	ND		3.74E-02	0.09765	8.51E-01